Tuning electrochemical CO$_2$ reduction pathways using pulsed potentials on silver

Inaugural-Dissertation
to obtain the academic degree
Doctor rerum naturalium (Dr. rer. nat.)

submitted to the Department of Biology, Chemistry, Pharmacy
of Freie Universität Berlin

by

Alexander Ulrich Arndt

July 2022

Time period for conducting the doctoral studies:

01.10.2018 – 31.07.2022

Institute where the research was conducted:

Helmholtz-Zentrum Berlin für Materialien und Energie GmbH,

Hahn-Meitner-Platz 1, 14109 Berlin

Supervisor and 1st reviewer:

Dr. Matthew Mayer

Young Investigator Group Electrochemical Conversion

Helmholtz-Zentrum Berlin für Materialien und Energie GmbH,

Hahn-Meitner-Platz 1, 14109 Berlin

2nd reviewer:

Prof. Dr. Beate Paulus

Theoretical Chemistry,

Institut für Chemie und Biochemie, Freie Universität Berlin,

Arnimallee 22, 14195 Berlin

Date of defense: 07.11.2022

Herewith I certify that I have prepared and written my thesis independently and that I have not used any sources and aids other than those indicated by me. Intellectual property of other authors has been marked accordingly. I also declare that I have not applied for an examination procedure at any other institution and that I have not submitted the dissertation in this or any other form to any other faculty as a dissertation.

……………………………..

Berlin, July 2022

Alexander Arndt

Acknowledgements

First of all, I would like to express my deep gratitude to my supervisor Dr. Matthew Mayer. His curiosity and knowledge were always a great inspiration for me during my time at HZB. His door was always open, and I am grateful for all the time he took for me and my work. I was always impressed by his ability to think quickly about complex issues and his talent to see the big picture. Matts precise and focused way of working supported me and contributed to the success of my work. I was fortunate to experience great guidance and support from him while being able to develop and test my own ideas.

Furthermore, I would like to thank Prof. Dr. Beate Paulus for her interest in my work. I am grateful for the insightful conversations, her guidance during the PhD and for the good advice she gave me. I am very pleased that she has guided and reviewed my work.

My thanks also go to Dr. Laura Pardo-Perez. She has been a great help to me from the very beginning. Laura always had an open ear for me, and I am grateful that I was able to profit from her knowledge, and her structured and goal-oriented way of working. Her positive manner, even beyond the laboratory, will remain in my special memory.

Further thanks go to Gumaa, Sasho, Sid and the rest of the NECC team for all the good conversations, helpful advice and the great working atmosphere. I would especially like to thank Theocharis Tzanoudakis for his work on the mass spectrometers. It was a great experience to pass on what I learned to him and to see how he mastered even challenging tasks with his quick grasp and his commitment.

A big thank you also goes to Dr. Peter Bogdanoff, to whom I could always go with small and big questions. His experience and hands-on mentality were a great support to me. I would also like to express my thanks to Karsten Harbauer. He, too, was always a help and tirelessly produced new samples for me.

Many thanks to my family, who also supported me during this exciting time. Even from a distance, they have been a great support to me. Thank you for never doubting my path.

Finally, I want to express my thanks to my love Luisa. You have tirelessly supported me on this adventure and especially the last few weeks you have had my back. Together we have started our own family, an experience that is indescribable. I'm thankful for you and Carlo, for your patience and the beautiful memories we have created. I am so looking forward to our next steps.

Abstract

Renewable energy powered electrochemical CO_2 reduction (CO_2ER) enables us to utilize the greenhouse gas and turn it into useful commodity chemicals, thus mitigating harmful carbon emissions and offering a more sustainable carbon source alternative to crude oil. Yet, a low selectivity, stability and activity hamper the industrial application.

We have studied pulsed potential CO_2ER (p-CO_2ER), which serves as an elegant way of controlling the product selectivity simply by modulating the applied electrical input. In pulse potential CO_2ER driven by square-wave voltammetry, four variables can be adjusted to drive the catalysts selectivity: the pulse potentials herein labeled "cathodic" (E_c) and "anodic" (E_a) (meaning that one is more negative than the other, while both are typically > 0 V) as well as the time of the applied cathodic pulse t_c and of the anodic pulse t_a. We have investigated the effect of p-CO_2ER on silver and found the unique behavior of high methane formation. The catalyst underwent an "activation" period of 4-5 h to reach its CH_4 selective state, which we have analyzed to be due to changes in the surface morphology as well as changes in adsorbates.

We have systematically studied the effect of pulse potential and pulse time in a classical H-cell as well as in a flow-cell connected to a mass spectrometer. We found that the CH_4 formation depends on the right combination of E_c and E_a and discovered significant rate enhancement towards CH_4 when applying millisecond pulses.

A thorough analysis of the product formation on a millisecond timescale by means of differential electrochemical mass spectrometry (DEMS) allowed us to gain a deeper understanding of the pulsing effect. The fast response product analysis by DEMS allowed us further to screen a plethora of pulse potential combinations, identifying new combinations for high CH_4 activity. We provide additional information about adsorbed intermediates and products on the silver surface by in-situ Raman spectroscopy, and hence were able to show that pulsing leads to an increase of local CO_2-concentration, which can promote CO_2ER, while suppressing the formation of hydrogen.

Zusammenfassung

Die mit erneuerbaren Energien betriebene elektrochemische CO_2-Reduktion (CO_2ER) ermöglicht es uns, das Treibhausgas zu nutzen und in wertvolle chemische Grundstoffe umzuwandeln. Hierdurch können sich schädliche Kohlendioxidemissionen verringern lassen sowie eine nachhaltige Kohlenstoffquelle als Alternative zu Erdöl etablieren. Allerdings behindern eine geringe Selektivität, Stabilität und Aktivität der Katalysatoren die industrielle Anwendung.

Wir haben die CO_2ER mit gepulstem Potenzial (p-CO_2ER) untersucht, welche eine elegante Möglichkeit zur Kontrolle der Produktselektivität darstellt. Bei der CO_2ER mit rechteckförmigem gepulstem Potenzial können vier Variablen eingestellt werden, um die Selektivität des Katalysators zu steuern: die Pulspotenziale, die hier als "kathodisch" (E_c) und "anodisch" (E_a) bezeichnet werden (was bedeutet, dass eines negativer ist als das andere, während beide typischerweise > 0 V sind), sowie die Zeit des angelegten kathodischen Pulses t_c und des anodischen Pulses t_a. Wir haben die Wirkung von p-CO_2ER auf Silber untersucht und das einzigartige Verhalten von hoher Methanbildung festgestellt. Der Katalysator durchlief eine "Aktivierungsphase" von 4-5 Stunden, um seinen CH_4-selektiven Zustand zu erreichen, was wir auf Veränderungen in der Oberflächenmorphologie sowie auf Veränderungen in adsorbierten Spezies zurückführen.

Wir haben die Auswirkung des Pulspotenzials und der Pulsdauer systematisch in einer klassischen H-Zelle sowie in einer an ein Massenspektrometer angeschlossenen Durchflusszelle untersucht. Wir fanden heraus, dass die Methanbildung von der richtigen Kombination von E_c und E_a abhängt und entdeckten eine signifikante Ratenerhöhung bezüglich CH_4 bei der Anwendung von Millisekunden-Pulsen.

Eine gründliche Analyse der Produktbildung auf einer Zeitskala von Millisekunden mit Hilfe der differentiellen elektrochemischen Massenspektrometrie (DEMS) ermöglichte es uns, ein tieferes Verständnis für den Pulseffekt zu gewinnen. Zusätzliche Informationen über adsorbierte Zwischenprodukte und Produkte auf der Silberoberfläche konnten wir durch in-situ Raman-Spektroskopie gewinnen. Die Produktanalyse mit hoher Zeitauflösung mittels DEMS ermöglichte es uns, eine Vielzahl von potenziellen Pulskombinationen zu untersuchen und neue Kombinationen für eine hohe CH_4-Aktivität zu identifizieren. Wir konnten zeigen, dass das Pulsen zu einer Erhöhung der lokalen CO_2-Konzentration führt, was die CO_2ER fördern kann, während die Bildung von Wasserstoff unterdrückt wird.

Table of contents

1 Introduction

1.1 Motivation

Human consumption of fossil fuels has led to a drastic rise in the atmospheric CO_2-concentration since the mid-19th century (see Figure 1). This has resulted in an increase in earth's surface temperature by +1.11 °C due to the greenhouse effect.[1,2] Svante Arrhenius (awarded a Nobel Prize in 1903) published on the relation between atmospheric carbon dioxide and its greenhouse effect already in 1896. He postulated an increase in earth's temperature by 4-6 °C in case of a doubling in atmospheric CO_2.[3] There is no doubt that the increase in CO_2 stems from human activities and that drastic measures have to be taken in order to keep global warming below 1.5 °C.[4]
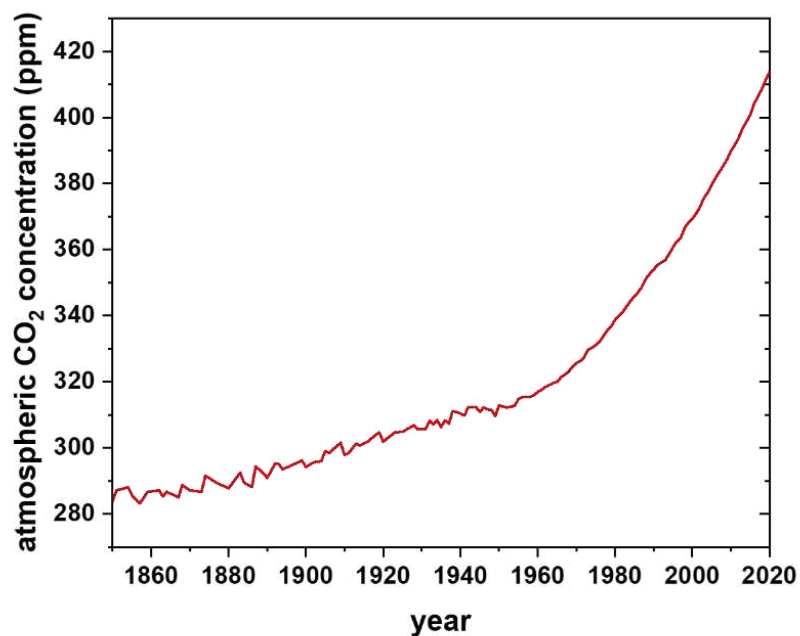
Figure 1: Atmospheric CO_2 concentration over the last 170 years. Data taken from [5].

Considerable efforts have been made in the past years to diverge from the use of fossil fuels as an energy source towards renewable energy (e.g., solar and wind). Significant progress has been made in the implementation and efficiency improvement of such technologies in the last decades. While this approach helps to significantly lower the carbon emissions based on energy consumption, it does not address our reliance on fossil fuels as a carbon source for an incredibly

wide range of non-fuel applications. The chemical/pharmaceutical industry consumes giant amounts of organic carbon derived from crude oil to supply modern society with polymers, fertilizers and medicine on a massive scale, essentially all of which eventually decompose to CO_2. If we are to reach carbon neutrality by 2050, not only the energy sector needs to change drastically but most chemical industries need to adapt to the energy transition. In the context of transition from crude oil and natural gas as sources of carbon to sustainable ones, electrochemical CO_2 reduction (CO_2ER) could play an important role. In the CO_2ER process, the harmful greenhouse gas carbon dioxide is transformed into small organic building blocks like CO, formate, alcohols and hydrocarbons etc. Ideally, the reaction is driven with electricity from a sustainable source and thus offers a pathway for the production of CO_2-neutral commodity chemicals. In order for this technology to be scaled up to an industrial size, the poor control of which products are formed (selectivity) has to be tackled, which will be addressed in the following chapters.

The work here employs pure research grade CO_2 and does not address the question of where the CO_2 comes from. Although governments have proposed rapid decreases in carbon emissions, the fact is that conventional industry will continue using carbon-emitting technologies for the foreseeable future, and thus so-called "point source" carbon capture will be a primary near-term CO_2 source for utilization. Meanwhile, it has become increasingly apparent that "negative emissions" technologies are needed to achieve a stable climate. Most IPCC models include assumptions of CO_2 removal from the atmosphere needs to occur on a massive scale[6], and as such "direct air capture" technologies will likely represent a long-term CO_2 source.

1.2 Electrochemical CO_2 reduction

In electrochemical CO_2 reduction (CO_2ER), carbon dioxide reacts with protons and electrons to form products following the general equation:

$$y\, CO_2 + x\, H^+ + x\, e^- \rightarrow n\, H_2O + \text{product(s)} \qquad (1)$$
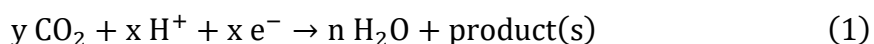
As stochiometric amounts of electrons and protons are needed to drive this reaction, an anode reaction that can supply these sufficiently is needed.

Thus, the most common anode reaction involves the oxygen evolution reaction (OER), where water molecules are oxidized to produce molecular oxygen (according to equation (2)).

$$2\,H_2O \rightarrow O_2 + 4\,H^+ + 4\,e^- \tag{2}$$

Due to the very positive standard potential (E^0= 1.23 V vs the reversible hydrogen electrode (RHE)) and overpotential needed to drive this reaction, other anode reactions like the oxidation of small organic molecules with considerably lower overpotentials[7,8] are being considered. While these reactions (e.g., glycerol oxidation) offer a chance of costs reduction by needing lower voltages to drive the reaction it cannot be considered a sustainable source if we target implementing CO_2ER to a TW scale. Therefore, so far water is considered the most sustainable reactant in the anode process for CO_2ER.

Accordingly, CO_2ER is most commonly conducted in aqueous media. Since the hydrogen evolution reaction (HER), (see equation (3)), has a standard potential (E^0= 0 V vs RHE) close to those of CO_2ER (discussed below) and is kinetically simpler, a major challenge in the research field is the constant competition of CO_2ER reaction with the HER.

$$2\,H^+ + 2\,e^- \rightarrow H_2 \tag{3}$$

Table 1: Major reduction products during CO_2ER and the standard equilibrium potentials corresponding to their conversion from CO_2 at a pH of 6.8 (vs the reversible hydrogen electrode (RHE)).[9,10]summarizes the thermodynamic standard potentials for the reduction of CO_2 to the most common reaction products. The values near 0 V vs the reversible hydrogen electrode (RHE) suggest that the transformation of CO_2 could possibly take place at potentials similar to those used for HER. However, significantly higher overpotentials must be applied in order to overcome the kinetic limitations.

Table 1: Major reduction products during CO_2ER and the standard equilibrium potentials corresponding to their conversion from CO_2 at a pH of 6.8 (vs the reversible hydrogen electrode (RHE)).[9,10]

Reaction product	E^0 (V vs RHE)	# of e^- needed
Carbon monoxide, $CO_{(g)}$	−0.10	2
Formic acid, $HCOOH_{(aq)}$	−0.12	2
Methanol, $CH_3OH_{(aq)}$	0.03	6
Methane, $CH_{4(g)}$	0.17	8
Ethanol, $C_2H_5OH_{(aq)}$	0.09	12
Ethylene, $C_2H_{4(g)}$	0.08	12

The group of Hori set a milestone in CO_2ER by discovering the ability of copper to electrochemically reduce CO_2 into hydrocarbons with reasonable efficiencies. His work established a foundation on which the current research is set on.[11,12] By screening many different metal catalysts in CO_2ER they arrived at a classification of the transition metals[13], which can be grouped into four groups, based on their major product formed under CO_2ER conditions. There are catalysts that form preferably formate, (such as Pb, Sn, In), catalysts that don't make significant CO_2ER products and instead produce mostly hydrogen (like Fe, Ni, Pt), and metals that primarily yield carbon monoxide under CO_2ER conditions (like Ag, Au, Zn). One transition metal stands out of this classification, copper, as the only metal catalyst able to form products requiring >2 e^- transfers as well as multicarbon products in significant amounts. The CO_2ER performance of the transition metals can be explained by their binding manner/strength to CO_2 and CO. Formate producers bind CO_2 typically in a bidentate manner by the two oxygen atoms, affording the OCHO intermediate, which is then further reduced to formate ($HCOO^-$). The platinum group metals, as well as iron and titanium, are known to produce mainly H_2 under CO_2ER. This is due to the fact that these metals are able to perform the reduction of CO_2 to CO efficiently, but then are poisoned by the evolved CO, due to their high binding strength to it. While coin metals like silver and gold reduce CO_2 to CO quite efficiently, they exhibit a significantly lower binding strength towards it, with the result of CO being released from the surface as the main product (and thus prohibiting further reduction). Only copper shows the optimal binding strength to the crucial intermediate CO which explains its ability to reduce CO_2 beyond carbon monoxide, in well agreement with the Sabatier principle.[14]

A common observation in potentiostatic CO_2ER is a "deactivation" of the catalyst. This refers to a loss in CH_4/C_2H_4 selectivity in favor of HER, happening rather quickly, often over the first hour of the experiment. This phenomenon is sometimes ascribed to the deposition of trace metals in the electrolyte.[15,16] This can be circumvented by applying occasional oxidative pulses which desorb the contaminants, pre-electrolyzing the electrolyte[15], or treating the electrolyte with chelating agents, which bind possible trace metals efficiently, keeping them from adsorbing.[17]

Another challenge in CO_2ER is the low solubility of CO_2 in aqueous electrolytes (~33 mmol/l at 1 atm and 298 K).[18] This can lead quickly to mass-transport limitations and thus prevents achieving high CO_2ER rates. Gas-diffusion electrodes have been development, which feed gaseous CO_2 directly to the catalyst. This leads to increased mass-transport and allows for current densities of 100-1000 mA/cm².[19,20] While it offers a great chance to convert CO_2 at much higher rates, it brings additional complications, which is why we focus our work on the classical H-cell reactor.

1.3 Electrochemical CO_2 reduction on copper

As copper has exhibited the unique ability to reduce CO_2 beyond 2 e⁻ products (CO, HCOOH) in a significant manner, it has been widely studied in order to further improve its selectivity, stability and activity. Kuhl et al. were able to show the formation of 16 different products on a polycrystalline copper foil under potentiostatic control.[10] While the formation of valuable higher reduction products (beyond 2 e⁻) such as acetaldehyde or n-propanol is appealing, Cu shows quite poor selectivity and instead typically produces a mixture of products, which is hampering industrial implementation, due to cost intensive product separation.[21] This makes further research efforts necessary, improving the selectivity, activity and stability.

One approach to affect the selectivity is nanostructuring copper. While it does not alter the intrinsic activity of Cu[9], high surface area copper catalysts have shown to improve C_{2+} selectivity due to higher number of undercoordinated sites (lowering kinetic barriers) and increased local pH (suppressing HER and promoting C-C coupling).[22,23]

Another way to alter the product distribution is via the electrolyte. As has been stated previously the local pH has implications on the selectivity, hence the buffer capacity of the electrolyte affects the pH in the electrode vicinity. In addition to the buffer strength, alkali metal cations have shown drastic effect on the reaction pathway[24,25]. They show a promoting effect towards

C_{2+} products, while suppressing HER in following order: $Li^+ < Na^+ < K^+ < Rb^+ < Cs^+$. This order is rationalized with the decrease in effective hydrated ion size, due to the smaller hydration shells at larger cations like Cs^+. Theoretical studies have suggested that cations with a smaller hydration shell (like Cs^+) increase the local electric field in its vicinity, stabilizing the adsorbed CO_2 intermediate[26], as well as promoting C-C coupling by stabilizing C_2 intermediates.[27] One has to note that some of the cited literature report on different reference scales.

1.4 Pulsed potential electrochemical CO_2 reduction

In contrast to altering the product formation by employing different synthetic methods to create nano-/mesostructures, pulsed potential electrochemical CO_2 reduction (p-CO_2ER) offers a simple alternative for reaction control. One of the first studies on this topic was published by Nogami et al. in the early 1990s. They investigated the effect of applying a square wave potential control program which alternates the potential between two values, one more negative labeled "cathodic" potential (E_c), and one more positive, labeled "anodic" (E_a), with the respective time at each potential labeled t_c and t_a.
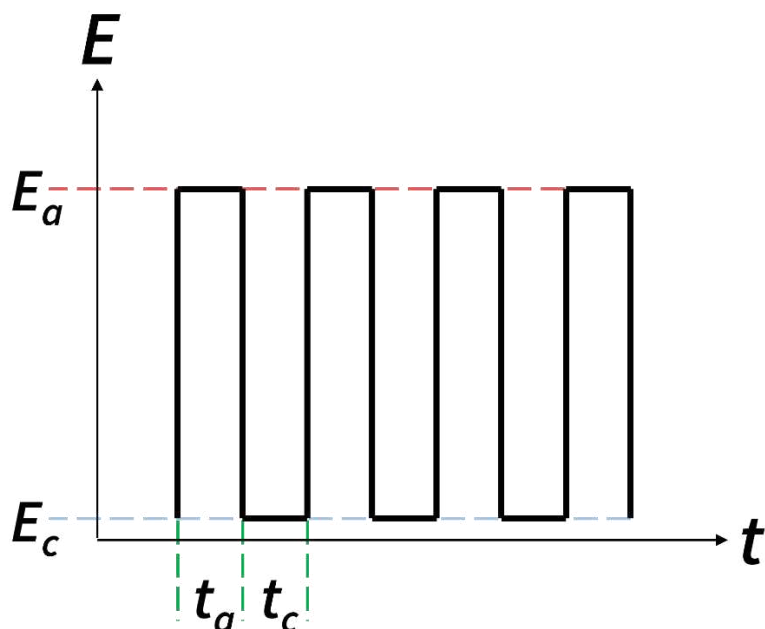
Scheme 1: Pulse potential technique applied in this study. E_c is the cathodic pulse potential, E_a the anodic pulse potential, with the corresponding time for each potential applied t_c and t_a respectively.

They applied $E_c = -1.8$ V and $E_a = 0$ V (both vs saturated calomel electrode (SCE), $t_c = t_a = 5$ s) on a copper catalyst and found significant HER suppression (up to 60 % for over 24 h) as well as enhanced C_2H_4 formation (10-15 % increase compared to potentiostatic catalysis).[28] The authors observed also the deactivation of the catalyst under potentiostatic conditions, which was ascribed based on XPS data, to the deposition of graphitic carbon resulting from the reduction of CO_2. Applying the p-CO_2ER prevented this deactivation, which they ascribed to reoxidation of the organic contaminants. Kimura et al. followed up the p-CO_2ER concept and studied the effect of shorter potential pulses on a polycrystalline Cu surface over various E_c.[29] They could show significantly higher CH_4 formation over a range of E_c at potential pulses of 5 s. They hypothesized that the suppressed H_2 and enhanced CH_4 formation is due to a lower surface coverage of hydrogen (and thus a higher coverage of carbon species) as a result of the anodic pulse.

A landmark paper was published by Bui et al.[30] in which the authors modelled the diffusion of species in p-CO_2ER on a copper electrode based on the experimental results of a previous study.[31] With their model, they predicted that under pulsing (at the conditions stated), CO_2 replenishes very fast during the anodic part of the pulse. In contrast to this, the local pH does not recover so quickly from the high alkaline state. This leads to a time domain at which there is high CO_2 concentration and high local pH, which pulsing can access, explaining the promotion of C_2H_4 formation and HER suppression.

1.5 Electrochemical CO_2 reduction on silver

Silver, a CO weak binding catalyst, is considered to produce only CO and H_2 under CO_2ER conditions, as mentioned earlier.[13,32,33] Although higher reduction products (>2 e⁻) are typically of great interest, due to their high market volume and price[34], silver has gotten great attention in recent years due to its high selectivity towards CO. It has been implemented in one of the first pilot plants for CO_2ER in Germany, operated by Siemens Energy and Evonik, where CO_2 is initially reduced to CO, which is subsequently converted into 1-Butanol and 1-Hexanol by a fermentation process using micro-organisms.[35]

While silver shows inherently good CO_2ER selectivity towards CO, it still displays a large overpotential to efficiently produce CO, due to the competition with the HER. Several groups have tried to improve this, for instance by using different surface morphologies or the employment of ionic liquids[36,37]. Ma et al. have demonstrated significantly lower overpotentials

compared to polycrystalline Ag, on an oxide derived silver catalyst (OD-Ag).[38] They created the pre-catalyst by running CVs in 0.2 M NaOH, followed by an in-situ reduction to metallic silver prior to the CO_2ER. Their so obtained catalyst showed high Faradaic efficiency (FE) for CO of 80 % and more at potentials as low as −0.6 V vs RHE. This illustrates the drastic effect on HER suppression and resulting CO promotion arguably due to higher surface area and thus higher local pH. Lu et al. have created high surface silver catalysts by dealloying an Ag-Al precursor and etching of the Al-atoms.[39] The resulting structure gave about 18 mA/cm² (based on the geometrical surface area) with 90 %FE_{CO} at an operating potential of −0.6 V vs RHE. The authors attributed this drop in overpotential due to the stabilization of the first CO_2ER intermediate (*CO_2^-) on the high index, low coordination sites. Dutta et al. investigated the CO_2ER on an Ag-foam catalyst with surprising results.[40] The catalyst was prepared by the hydrogen bubble templated electrodeposition, resulting in high surface foam-like structures. The so obtained Ag-foam catalyst showed high FE_{CO} of 90 % at −0.8 V vs RHE in a 0.5 M $KHCO_3$ electrolyte. The most intriguing result of their study was the efficient formation of CH_4 at potentials between −1.4 V to −1.6 V vs RHE. In this potential range (corresponding to −2.05 V to −2.25 V vs Ag/AgCl) they detected methane with a FE_{CH4} of 16-40 %, and a total FE for Hydrocarbons (CH_4 + C_2H_4) of 17-59 %. Such high selectivity towards hydrocarbons on silver had not been reported before. The authors explain this behavior by a significant change in *CO adsorption energy towards more copper-like values, resulting in a copper like CO_2ER behavior.

Aside from altering the surface morphology, another elegant way for selectivity enhancement has been presented. Shiratsuchi et al. were able to alter the product distribution on silver in CO_2ER by applying a potential pulsing.[41] They tested the effect of multiple pulse potentials on the product distribution and were able to observe the formation of methane, formate and even ethanol with reasonable efficiencies. The electrolysis was performed in CO_2-saturated 0.1 M $KHCO_3$ solution at 10 °C. The authors could observe CH_4 formation at potentials of E_c= −2.25 V and E_a= −0.4 V vs Ag/AgCl up to 55 % FE. At a more positive E_a (e.g., −0.125 V) the selectivity towards >2 e⁻ products decreases and CO and formate are preferentially formed. They ascribe this unique behavior to be due to an increased amount of adsorbed H* species on the surface at E_a≥ −0.4 V. Based on Raman evidence[42,43], which suggested a graphitic carbon intermediate, they postulate the higher surface coverage of H* to result in an increase towards higher reduction products, according to the following equations:

$$CO_2 + 4\,H^* \rightarrow C + H_2O \qquad\qquad (4)$$

At more negative E_a the reaction proceeds via the following equation:

$$C + 4\,H^* \rightarrow CH_4 \tag{5}$$
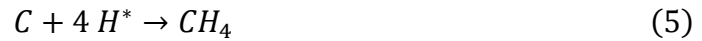
Whereas at less negative E_a the [C] intermediate reacts according to equation (6), yielding CO and formate:

$$C + HCO_3^- \rightarrow CO + HCOO^- \tag{6}$$

While these proposed reactions seemed reasonable with the information available to the authors at the time, recent research (including the one in this thesis) revealed discoveries that strongly argue against their proposed mechanism, which will be discussed in the following chapters.

These findings served as an inspiration for research presented in this thesis which is focuses on the investigation p-CO_2ER on silver catalysts. In Chapter 3 the effect of p-CO_2ER on activity and selectivity of an Ag-foil is investigated, while particular attention is paid in this chapter to an observed sample activation period. Chapter 4 focuses on the investigation of the effect of pulsing conditions such as exploring E_c and E_a across a wider range, as well as t_c and t_a modulations using time resolved product detection on a millisecond time domain. In chapter 5 in-situ Raman spectroscopy will be discussed which gives an insight about possible adsorbates during p-CO_2ER and thereby complementing our observations.

1.6 Literature

(1)   Nullis, C.; Perrin, B. 2021 one of the seven warmest years on record, WMO consolidated data shows. https://public.wmo.int/en/media/press-release/2021-one-of-seven-warmest-years-record-wmo-consolidated-data-shows.

(2)   Rahmstorf, S. Anthropogenic Climate Change: Revisiting the Facts. In *Global Warming: Looking Beyond Kyoto*; Zedillo, E., Ed.; Brookings Institution Press: Paris, 2008; pp 34–53.

(3)   Arrhenius, S. On the Influence of Carbonic Acid in the Air upon the Temperature of the Ground. *Philos. Mag. J. Sci. Ser.* **1896**, *5*, 237–276.

(4)   Masson-Delmotte, V.; Zhai, P.; Pörtner, H.-O.; Roberts, D.; Skea, J.; Shukla, P. R.; Pirani, A.; Moufouma-Okia, W.; Péan, C.; Pidcock, R.; Connors, S.; Matthews, J. B. R.; Chen, Y.; Zhou, X.; Gomis, M. I.; Lonnoy, E.; Maycock, T.; Tignor, M.; Waterfield, T. *IPCC, 2018: Summary for Policymakers*; 2018. https://doi.org/10.1017/9781009157940.001.

(5)   Ritchie, H.; Roser, M.; Rosado, P. CO2 and Greenhouse Gas Emissions https://ourworldindata.org/co2-and-other-greenhouse-gas-emissions.

(6)   IPCC. Mitigation Pathways Compatible with 1.5°C in the Context of Sustainable Development. In *IPCC reports*; Cambridge University Press, 2022; pp 93–174. https://doi.org/10.1017/9781009157940.004.

(7)   Vass, Á.; Kormányos, A.; Kószó, Z.; Endrődi, B.; Janáky, C. Anode Catalysts in CO 2 Electrolysis: Challenges and Untapped Opportunities. **2022**. https://doi.org/10.1021/acscatal.1c04978.

(8)   Vass; Endrődi, B.; Janáky, C. Coupling Electrochemical Carbon Dioxide Conversion with Value-Added Anode Processes: An Emerging Paradigm. *Curr. Opin. Electrochem.* **2021**, *25*. https://doi.org/10.1016/J.COELEC.2020.08.003.

(9)   Nitopi, S. A.; Bertheussen, E.; Scott, S. B.; Liu, X.; Engstfeld, A. K.; Horch, S.; Seger, B.; Stephens, I. E. L.; Chan, K.; Hahn, C.; Nørskov, J. K.; Jaramillo, T. F.; Chorkendorff, I. Progress and Perspectives of Electrochemical CO 2 Reduction on Copper in Aqueous Electrolyte. *Chem. Rev.* **2019**, *119* (12), 7610–7672. https://doi.org/10.1021/acs.chemrev.8b00705.

(10)	Kuhl, K. P.; Cave, E. R.; Abram, D. N.; Jaramillo, T. F. New Insights into the Electrochemical Reduction of Carbon Dioxide on Metallic Copper Surfaces. *Energy Environ. Sci.* **2012**, *5* (5), 7050. https://doi.org/10.1039/c2ee21234j.

(11)	Hori, Y. ELECTROCHEMICAL CO2 REDUCTION ON METAL ELECTRODES. In *MODERN ASPECTS OF ELECTROCHEMISTRY*; Vayenas, C., White, R., Gamboa-Aldeco, M., Eds.; 2008; pp 89–190. https://doi.org/10.1007/978-0-387-49489-0.

(12)	Hori, Y.; Murata, A.; Takahashi, R. Potential Dependencies of the Products on Electrochemical Reduction of Carbon Dioxide at a Copper Electrode. *J. Chem. Soc. Faraday Trans.* **1989**, *85* (8), 2309–2326. https://doi.org/10.1246/cl.1989.289.

(13)	Bagger, A.; Ju, W.; Varela, A. S.; Strasser, P.; Rossmeisl, J. Electrochemical CO 2 Reduction: A Classification Problem. *ChemPhysChem* **2017**, *18* (22), 3266–3273. https://doi.org/10.1002/cphc.201700736.

(14)	Sabatier, P. Hydrogénations et Déshydrogénations Par Catalyse. *Berichte der Dtsch. Chem. Gesellschaft* **1911**, *44* (3), 1984–2001. https://doi.org/10.1002/CBER.19110440303.

(15)	Hori, Y.; Konishi, H.; Futamura, T.; Murata, A.; Koga, O.; Sakurai, H.; Oguma, K. "Deactivation of Copper Electrode" in Electrochemical Reduction of CO2. *Electrochim. Acta* **2005**, *50* (27), 5354–5369. https://doi.org/10.1016/j.electacta.2005.03.015.

(16)	Chen, Y.; Li, C. W.; Kanan, M. W. Aqueous CO2 Reduction at Very Low Overpotential on Oxide-Derived Au Nanoparticles. *J. Am. Chem. Soc.* **2012**, *134* (49), 19969–19972. https://doi.org/10.1021/ja309317u.

(17)	Wuttig, A.; Surendranath, Y. Impurity Ion Complexation Enhances Carbon Dioxide Reduction Catalysis. *ACS Catal.* **2015**, *5* (7), 4479–4484. https://doi.org/10.1021/acscatal.5b00808.

(18)	Janáky, C.; Hursán, D.; Endrödi, B.; Chanmanee, W.; Roy, D.; Liu, D.; De Tacconi, N. R.; Dennis, B. H.; Rajeshwar, K. Electro- and Photoreduction of Carbon Dioxide: The Twain Shall Meet at Copper Oxide/Copper Interfaces. *ACS Energy Lett.* **2016**, *1* (2), 332–338. https://doi.org/10.1021/acsenergylett.6b00078.

(19) Rabiee, H.; Ge, L.; Zhang, X.; Hu, S.; Li, M.; Yuan, Z. Gas Diffusion Electrodes (GDEs) for Electrochemical Reduction of Carbon Dioxide, Carbon Monoxide, and Dinitrogen to Value-Added Products: A Review. *Energy Environ. Sci.* **2021**, *14* (4), 1959–2008. https://doi.org/10.1039/D0EE03756G.

(20) Weekes, D. M.; Salvatore, D. A.; Reyes, A.; Huang, A.; Berlinguette, C. P. Electrolytic CO 2 Reduction in a Flow Cell. *Acc. Chem. Res.* **2018**, *51* (4), 910–918. https://doi.org/10.1021/acs.accounts.8b00010.

(21) Greenblatt, J. B.; Miller, D. J.; Ager, J. W.; Houle, F. A.; Sharp, I. D. The Technical and Energetic Challenges of Separating (Photo)Electrochemical Carbon Dioxide Reduction Products. **2018**. https://doi.org/10.1016/j.joule.2018.01.014.

(22) Lum, Y.; Binbin, Y.; Lobaccaro, P.; Bell, A. T.; Ager, J. W. Optimizing C−C Coupling on Oxide-Derived Copper Catalysts for Electrochemical CO2 Reduction. *J. Phys. Chem. C* **2017**, *121* (13–14), 14191–14203. https://doi.org/10.1021/acs.jpcc.7b03673.

(23) Raciti, D.; Mao, M.; Wang, C. Mass Transport Modelling for the Electroreduction of CO 2 on Cu Nanowires. *Nanotechnology* **2018**, *29* (4), 044001. https://doi.org/10.1088/1361-6528/aa9bd7.

(24) Resasco, J.; Chen, L. D.; Clark, E.; Tsai, C.; Hahn, C.; Jaramillo, T. F.; Chan, K.; Bell, A. T. Promoter Effects of Alkali Metal Cations on the Electrochemical Reduction of Carbon Dioxide. *J. Am. Chem. Soc.* **2017**, *139* (32), 11277–11287. https://doi.org/10.1021/jacs.7b06765.

(25) Ringe, S.; Clark, E. L.; Resasco, J.; Walton, A.; Seger, B.; Bell, A. T.; Chan, K. Understanding Cation Effects in Electrochemical CO 2 Reduction. *Energy Environ. Sci.* **2019**, *12* (10), 3001–3014. https://doi.org/10.1039/C9EE01341E.

(26) Chen, L. D.; Urushihara, M.; Chan, K.; Nørskov, J. K. Electric Field Effects in Electrochemical CO 2 Reduction. *ACS Catal.* **2016**, *6* (10), 7133–7139. https://doi.org/10.1021/acscatal.6b02299.

(27) Montoya, J. H.; Shi, C.; Chan, K.; Nørskov, J. K. Theoretical Insights into a CO Dimerization Mechanism in CO2 Electroreduction. *J. Phys. Chem. Lett.* **2015**, *6* (11), 2032–2037. https://doi.org/10.1021/acs.jpclett.5b00722.

(28)   Shiratsuchi, R.; Aikoh, Y.; Nogami, G. Pulsed Electroreduction of CO2 on Copper Electrodes. *J. Electrochem. Soc.* **1993**, *140* (12), 3479–3481. https://doi.org/10.1149/1.2221113.

(29)   Kimura, K. W.; Fritz, K. E.; Kim, J.; Suntivich, J.; Abruña, H. D.; Hanrath, T. Controlled Selectivity of CO 2 Reduction on Copper by Pulsing the Electrochemical Potential. *ChemSusChem* **2018**, *11* (11), 1781–1786. https://doi.org/10.1002/cssc.201800318.

(30)   Bui, J. C.; Kim, C.; Weber, A. Z.; Bell, A. T. Dynamic Boundary Layer Simulation of Pulsed CO 2 Electrolysis on a Copper Catalyst. *ACS Energy Lett.* **2021**, 1181–1188. https://doi.org/10.1021/acsenergylett.1c00364.

(31)   Kim, C.; Weng, L.-C.; Bell, A. T. Impact of Pulsed Electrochemical Reduction of CO 2 on the Formation of C 2+ Products over Cu. *ACS Catal.* **2020**, *10* (21), 12403–12413. https://doi.org/10.1021/acscatal.0c02915.

(32)   Hatsukade, T.; Kuhl, K. P.; Cave, E. R.; Abram, D. N.; Jaramillo, T. F. Insights into the Electrocatalytic Reduction of CO2 on Metallic Silver Surfaces. *Phys. Chem. Chem. Phys.* **2014**, *16* (27), 13814–13819. https://doi.org/10.1039/C4CP00692E.

(33)   Feaster, J. T.; Shi, C.; Cave, E. R.; Hatsukade, T.; Abram, D. N.; Kuhl, K. P.; Hahn, C.; Nørskov, J. K.; Jaramillo, T. F. Understanding Selectivity for the Electrochemical Reduction of Carbon Dioxide to Formic Acid and Carbon Monoxide on Metal Electrodes. *ACS Catal.* **2017**, *7* (7), 4822–4827. https://doi.org/10.1021/acscatal.7b00687.

(34)   De Luna, P.; Hahn, C.; Higgins, D.; Jaffer, S. A.; Jaramillo, T. F.; Sargent, E. H. What Would It Take for Renewably Powered Electrosynthesis to Displace Petrochemical Processes? *Science (80-.).* **2019**, *364* (6438), eaav3506. https://doi.org/10.1126/science.aav3506.

(35)   Haas, T.; Krause, R.; Weber, R.; Demler, M.; Schmid, G. Technical Photosynthesis Involving CO2electrolysis and Fermentation. *Nat. Catal.* **2018**, *1* (1), 32–39. https://doi.org/10.1038/s41929-017-0005-1.

(36)   Feaster, J. T.; Jongerius, A. L.; Liu, X.; Urushihara, M.; Nitopi, S. A.; Hahn, C.; Chan, K.; Nørskov, J. K.; Jaramillo, T. F. Understanding the Influence of [EMIM]Cl on the Suppression of the Hydrogen Evolution Reaction on Transition Metal Electrodes. *Langmuir* **2017**, *33* (37), 9464–9471. https://doi.org/10.1021/acs.langmuir.7b01170.

(37)   Rosen, B. A.; Salehi-Khojin, A.; Thorson, M. R.; Zhu, W.; Whipple, D. T.; Kenis, P. J. A.; Masel, R. I. Ionic Liquid-Mediated Selective Conversion of CO2 to CO at Low Overpotentials. *Science (80-.).* **2011**, *334* (6056), 643–644. https://doi.org/10.1126/SCIENCE.1209786.

(38)   Ma, M.; Trześniewski, B. J.; Xie, J.; Smith, W. A. Selective and Efficient Reduction of Carbon Dioxide to Carbon Monoxide on Oxide-Derived Nanostructured Silver Electrocatalysts. *Angew. Chemie Int. Ed.* **2016**, *55* (33), 9748–9752. https://doi.org/10.1002/anie.201604654.

(39)   Lu, Q.; Rosen, J.; Zhou, Y.; Hutchings, G. S.; Kimmel, Y. C.; Chen, J. G.; Jiao, F. A Selective and Efficient Electrocatalyst for Carbon Dioxide Reduction. *Nat. Commun.* **2014**, *5*, 1–6. https://doi.org/10.1038/ncomms4242.

(40)   Dutta, A.; Morstein, C. E.; Rahaman, M.; Cedeño López, A.; Broekmann, P. Beyond Copper in CO 2 Electrolysis: Effective Hydrocarbon Production on Silver-Nanofoam Catalysts. *ACS Catal.* **2018**, *8* (9), 8357–8368. https://doi.org/10.1021/acscatal.8b01738.

(41)   Shiratsuchi, R.; Nogami, G. Pulsed Electroreduction of CO2 on Silver Electrodes. *J. Electrochem. Soc.* **1996**, *143* (2), 582–586. https://doi.org/10.1149/1.1836484.

(42)   Mahoney, M. R.; Howard, M. W.; Cooney, R. P. Carbon Dioxide Conversion to Hydrocarbons at Silver Electrode. *Chem. Phys. Lett.* **1980**, *71* (1), 59–63. https://doi.org/https://doi.org/10.1016/0009-2614(80)85289-4.

(43)   Cooney, R. P.; Mahoney, M. R.; Howard, M. W. Intense Raman Spectra of Surface Carbon and Hydrocarbons on Silver Electrodes. *Chem. Phys. Lett.* **1980**, *76* (3), 2–6. https://doi.org/https://doi.org/10.1016/0009-2614(80)80645-2.

2 Materials and Methods

2.1 Materials

High purity silver foils (0.5 mm thick, AlfaAesar Premion®, 99.9985 wt%) were mechanically polished with silicon carbide sandpaper (Würth, 1200 grain size) and alumina polishing suspension (Buehler MicroPolish™, particle sizes of 0.3 μm) to a mirrorlike finish. The samples were sonicated in iPrOH, dried in air and subsequently covered with Teflon tape to expose a fixed geometrical area. The catalyst for the Differential electrochemical mass spectrometry (DEMS) experiments was a 600 nm layer of silver sputtered onto porous, gas permeable membrane (ethylene-tetrafluoroethylene copolymer, Scimat 200/40/60).

All experiments were conducted in CO_2-saturated 0.1 M $KHCO_3$ made from dissolving $KHCO_3$ (Merck, EMSURE® ACS) in ultra-pure water (18.2 MΩ·cm) and saturating with CO_2 (Linde, 4.8N) for 30 minutes prior to the experiment.

2.2 Electrochemistry

We used a SP-200 potentiostatic (Bio-Logic Science Instruments) with the accompanying EC-Lab software to conduct our electrochemical measurements. The ohmic drop was not compensated unless stated otherwise due to changes in selectivity upon compensation. This could be due to the delay of the potentiostat in calculating and applying the corrected pulse potential. A custom-made glass cell that consisted of two compartments, separated by a Nafion® 115 membrane was used. To avoid contamination by other trace metals, the cell was exclusively used for silver catalysts and cleaned thoroughly by soaking in aqua regia for +12 h and subsequent sonication in ultrapure water (18.2 MΩ·cm) until all acid was washed out. The Nafion® membrane was stored in 2 M H_2SO_4 between experiments to assure full protonation of the sulfonic acid groups and wash out trace metal contaminations. A platinum mesh with high surface area was employed as a counter electrode. An Ag/AgCl reference electrode (3 M KCl, PalmSens) was used, and all reported potentials are referred to it, unless otherwise stated.

For all pulse experiments a prior linear sweep voltammetry (LSV) was conducted ranging from open circuit potential (OCP) to −1.8 V with a scan rate of 50 mV/s, to ensure full reduction of the silver catalyst.

For the pulse program the potential was stepped between the E_c and E_a according to Scheme 2. E_c is the "cathodic" pulse potential, referring to the more negative potential applied, while E_a stands for the "anodic" pulse potential, which is more anodic than the E_c hence the name.
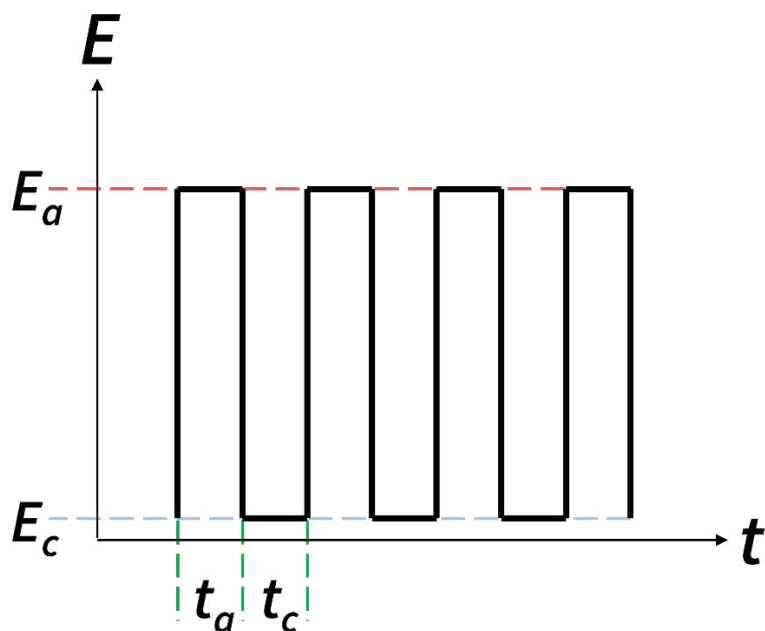
Scheme 2: Pulse potential technique applied in this study. E_c is the cathodic pulse potential, E_a the anodic pulse potential, with the corresponding time for each potential applied t_c and t_a respectively.

2.3 Gas Chromatography

For accurate product detection of gaseous products, we employed a gas chromatographer Thermo TRACE 1310 with a He carrier gas flow. The chromatographer has two columns for product separation: a HayeSepS (1 mm ID, Restek) and a molecular sieve MS5a column (1 mm ID, Restek). It uses two detectors: one Pulse Discharge Detector (PDD) and one Flame Ionization Detector (FID). The electrochemical cell was connected to the GC, by feeding the gases from the headspace of the cathode compartment via a heated transfer line (60 °C) into the chromatographer. The cell was fed with CO_2 at a flow rate of 20 mL/min.

The partial current for a gaseous product *A* were calculated by the following equation:

$$I_A(mA) = F * z_A * c_A * Flowrate * 0.06 \tag{7}$$

where F is the faraday constant (96485 C/mol), z_A is the number of electrons required to produce 1 molecule of product A, c_A is the concentration of the product as determined by the gas chromatographer (in mol/mL) and the *Flowrate* corresponds to the CO_2 feed into the cell at 20 mL/min.

A common figure of merit in CO_2ER is the faradaic efficiency (FE). Here it describes the efficacy with which current (electrons) is turned into a certain product A.

$$FE_A\ (\%) = \frac{i_A}{i_{total}} \times 100 \tag{8}$$

While i_{total} refers to the total current density during an experiment, which can be obtained from the potentiostat, i_A is the current density that has been used to create product A, and can to be determined by equation (7).

While in the field of CO_2ER, often only the FE is reported, this lacks the information of actual product formation rates. The FE of a catalytic product can change drastically, just due to the decrease of another product, while its formation rate stays the same. FE measurements are also affected by accurate determination of i_{total} , under steady state potentiostatic electrolysis measurements i_{total} vary little over time and is easily extracted from the chronoamperometry data. In the case of pulse electrolysis, the constant potential alternation between Ec and Ea leads to convoluted current profiles of faradaic and non-faradaic processes such as double layer charging processes and adsorption of species. For these reasons, in this thesis the CO_2ER activity results are presented and discussed in terms of the partial current densities i_A for each product.

2.4 Scanning Electron Microscopy and Electron Backscatter Diffraction

Top view scanning electron microscopy (SEM) images and energy dispersive X-ray spectroscopy (EDX) spectra were collected on a Zeiss LEO 1530 Gemini SEM system with a ThermoFisher UltraDry EDX detector. The SEM images were acquired at 3 kV using the secondary electron detector. All electron backscatter diffraction (EBSD) analyses were performed on a Zeiss UltraPlus scanning electron microscope equipped with an Oxford Instruments NordlysNano EBSD camera at 15 keV and about 1 nA.

2.5 Differential Electrochemical Mass Spectrometry

The analytical unit consisted of a PC-controlled quadrupole mass spectrometer (QMG 220 M1, PrismaPlus 1–100 amu) connected via a variable leak valve with a pre-vacuum chamber pumped by a rotary vane pump. The inlet system between the electrochemical cell and the pre-vacuum chamber was of a stainless-steel frit which served as a mechanical support for the porous gas permeable membrane. The working electrode was prepared by sputtering Ag (600 nm) onto the membrane. The area exposed to the electrolyte is determined by an O-ring with a 9 mm inner diameter. The electrochemical cell was fixed on top of the membrane and contained a conventional three electrode arrangement (see Figure 2). An Ag/AgCl (3 M KCl, World Precision Instruments, Dri-Ref 2) and a platinum mesh served as reference and counter electrode, respectively. The electrical contact to the working electrode was made via the Ag layer outside of the electrolyte. The time response of product detection is about 1 s-3 s.
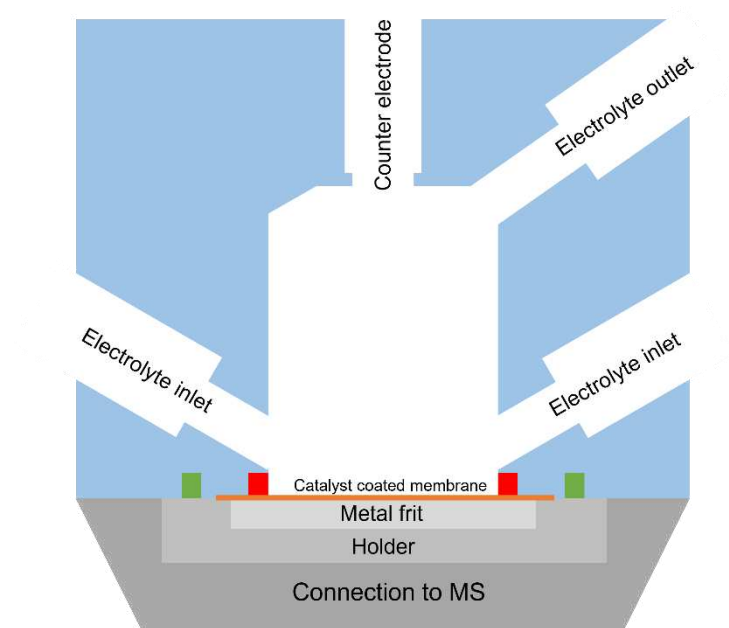
Figure 2: Sketch of the electrochemical DEMS cell used. The orange rectangle represents the catalyst coated membrane, the red and green squares represent individual O-rings of different sizes.

2.6 In-situ Raman spectroscopy

Raman spectra were acquired by a Renishaw in Via confocal Raman spectrometer. A 633 nm laser was used as the scattering source with a power of 1.3 mW; the laser was focused (by a cylindrical lens) to a streamline on the Ag surface resulting on a spot of 100 μm long and 10 μm wide. A water immersive objective was used with 40× magnification ratio and N.A. 0.8.

A modified version of the cell reported by D'Amario et al. [1] was used, equipped with electrolyte flow, which allowed for measurements at highly cathodic potentials. The sample was wrapped in Teflon tape and a hole of 2 mm diameter was made, resulting in an exposed area of 0.0314 cm². The sample was subjected to a roughening treatment in order to generate a plasmonic surface for surface-enhanced Raman probing. This was done by running 26 consecutive oxidation/reduction cycles on a polished silver foil with a 1.5 s step at 0.2 V vs. Ag/AgCl per each cycle, in a 0.1 M KCl according to Bohra et al.[2]
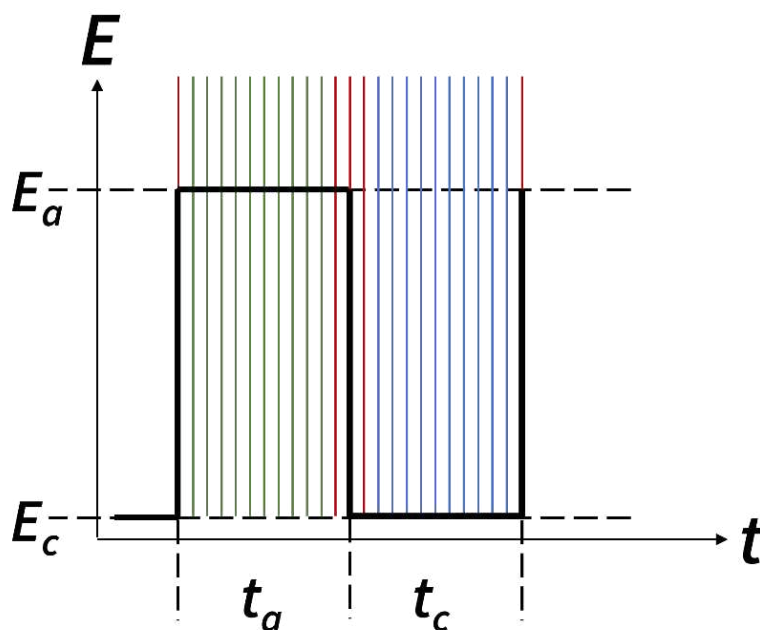
Scheme 3: Raman spectrum acquisition over one pulse cycle. Solid green lines represent the acquisition point of the spectra used for analysis during anodic pulse, the blue solid lines correspond to the ones during the cathodic pulse, while the ones in red are omitted from the analysis.

During the pulse experiments Raman spectra were recorded every 400 ms (200 ms data acquisition + 200 ms deadtime). For a total pulse cycle of 10 s ($t_c + t_a$) we recorded 25 spectra

(cf. Scheme 3), and a total of 6000 spectra over the 40-minute pulse experiment. These 6000 spectra were then split into three segments for data processing. Of the 25 spectra per pulse cycle, only 20 were used for data analysis (blue lines in Scheme 3), so one spectrum in the beginning and at the end of each potential pulse was cut off, as well as the one spectrum acquired during the potential switching (represented by red lines in Scheme 3).

2.7 Literature

(1)   D'Amario, L.; Stella, M. B.; Edvinsson, T.; Persico, M.; Messinger, J.; Dau, H. Towards Time Resolved Characterization of Electrochemical Reactions : Electrochemically-Induced Raman Spectroscopy. *ChemRxiv* **2022**.

(2)   Bohra, D.; Ledezma-Yanez, I.; Li, G.; de Jong, W.; Pidko, E. A.; Smith, W. A. Lateral Adsorbate Interactions Inhibit HCOO − While Promoting CO Selectivity for CO 2 Electrocatalysis on Silver. *Angew. Chemie* **2019**, *131* (5), 1359–1363. https://doi.org/https://doi.org/10.1002/anie.201811667.

3 Pulsed potential effect on the CO_2ER selectivity on silver foil catalyst

3.1 Studying the activation process

This thesis is focused on studying the effect of pulsed potential on the product distribution in the electrochemical CO_2 reduction reaction (CO_2ER). As mentioned in previous chapters most work using this technique has been focusing on copper and copper−containing catalysts. We investigated mechanically polished silver foil catalysts without further pretreatment, aiming to alter the product formation without synthesizing a complex catalyst prior. The experiments were conducted in a CO_2-saturated 0.1 M $KHCO_3$ solution (as stated in section 2.1).
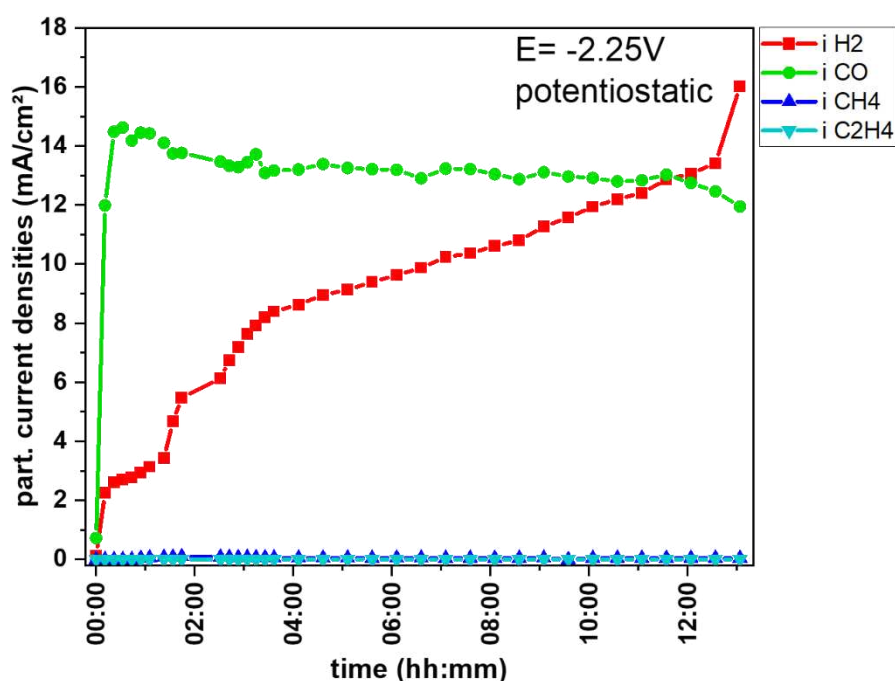
Figure 3: CO_2ER performance of an Ag−foil under potentiostatic control at −2.25 V.

Under potentiostatic conditions, at similar potentials as we apply for the pulsed electrolysis, carbon monoxide and hydrogen are detected. This is in line with previous reports[1,2] (also see CO_2ER on silver in the introduction chapter) and based on the fact that silver shows a weak binding strength[3] towards *CO and is thus not able to further reduce it to more electron

products (with significant selectivity). Figure 3 shows the partial current density of gaseous products formed from CO_2ER on a silver foil catalyst at −2.25 V. We observe only CO as CO_2ER product, along with a continuous rise in HER over the time of the experiment. This has been observed in several studies and is ascribed to a poisoning of the catalyst surface by graphitic carbon, or deposition of trace metals from the electrolyte.[4,5] We note that no hydrocarbon formation was detected.

We have investigated the effect of various potentials and pulse times using a square-wave potential, where one potential is capable of producing significant cathodic current (E_c) and one resulting in near-zero current (E_a). The time domain of each potential pulse is referred to as t_c and t_a respectively (cf. Scheme 2: Pulse potential technique applied in this study. E_c is the cathodic pulse potential, E_a the anodic pulse potential, with the corresponding time for each potential applied t_c and t_a respectively.). It has been suggested that a high overpotential is needed in order to compete with the fast CO desorption on a weak binding catalyst like silver[3,6], hence the E_c is set accordingly. The low current domain gives time for the mass-transport of CO_2 and protons to the electrode surface, while avoiding silver oxidation. From simply pulsing the applied potential (essentially on and off with 5 s steps), the selectivity drastically changed as compared to constant potential. Furthermore, the selectivity evolved gradually over the course of several hours under pulsed conditions. This suggests there are two important timescales which influence selectivity under these conditions, the ~second timescale of electrochemical pulsing, and ~hours timescale during continuous operation. The central aim of this present work is to disentangle and understand in detail the different processes resulting from pulsing which are contributing to these observations of dynamic selectivity.

The effects of variation of the pulsing timescales and potentials will be presented in a later section. But first we sought to understand the origin of the slow change which occurs over several hours. In an electrochemical system, there are a number of things which could be changing on this timescale, including the formation of a concentration gradient (of ions and/or pH), the deposition of trace contaminants such as Cu or Fe onto the cathode, a slow formation/accumulation of adsorbed species modifying the electrode surface or structural transformation of the electrode surface material.

We set E_c= −2.25 V and E_a= −0.6 V, with 5 s for each potential (denoted from now on as −2.25 V/−0.6 V, 5 s/5 s), resulting in the formation of methane with significant selectivity, while the competing HER was being suppressed. Figure 4 shows the detected gaseous products over

an 8 h experiment. H_2 appears to be suppressed from the beginning, whereas carbon monoxide decreases in the first 3 h of the experiment. The formation of CH_4 increases over the first 4-5 h of catalysis and reaches a plateau at a current density of around 4 mA/cm². These findings sparked our interest, for two reasons: I) hydrocarbon formation on silver is a rare observation and II) pulsing on copper is known to affect its selectivity instantaneously.[7,8] (compare section 1.4)
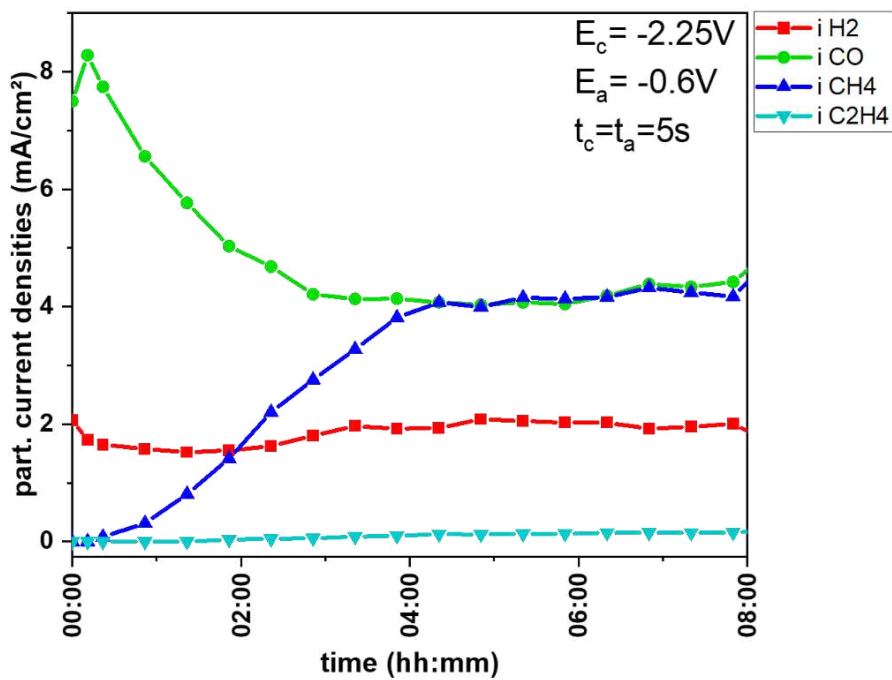
Figure 4: Pulsed potential CO₂ER performance of a silver foil catalyst. Conditions applied were: E_c= −2.25 V, E_a= −0.6 V, t_c & t_a= 5 s.
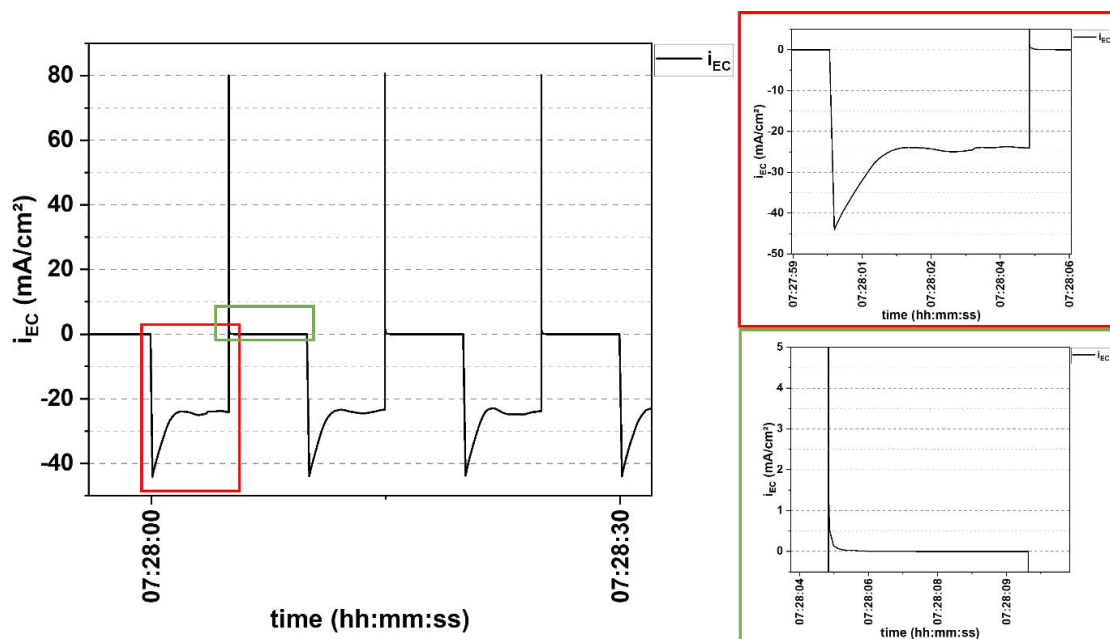
Figure 5: Current response to potentials pulses (−2.25 V/−0.6 V, 5 s/5 s). Red and green boxes show a zoom in on the cathodic and anodic part of the pulse, respectively.

Assessing the current response of the system can already give us an information about possible processes. Figure 5 depicts the current signal for one potential pulse as obtained from the potentiostat. We can see during the cathodic pulse (red box) a region of higher current density during the first 1-1.5 s of the pulse, while an almost constant current regime for the remainder of the pulse. We don't observe a pronounced transient of the double layer charging during the cathodic pulse (as we do for the anodic pulse), either because of insufficient data collection or because it is convoluted with the high current density regime. For the anodic pulse (green box) we see initial a large current transient, representing the double layer charging, followed by little to no reductive current flowing. Hence, we it is likely that all the product formation for a pulsed potential experiment takes place during the cathodic pulse. During symmetrical pulsing (e.g., 5 s/5 s) significant cathodic currents are only flowing during half the time, yet the CO_2 gas bubbling through the cell and into the GC is continuous. Therefore, relating the measured currents to the measured product formation rates requires application of a correction factor. We choose to do this by multiplying the GC-measured product formation rates by two, which makes them relevant to the observed currents during the cathodic pulse steps.

To examine the possibility of surface structure change, we carefully examined the surface before and after by SEM.
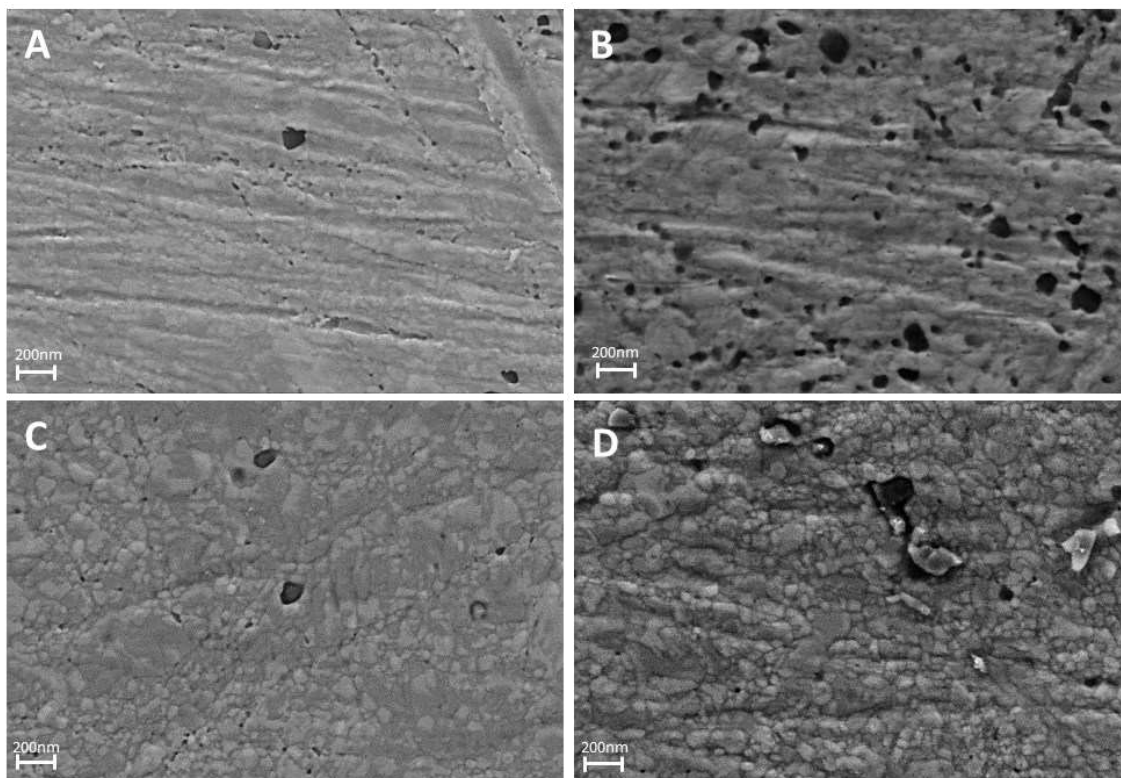
Figure 6: SEM images of silver foil samples before and after catalysis. A before, B after 7 h of potentiostatic catalysis at −2.1 V, C after 3 h of pulsed electrolysis, D after 17 h of pulsed electrolysis at E_c= −2.15 V, E_a= −0.5 V, t_c= t_a =5 s.

Figure 6 A depicts the sample surface as received after mechanical polishing, prior to any electrocatalysis, whereas Figure 6 B shows the sample surface after 7 h of potentiostatic catalysis at −2.1 V, which did not form any methane (see Figure 3). No significant changes in the surface morphology over the 7 h experiment can be detected, as the streaks from polishing persist. There might be a slight increase in pore size, yet we find no significant formation of grains. As can be seen in Figure 6 C and D, the surface does undergo some changes during the pulsed experiment. The formation of grains can be detected, which become more pronounced with increasing electrolysis time.

Electron backscatter diffraction (EBSD) was employed to gain further information about the microstructure. EBSD provides information on diffraction planes which when mapped in 2D, reveals orientation trends for surface grains. Figure 7 A & B show EBSD maps of a sample before and after pulsed catalysis respectively. Evaluation of these data suggests an increase of the average grain size (from 1.7 µm prior to catalysis to 2.7 µm after the electrolysis). However, the areas investigated by means of EBSD were rather small; thus, the statistics are limited. Thus, it

was not possible to relate the change in selectivity between the state prior to catalysis and the one after the electrolysis to changed crystal facets at the surface; this would be one line of explanation, since different activities and selectivity have already been demonstrated for Ag(100), Ag(110) and Ag(111) under CO_2ER conditions[9]. Identical location EBSD (IL-EBSD) could allow for a more robust statement. Hence our results suggest that reorientation of facets does happen and can contribute to the change in selectivity observed. As a control experiment, we collected an EBSD map for a sample before and after potentiostatic catalysis (at −2.1 V for 7 h) shown in Figure 7 C & D, and did not observe a growth in grain size, nor a significant change in orientation.
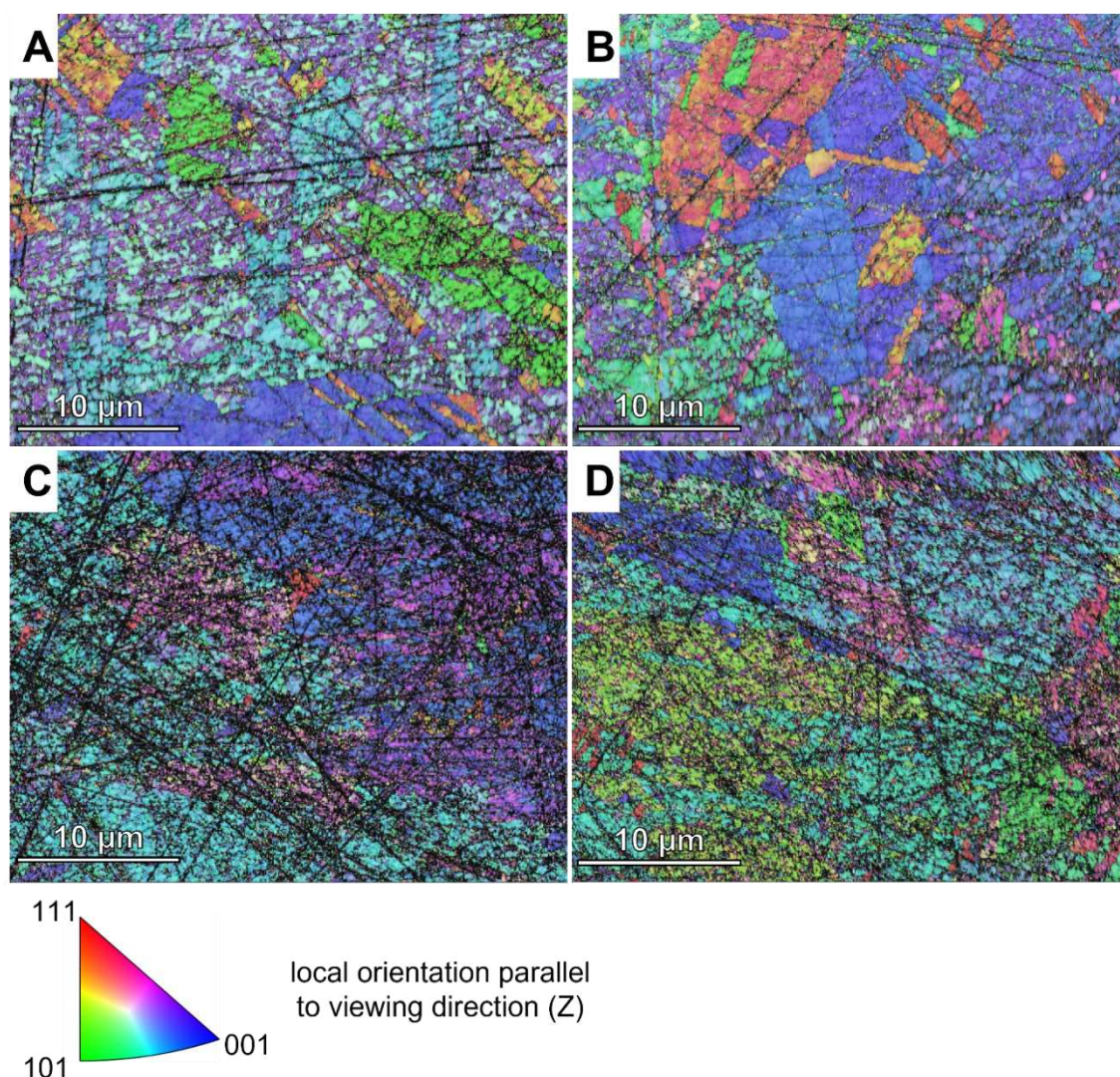
Figure 7: EBSD map of a sample before (A) and after (B) pulsed potential electrolysis at (−2.1 V/−0.5 V, 5 s/5 s) for 17 h, while C) and D) show before and after potentiostatic catalysis (-2.1 V, 7 h) respectively.

The combination of SEM and EBSD data suggested that the electrochemical pulsing resulted in a significantly different catalyst surface structure, which could lead to the hypothesis that the role of the pulsing was simply to modify the surface structure into one which becomes selective to CH_4 formation. Putting the hypothesis to test we conducted a control experiment, where we ran a silver foil catalyst under pulsed control (−2.25 V/−0.6 V, 5 s/5 s) for about 7 h and 45 min and then switched to potentiostatic control (cf. Figure 8; transition is indicated by the black vertical line). Figure 8 A depicts the partial current densities with a correction factor for the dilution (vide supra; Figure 5 and discussion), while Figure 8 B shows the data without accounting for the dilution.

The formation of CH_4 grows over the first 5 h of the experiment while CO and H_2 are significantly suppressed early on. We can observe the preservation of CH_4 evolution to some extent (Figure 8 B), though when looking at the dilution corrected graph (Figure 8 A), we can see a significant loss in methane activity. The CO partial current density decreases slightly, while the H_2 formation grows steeply at the expense of methane formation. Hence the methane formation cannot originate solely from the surface restructuring, but pulsing has to have some other contributing effect enabling its formation with the shown selectivity.
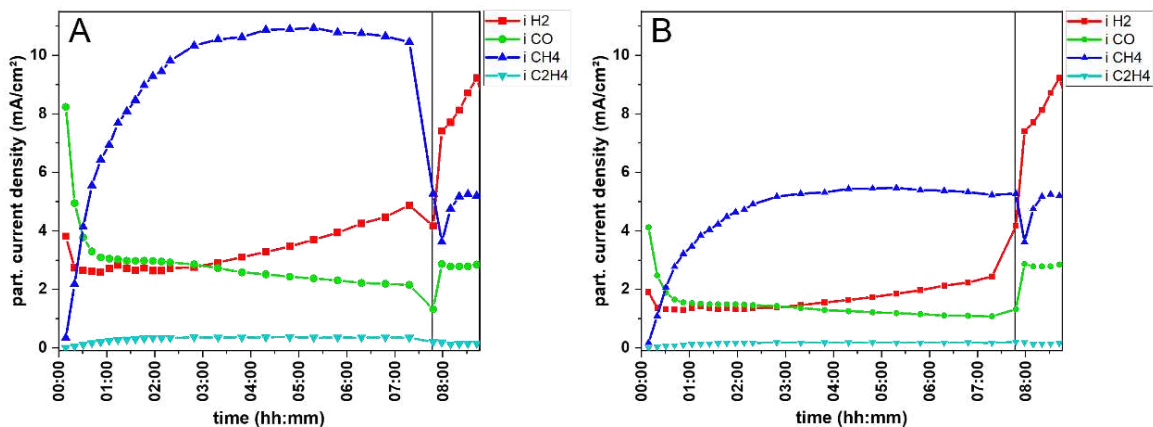
Figure 8: CO_2ER results of an Ag-foil under pulsed electrolysis at −2.25 V/−0.6 V, 5 s/5 s followed by potentiostatic catalysis at −2.25 V. The vertical line indicates the switch from pulsed to potentiostatic control. A shows results with correction factor applied, B is without.

Further testing the hypothesis of surface morphology governing the selectivity, Figure 9 shows the results of a pulse experiment in which the catalyst was activated and then placed in a cell with fresh electrolyte. Here we can observe the initial activation of the sample under pulsed potential (though slower than usual), where HER is significantly suppressed and CH_4 grows at

the expense of CO. When removing the bias on the sample and placing it in a cell with fresh electrolyte, we see the hydrocarbon formation drops down to near zero, the CO formation rate goes back up, and the process of "activation" over several hours of continued pulsing was required to recover the selectivity toward CH_4. Interestingly this re-activation seems to proceed more rapidly, and the sample reaches higher methane rates than in the first activation.
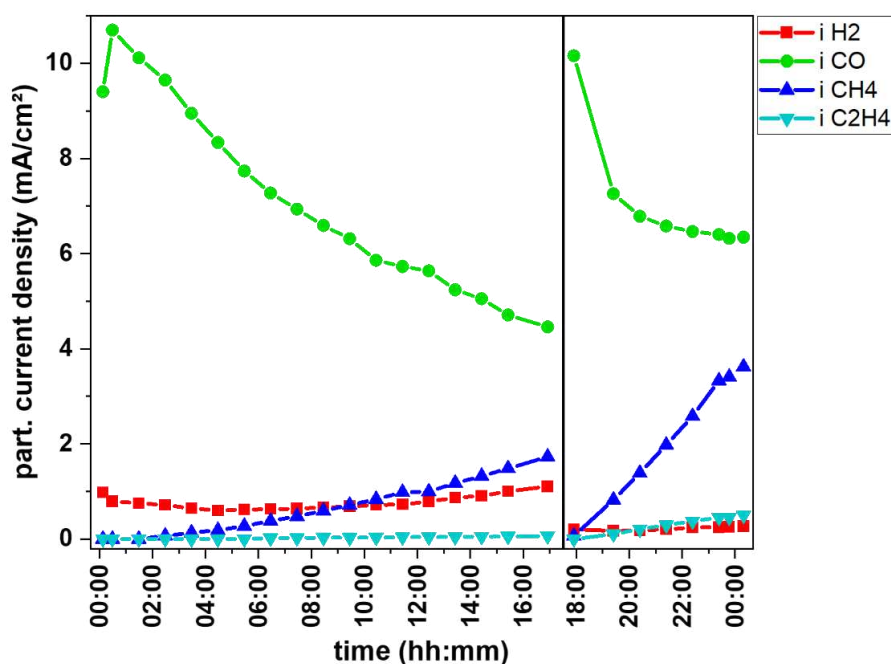
Figure 9: CO_2ER performance of a sample pulsed at −2.25 V/−0.5 V, 5 s/5 s initially activated and then placed in a cell with fresh electrolyte and pulsed for another 5 h. Black line indicates exchange.

As a slow change in selectivity can also hint towards deposition of trace metals from the electrolyte, which can accumulate during the extended experiments and alter the catalyst surface and selectivity. In order to rule out this possibility of trace metal contaminations on our samples, we not only used high purity chemicals, but also ran an experiment in an electrolyte solution, which was previously treated with a chelating agent (Chelex® 100). This chelating agent has a high affinity towards transition metals and would bind any trace metals in the electrolyte.[5] Figure 10 depicts the results obtained from this experiment, which show similar behavior as seen in previous experiments. Although the trends are in good agreement to preceding experiments, we note an unusually high i(CO). This is of unknown origin and has appeared in several experiment since, despite considerable efforts. We tried thorough cell cleaning, exchanging cell parts and membrane for fresh ones and applied different surface and sample treatments unfortunately without success. To this day we cannot explain this behavior, since it does not

stem from contaminations. We applied an annealing treatment at 500 °C, aiming to relieve possible strain within the sample, yet catalysts after the treatment continued to show elevated CO signals.
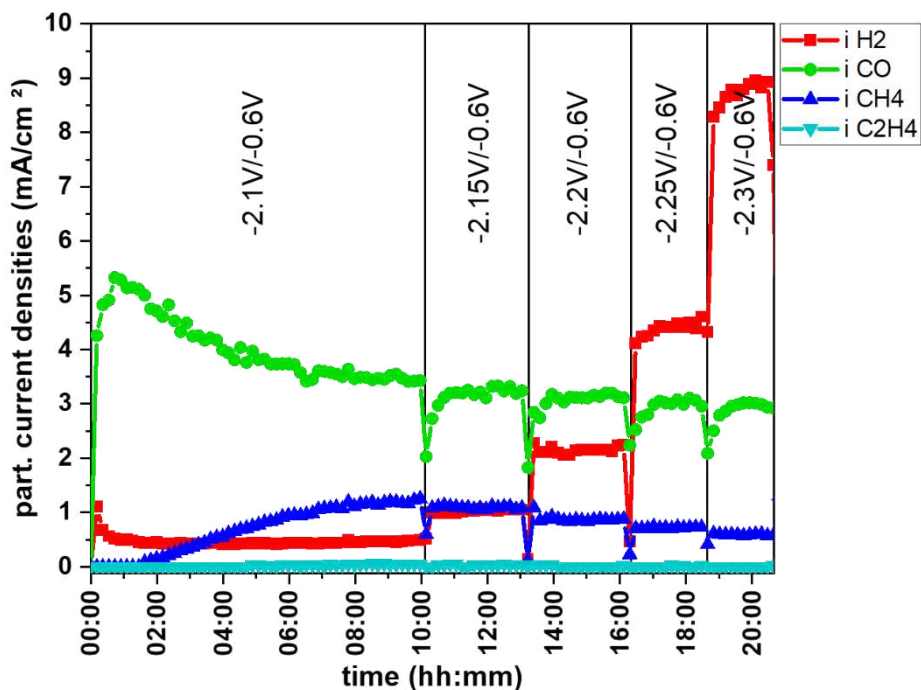
Figure 10: Ag-foil sample in a Chelex® treated electrolyte under pulse potential control with varying E_c.

Slow changes in behavior may suggest changes to the electrolyte, possibly including accumulation of species resulting from catalysis, build-up of concentration gradients of electrolyte species (ions), or pH gradients, for instance. We therefore performed a control experiment, in which we aimed to investigate a possible build-up of ion or pH gradients across the membrane, which could affect the selectivity. We employ a cation exchange membrane with the expectation that it selectively transports H^+, balancing the anode and cathode reactions. If K^+ was instead contributing as current-carrying ion through the membrane, the cell would eventually develop different pHs and ion concentrations in the anode and cathode chambers. To examine whether such a phenomenon might be influencing our observed selectivity trends, a control experiment was performed which simply omitted the membrane, thus operating as a single compartment cell. The results are plotted in Figure 11 and show similar results to previous experiment. We observe the slow growth in CH_4 formation over 6 h, with a simultaneous decrease in CO rate. H_2 grows along with the CH_4 signal up to over 4 mA/cm² after 15 h. This

30

unusually high HER can be explained in parts by unintentional sample flooding, during which electrolyte trickles underneath the sample wrapping and thus exposing a large part of the electrode to (quickly CO_2 depleted) electrolyte. Since we observe a similar timescale for activation for the formation of methane when measuring in absence of a membrane, we can conclude that a pH or potassium gradient between the anolyte and catholyte is not likely to be forming and inducing the observed activation behavior. Nevertheless, this does not exclude the possibility of change in the local pH or the cation concentration in the diffusion layer on the timescales of potential pulsing.
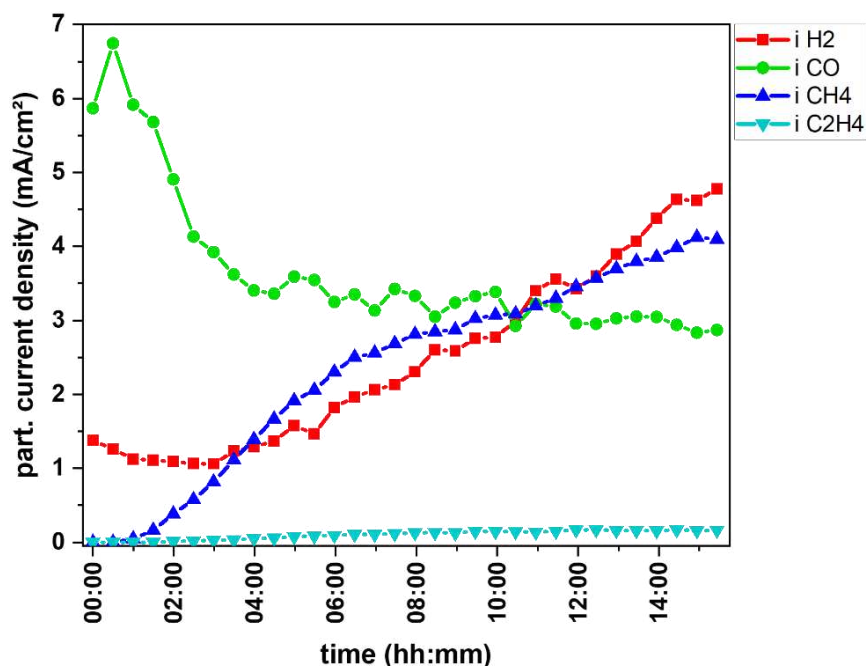
Figure 11: Membraneless pulse experiment. E_c= −2.25 V, E_a= −0.6 V, 5 s/5 s.

Besides gradients in concentration or pH, electrolyte compositions can also change due to chemical transformations, dissolution of electrode material, or accumulation of impurities. We examined this possibility by two approaches: activate a catalyst sample and then swap it for a pristine one or activate a sample and then swap the electrolyte for fresh solution. With this we aim to discern whether the selectivity trend is dictated by changes to the electrode, or changes to the electrolyte. Running a pulsed potential experiment for an extended time, followed by an exchange of electrode has been discussed for Figure 9. In this we observed a "reset" of the catalyst selectivity after the exchange of electrolyte, suggesting that the selectivity is not solely governed by the structure of the electrode. To test whether the selectivity is driven by solution

species, we conducted a pulse experiment, followed by an exchange of the catalyst for a fresh sample after the initial sample ran for hours. During the 17 h experiment (Figure 12) we observe the sample activation over the first 5 h followed by a slight increase in HER over the first 8 h. CH_4 production was constant, while CO formation decreased from initially 10.5 mA/cm² to around 3 mA/cm² after 8 h. We switched from 5 s pulses to 1 s pulses after ca 9 h (which will be discussed in chapter 4), which was applied for another 8 h. After a total of ~ 17 h, the experiment was stopped, and the catalyst was exchanged for a freshly polished silver foil but continuing to use the same electrolyte solution as before. We resumed applying the previous potential conditions with 5 s pulses. Figure 12 shows the CO_2ER product rates plotted vs time. We see the end of the initial pulse experiment during which we reach a partial current density of about 4 mA/cm² for methane after 17 h of pulsed potential control. Upon exchanging the catalyst, we detect a sudden loss of CH_4 formation and observe sample activation over 4-5 h as we have previously seen.
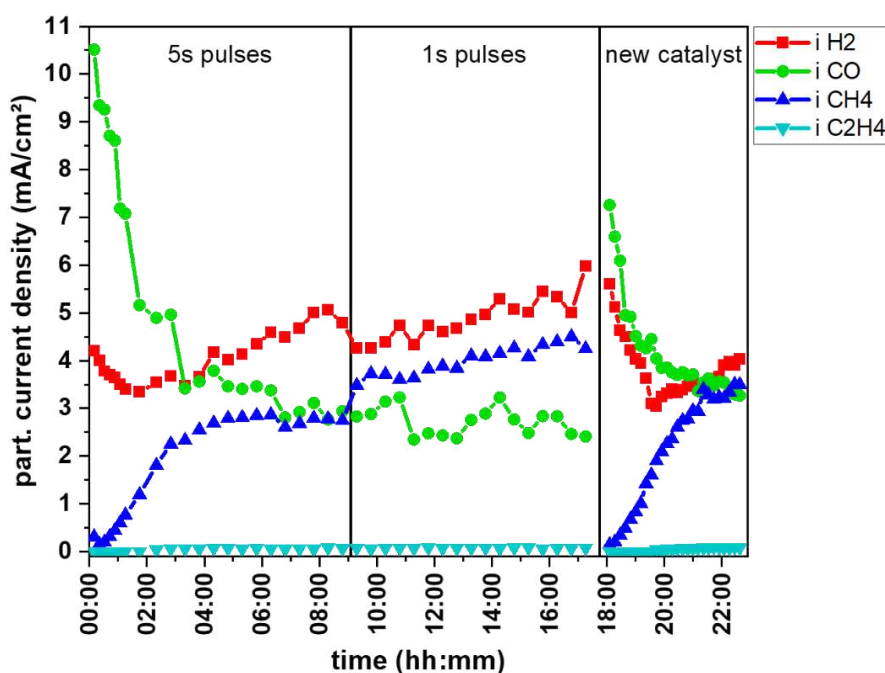
Figure 12: Pulsed potential electrolysis for 17 h, at −2.25 V/−0.6 V, 5 s/5 s; followed by −2.25 V/−0.6 V, 1 s/1 s and subsequently pulsed EC with a fresh Ag sample in the same electrolyte/cell at −2.25 V/−0.6 V, 5 s/5 s.

Since a freshly polished electrode tested in electrolyte from the previous experiment did not immediately give high CH_4 yields, but instead demonstrated the typical activation behavior over a few hours, we conclude that the activation behavior over several hours is attributable not to

changes in the bulk electrolyte, but rather due to slow changes of the electrode itself. Thorough in-situ analysis of the catalyst (e.g., in-situ AFM) is needed to unravel the effect of the potential threshold on the surface and possible restructuring. Adsorbates on the catalyst under can also affect the selectivity and would show a potential dependent behavior. This could be elucidated by means of in-situ vibrational spectroscopy like Raman, which will be subject to a following chapter.

3.2 Varying pulse potential parameter

As we have stated earlier (in section 1.4), four pulse parameters can be used to tune the reaction selectivity in square-wave p-CO_2ER. We've established that pulsing causes significant selectivity trends, so far just looking at a single configuration. It is likely that there exists an optimal combination of pulse parameters (potentials, times) which maximizes the yields of certain products (i.e., CH_4). While this presents a very large possible parameter-space, we addressed this challenge stepwise by varying one parameter at a time whilst keeping the others constant and observing the resulting selectivity trends.

For consistency with our previous results, we activated the sample in the same manner as we did in previous experiments, before applying the varied potential combinations. During the activation of the sample at E_c= −2.1 V, E_a= −0.6V, 5 s/5 s for 5 h, we observed typical growth in CH_4 formation rate, with suppressed HER and a slightly decreasing CO signal (cf. initial part of Figure 13 A). Aiming to study the effect of the cathodic pulse potential, we kept E_a fixed (−0.6 V), varying E_c from −1.7 V to −2.3 V, while each potential combination was applied for 2 h. Figure 13 A shows the product distribution over the duration of the experiment, while Figure 13 B shows the averaged partial current densities for the gases formed, plotted vs the corresponding cathodic pulse potential. As seen in Figure 13 B, the cathodic pulse potential has a distinct effect on all the gaseous products (except for ethylene, which was left out of the summary, due to low formation rates). At very high overpotentials (more negative than −2.1 V), we observe a steep increase in i(H_2), along with a decrease in CH_4 and CO formation. In contrast, at lower overpotentials (less negative than −2.1 V), we observe a decrease in i(H_2) and CH_4 formation, while CO formation is promoted, giving rise to similar selectivity as observed under potentiostatic control. We observe the highest CH_4 formation rate at E_c= −2.1 V, a condition we thus maintained for subsequent studies varying other parameters. To test the reversibility of the

potential-dependence over the course of the experiment, we periodically returned to the original parameters (−2.1 V/−0.6 V). A growth in total (cathodic) current density at these control potentials over time can be explained by surface roughening as observed in the SEM images in Figure 6. It seems that an E_c of at least −1.9 V is needed to produce detectable amounts of methane. This points to a high thermodynamic barrier in the formation of CH_4 on silver, which would be consistent with literature results[10], while possible kinetic factors can't be ruled out (as this potential might correspond to a threshold current resulting in a certain local pH). The drastic increase in $i(H_2)$ at high overpotentials, might be explained by reaching a mass transport-controlled regime, in which CO_2 can no longer be sufficiently supplied by diffusion to the electrode surface, hence a drop in CO_2ER activity and growth in H_2 formation.
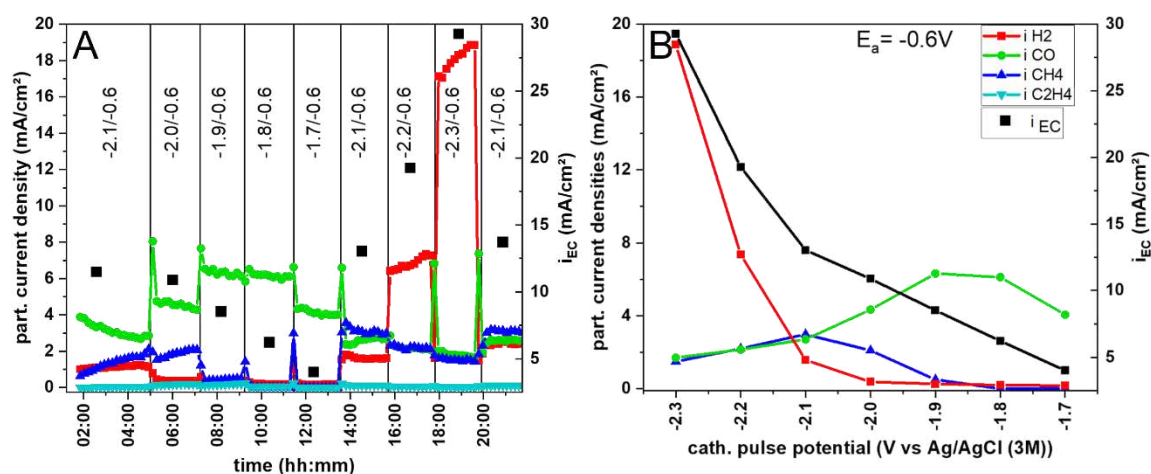
Figure 13: A) cathodic pulse potential variation. E_a was fixed to −0.6 V and each new potential combination was applied for 2 h. B) summary graph showing the average partial current densities for gaseous products and the total current density as a function of varied E_c.

Having identified E_c= −2.1 V as a condition resulting in a local maximum in CH_4 evolution rate, we then fixed this value for subsequent study of the influence of E_a variation. Again, we kept revisiting the starting potential combinations evaluating the sample stability. Variation in total current density and partial current density between these potential combinations (−2.1 V/−0.6 V at different times throughout the experiment) can be interpreted as an increase in roughness. In the screening of E_a, we can detect the strong impact on product selectivity that the anodic pulse potential has and group the data into three segments (see Figure 14 A and Figure 14 B). At E_a more negative than −0.6 V, we observe less pronounced methane formation, while there is only a minor change observable in all gases between the three potentials in this regime.

Intermediate anodic pulse potentials (−0.4 V to −0.6 V) resulted in methane being the major product, with a rise of i(H$_2$) and a decrease in CO towards less negative pulse potentials. Along this line, we detect an increase in total current density (cf. Figure 14 B). At the third regime tested, potentials above −0.4 V, we observe the most drastic changes in selectivity. As one can see in Figure 14 A switching to −0.3 V resulted in a steep rise in both i(H$_2$) and i(CH$_4$) during the first 30-40 min, accompanied by a sharp rise in total current density. This is followed by an abrupt curb in H$_2$, CH$_4$ formation rate and total current density, while CO formation grows at the same time. Upon switching to −0.2 V, all the methane formation is lost, and we detect only CO and H$_2$. The ability to form methane appears to be lost, since we no longer detect any CH$_4$ when revisiting the starting conditions after 37 h. We therefore conclude that the E$_a$ of −0.2 V/−0.3 V represents a threshold condition at which the sample activation is reversed, and the methane selectivity is lost.
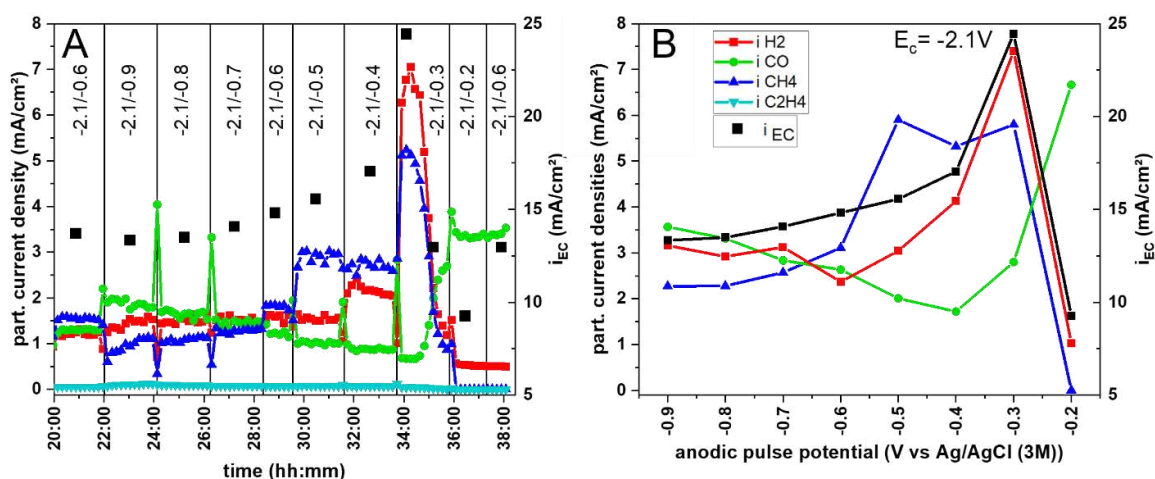
Figure 14: A) anodic pulse potential screening. E$_a$ was changed, while E$_c$ was fixed to −2.1 V. Each new potential combination was applied for 2 h. B) summary graph showing the average partial current densities for gaseous products and the total current density as a function of varied E$_a$.

Our observations so far have shown that pulsing is critical for both activating the sample, as well as for inducing the CH$_4$ pathway. We have also found that certain conditions (such as the critical E$_a$ threshold potential) can lead to the loss of CH$_4$ activity. Thus, the open question is whether an activated sample would retain its activity after a resting period (without removal from the solution) if pulsing is resumed. Therefore, we conducted experiments during which a sample was activated under pulsed potential control and then allowed to rest at open circuit, whilst measuring the open circuit potential (OCP), followed by potential pulsing again. The results are

depicted in Figure 15 and in Figure 16. Both experiments were conducted under the same applied pulse conditions (−2.25 V/−0.6 V, 5 s/5 s), meaning they only differ in the total duration that the potential pulsing was applied and ultimately in the OCP potential they reach.

In the first experiment conducted, we observed a reduction in CO current density from 8.6 mA/cm² to 4.1 mA/cm² during the initial 3.5 h, where methane production slowly grows to about 0.9 mA/cm², while HER remains quite stable over this time. We then introduced a 10-minute period without applied potential, which allowed the system to relax at OCP. During this, the potential at the working electrode shifted in ~11 min from −0.6 V to −0.25 V (see inset in Figure 15). We therefore note, that the OCP seemed to be within the threshold potential range, where we observed deactivation in the previous experiment. After resuming pulsed potential control, we observe pre-OCP behavior i.e., similar partial current densities for all products as before the OCP period.
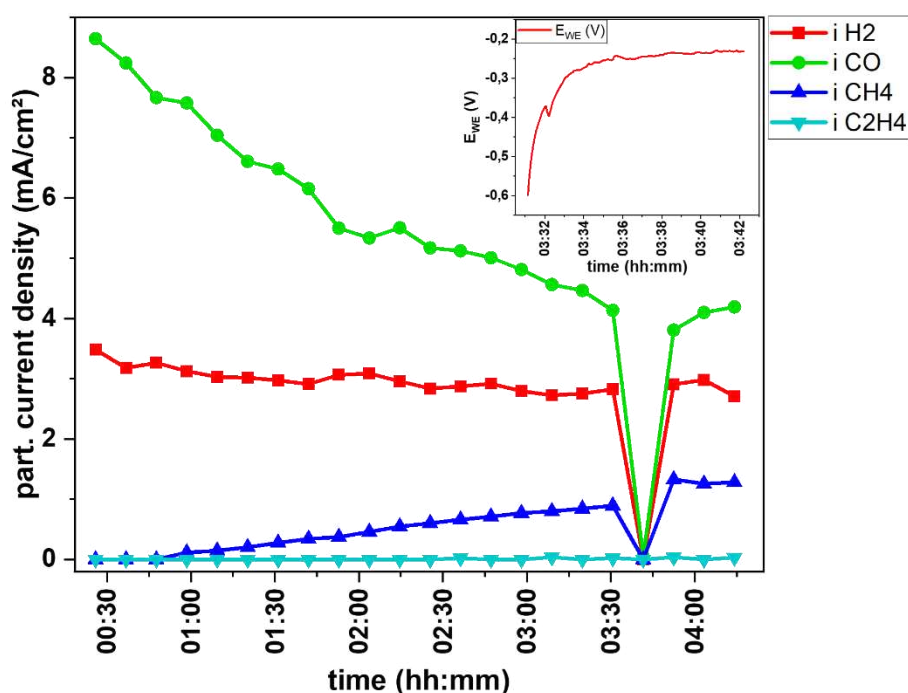
Figure 15: Partial current densities for gaseous products formed at −2.25 V/−0.6 V, 5 s/5 s with a 10−minute OCP period in between. Inset shows potential shift during the OCP.

In the other experiment the initial potential pulsing was only applied for 1 h 20 min before the OCP period. During this time, we observe the typical activation behavior, with CO decreasing, a constant H_2 signal and an increase in $i(CH_4)$ (see Figure 16). Allowing the working electrode

potential to relax under open circuit conditions, resulted in a shift of potential to about from −0.6 V to −0.1 V in 10 min (cf. inset Figure 16). Hence the OCP was significantly more positive than the identified threshold potential. Applying the potential pulsing again, yielded CO and hydrogen initially while no methane was formed during the first 10 min after the OCP. The CH_4 signal grew with a similar rate as it did during the initial activation and reached about 1.6 mA/cm² after 37 min.
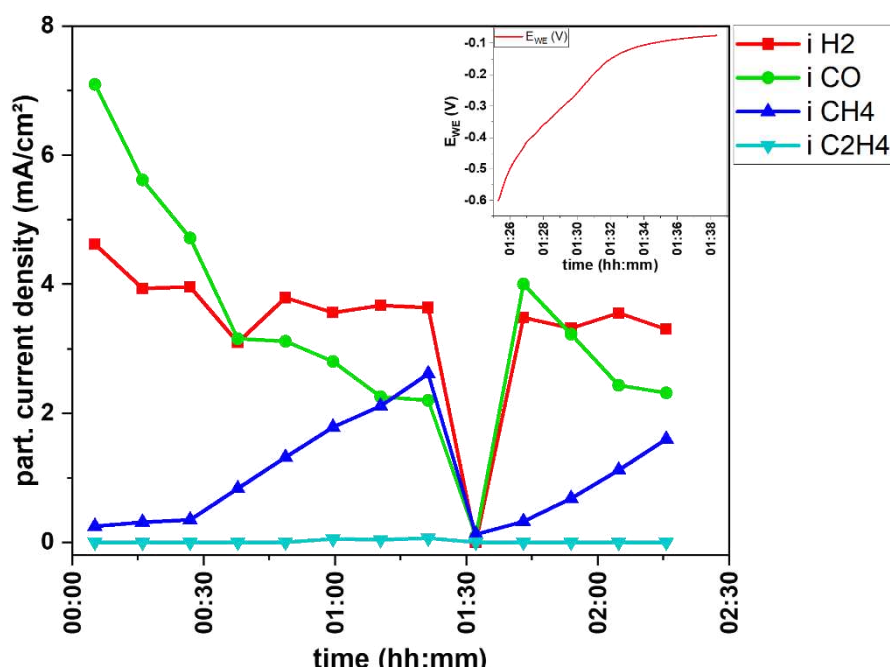
Figure 16: Partial current densities of gaseous products formed under pulsed potential control at −2.25 V/−0.6 V, 5 s/5 s, with a 10−minute OCP period at 01:26. Inset shows the potential shift during the OCP period.

This observation is consistent with the E_a screening experiments, where a threshold potential for losing activation was identified. Possible explanations for this threshold potential include the ad-/desorption of species on the catalyst surface, as well as possible electrode surface reconstruction[11] and electrode oxidation. Careful analysis by in-situ vibrational spectroscopy could give information about the state of adsorbates during each potential pulse and hence lead to a better understanding of the pulsing effect. A paper by Corson et al.[12] has shown that the re-organization of water molecules along a silver surface in CO_2ER takes place at a potential coinciding with our threshold value. The authors studied an Ag-catalyst during in-situ CO_2ER conditions, using ATR-SEIRAS. Their paper reports the potential dependent alignment of water molecules in either a H-down, mixed, or O-down orientation towards the electrode surface

depending on the applied potential. At potentials more negative than the point of zero charge (pzc), the water molecules in the double layer orient H-down, with hydrogen facing the electrode surface. This is due to the negative polarization of the electrode and the interaction with the partially positive hydrogen. At the pzc, the molecules will align with the H-OH bond in parallel to the catalyst, while at potentials more positive, they will orient O-down. The point of zero charge in dilute solutions (as in our case 0.1 M KHCO$_3$) is not affected by the interaction with non-specific adsorbed species, such as alkali ions and carbonates, suggesting it to be close the literature values reported in 0.005 M NaF.[13]

The point of zero charge for several silver facets are listed in Table 2. While the cathodic pulse potentials tested here are all far more negative than the reported values, the anodic pulse potentials are almost entirely more positive. One would assume a change in water orientation upon passing the pzc, findings of Corson et al.[12] suggest that the water molecules keep their orientation – once they are aligned – far beyond the pzc. The oriented water molecules (H-down, due to prior CA at −0.6 V vs RHE for 90 s) were observed to take 1 to 2 h to relax into steady state conditions. The thereby formed densely packed water layer, has been reported to be able to significantly affect the proton transfer to the surface and thus impact the HER and potentially the H* coverage/ formation of the H* intermediate.[14–17]

Table 2: Values for the point of zero charge on several silver facets.[13]

	pzc vs Ag/AgCl (3M)
Ag(111)	−0.67 V
Ag(100)	−0.82 V
Ag(110)	−0.95 V

Upon screening in the anodic direction, Corson et al. have observed the presence of the proposed H−down orientation up to a potential of 0.5 V vs RHE (−0.1 V vs Ag/AgCl). These findings match our observations perfectly in terms of the threshold E_a which leads to the selectivity switch. We thus propose that the deactivation of the CH_4 selectivity stems in parts from the re-orientation of water molecules in the double layer and hence the observed CH_4 formation is dependent on the H-down of water molecules.
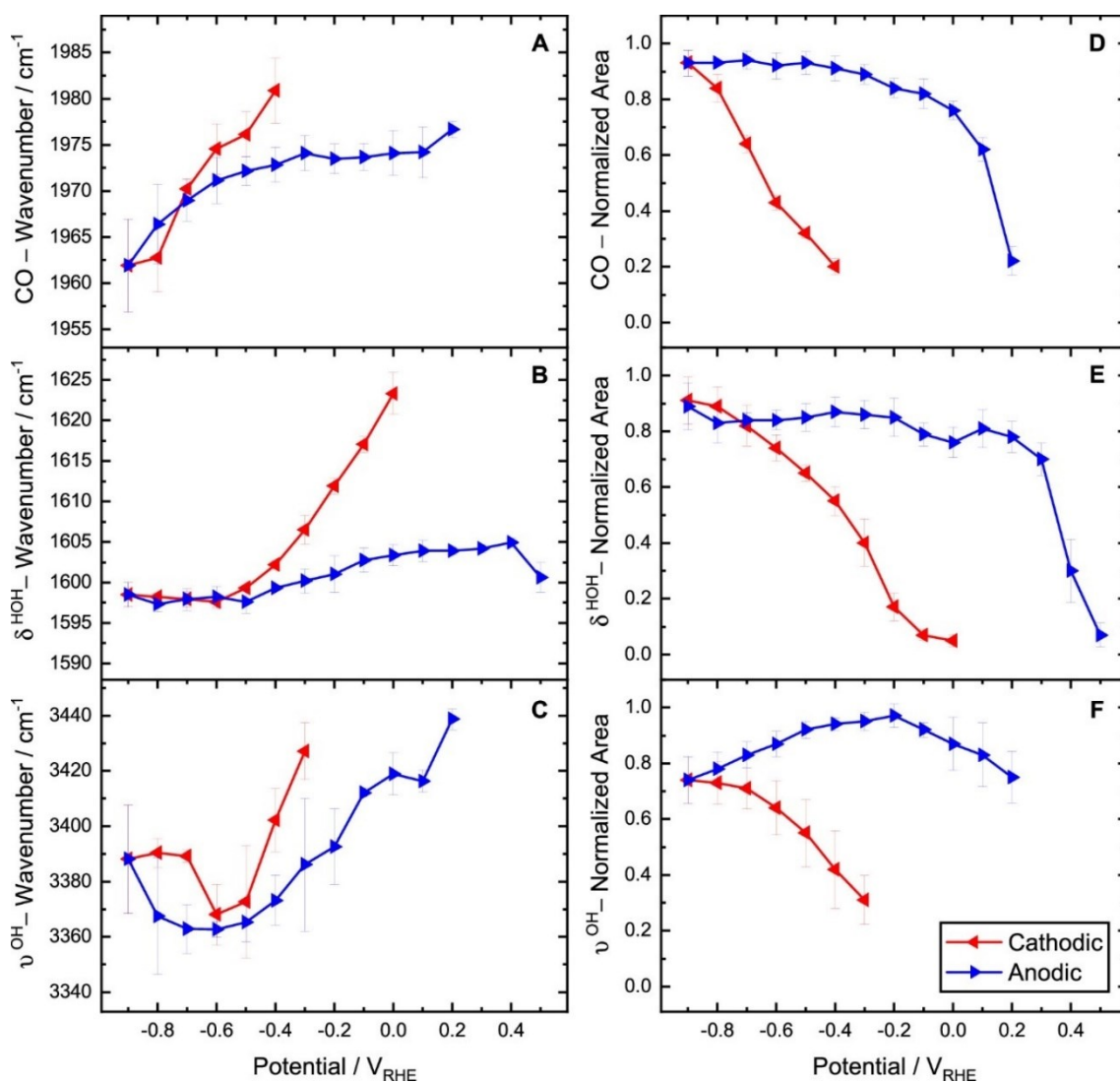
Figure 17: Average peak position (A−C) and normalized area (D−F) of three SEIRAS peaks during CV: CO (A and D), δ_{HOH} (B and E), and ν_{OH} (C and F). Average values and standard deviations are calculated from five CV experiments performed at 2 mV/s. The area is normalized by the largest area in each individual data set. Error bars represent one standard deviation. Red lines show the cathodic scan from 0.2 to −0.9 V_{RHE}, and blue lines show the anodic scan from −0.9 to 0.6 V_{RHE}. The activated Ag cathode on a Ge ATR crystal was in 0.1 M $KHCO_3$ with continuous CO_2 flow through the electrolyte. Reprinted with permission from[12]. Copyright 2020 American Chemical Society
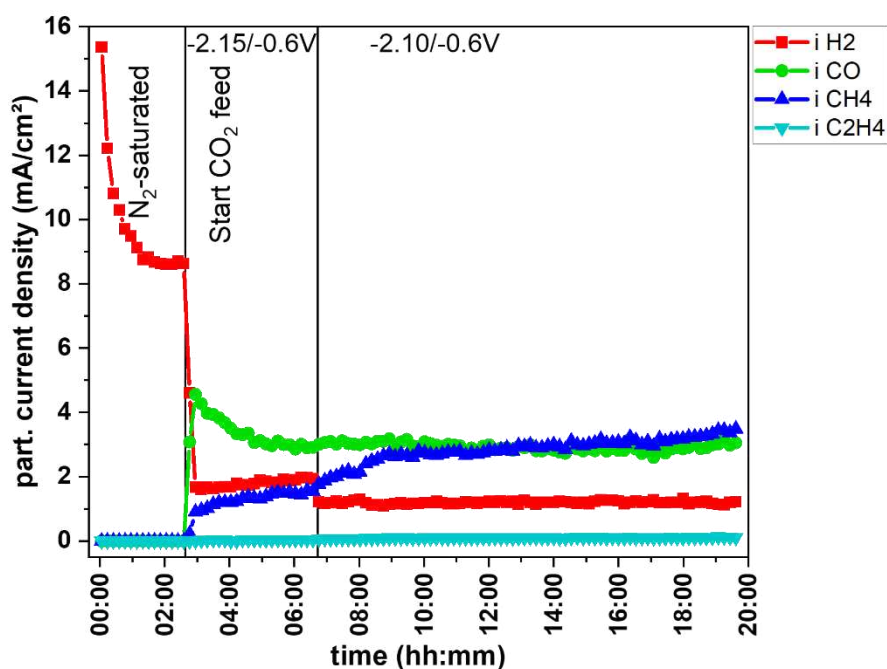
Figure 18: Pulse experiment (−2.15 V/−0.6 V, 5 s/5 s) started in N_2-saturated electrolyte. After about 2.5 h CO_2 was added to the electrolyte which is indicated by the first black line in the graph. The second black line indicates transition from E_c= −2.15 V to E_c= −2.1 V.

In order to investigate the source of carbon in our experiment – determining whether it stems completely from solvated CO_2 supplied by the gas feed, or if reduction of the bicarbonate electrolyte solution might occur, we conducted a pulse experiment in the absence of a CO_2, using nitrogen-saturated electrolyte instead. Herein we applied potential pulsing as defined in Figure 18 for about 2.5 h, before we started introducing CO_2 into the solution. During the CO_2-free part of the experiment, the only gas detected was hydrogen, from which we can conclude that no bicarbonate reduction took place, hence no carbon-containing gases were detected. Upon introduction of CO_2 in the solution, we observe a sharp rise in CO and CH_4 partial current densities, while H_2 formation abruptly drops from ~9 mA/cm² to 2 mA/cm². Within 30 min of CO_2 addition $i(CH_4)$ has reached over 1 mA/cm² and from thereafter grows only slowly for the next 3.5 h. As we change the cathodic potential, we can observe another instantaneous drop in $i(H_2)$, while $i(CO)$ remains at previous levels and methane formation continues to rise over the following 13 h experiment. The sharp increase in methane formation upon CO_2 addition suggests that the sample activation process under potential pulsing – at least partially – occurs also in a CO_2-free environment.

From our results and discussion shown we can conclude that applying an alternating potential (pulsed potential) on a silver foil catalyst in CO_2ER can significantly change the reaction selectivity. As compared to potentiostatic experiments, potential pulsing leads not only to suppression of the HER but can also yield methane as a major product – a behavior that is unique for flat Ag catalysts. We have shown that this selectivity is established over several hours of catalysis. The fact that methane is formed on a catalyst otherwise known to release CO before it can be further reduced and the timeframe in which the selectivity changes, make this system an interesting model to study. We propose the interplay of surface restructuring (as seen in the SEM and EBSD data)[18], pulsing effects (like elevated CO_2 concentration and high local pH – as modelled by Bui et al.[19]), along with adsorbed species[10] and water orientation in the electrode's vicinity[12] as causes for the formation of methane.

As for future experiments, conducting in-situ vibrational spectroscopy like Infrared (IR) or Raman is of high interest, since this information could help getting insight into formed adsorbates and intermediates. While the in-situ roughening during the activation could lead to surface enhancement of Raman signals for example, the high overpotentials needed to drive the methane formation could hinder the collection due to strong bubble formation on the surface. In-situ AFM could help to get a clearer of the surface restructuring taking place during p-CO_2ER

In the above we have tested various potential combinations, which was due to the experimental set-up quite time consuming. Covering a wider experimental space will be part of the next chapter, utilizing faster product detection by mass spectrometry. After addressing thermodynamics, we will now focus on kinetic effects, by probing the of pulse time (t_c and t_a) modulation.

3.3 Effect of pulse time variation

After focusing on the effect of varying the pulse potentials, we turned to investigating the effect of altering the other pulse parameter – the pulse time. This refers to the duration of each potential applied and can – as will be shown in the following chapter – significantly alter the product formation. In the experiments conducted in the H-cell, where products were detected by use of gas chromatography, the focus was on symmetrical pulses, meaning equal pulse length for the cathodic and the anodic pulse ($t_c = t_a$). In the experiments conducted with the use of the

mass spectrometer, we investigated the effect of asymmetrical pulses, where one of the potentials was applied for a longer time than the other ($t_c \neq t_a$).

In an initial experiment (Figure 19) we applied a pulsed potential (E_c= −2.25 V, E_a= −0.6 V) at 5 s for each potential. We kept this condition for over 15 h in order to complete the sample activation period and create a stable reaction condition under which we can study the effect of shorter pulse duration. At about the 16 h mark, we switched from 5 s pulses to 1 s pulses, at which point we observed an immediate response in form of a sharp rise in i(CH$_4$) and a drop in HER. Interestingly, the CO formation remains largely unaffected by the shift in pulse time. It is important to note that although changes in t_c and t_a result in changes to the overall pulse frequency (here, a 5-fold increase in frequency), we are still using a square wave function (where $t_c = t_a$) and thus the correction factor described previously still applies (see Figure 5 and discussion). This initial experiment was striking in that it showed that even after the sample was "activated" over hours and producing stable rates of product formation, different pulse conditions could still induce strikingly different selectivity trends.
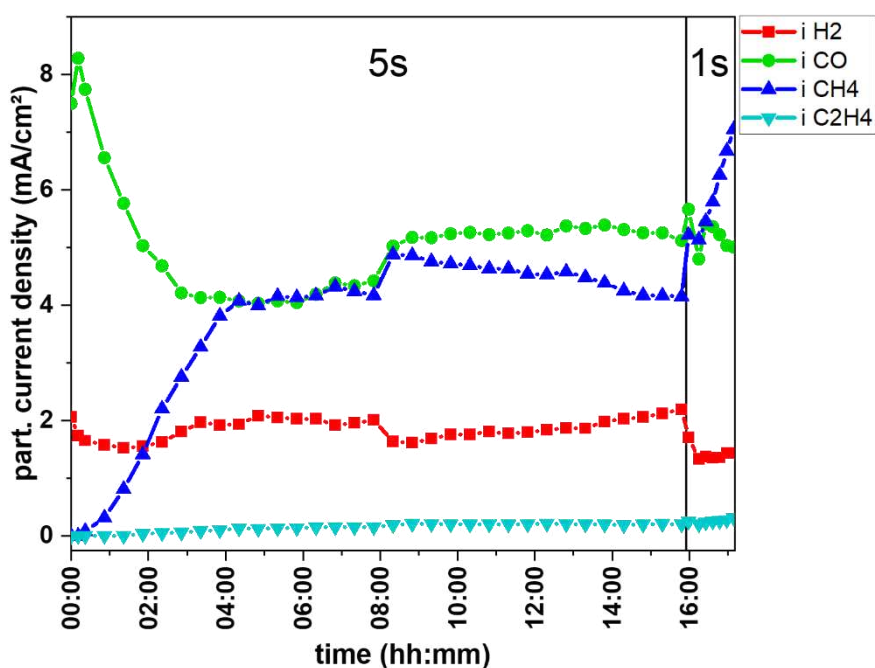
Figure 19: Effect of shorter pulse time when switching after ~16 h (as indicated by black line) from 5 s/5 s pulses to 1 s/1 s pulses at −2.25 V/−0.6 V.

In another experiment we examined a broader range of shorter pulse times (Figure 20). After activating the sample for 6 h under pulsed potential control (with t_c= t_a= 5 s), we switched to 2 s

pulses, upon which we detected no change in the partial current density for CO, while the H_2 signal decreased in favor of CH_4. This trend continues with shorter pulse times going from 2 s to 1 s to 0.5 s. We then applied the initial conditions of 5 s pulses again, to check whether much has changed during the shorter pulse period and could observe a significant increase compared to the beginning of the experiment. Thus, not all the increase in methane formation can be attributed to the effect of shorter pulses but seems to be an effect of higher activated state. Yet we note a drop in methane formation going from 0.5 s to 5 s pulses, with a simultaneous increase in HER. This confirms the effect of shorter pulses on HER suppression and CH_4 promotion. While E_c and E_a vary a bit (since optimal conditions haven't been established, when this data was acquired) it shows that effect pulse time modulation persists even when the applied potentials change.
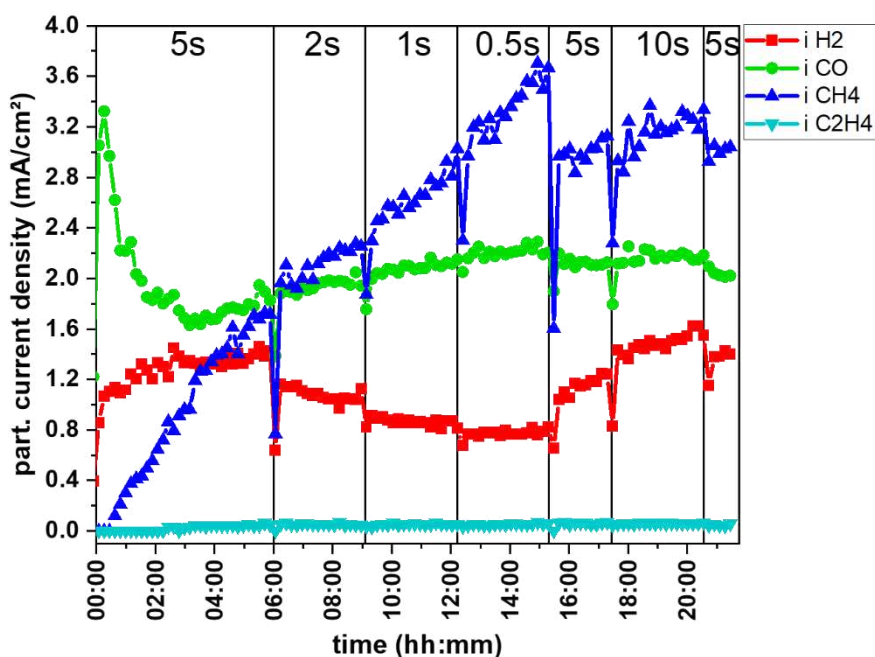
Figure 20: Effect of various pulse durations (labeled on the figure) adjusted periodically during continuous operation. Applied potentials were E_c= −2.1 V & E_a= −0.5 V.

The results of Figure 20 showed a trend that shorter pulses progressively led to larger i(CH_4) and greater HER suppression, so we performed further experiments using even shorter sub-second pulses. The sample was "activated" by applying conditions previously established (E_c= −2.1 V, E_a= −0.5 V) to produce a stable methane signal, followed by a transition to pulses of 100 ms and below (see Figure 21). We observe a growing partial current density of methane

over the first 6 h of the experiment (up to ~6 mA/cm²) while i(CO) and i(H$_2$) stabilize quite quickly after an initial drop. Upon switching to 100 ms pulse, we observe a steep rise in i(CH$_4$) and a continuous growth of the signal over the following 6 h. The methane formation seems to grow at the expense of the H$_2$ formation, since we detect a decrease in HER upon applying the shorter pulses. Over the time of the experiment the methane rate triples from 4.8 mA/cm² after ~3 h, to 15.4 mA/cm² after 10 h 45 min. Aiming to get information about the time frame of product formation, we went to even shorter pulse duration. Applying 50 ms pulses, yielded even higher rates of methane production of over 18 mA/cm². While the CO formation decreased slightly over time, HER showed little response to the even shorter pulses and could not be further suppressed.
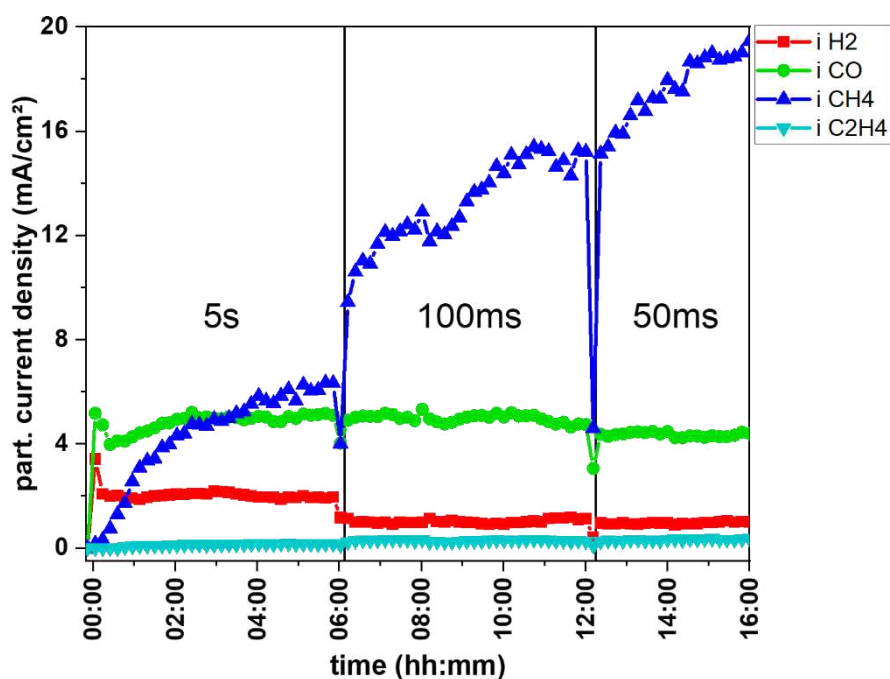
Figure 21: Pulse experiment at −2.1 V/−0.5 V at different pulse durations, while both potentials were applied for the same length (t_c=t_a) as labeled on the figure.

At this point, with the observations that I) CH$_4$ forms significantly only under potential pulsing, and II) the time-averaged rate of CH$_4$ production increases with shortened pulse time (increase pulse frequency), it seemed likely that the formation of methane is not uniform over the pulse duration, but rather is formed mainly during an initial period during E_c/t_c, before steady-state conditions (e.g., of CO$_2$ concentration, local pH) are reached. Thus, shortening the pulse time effectively increases the relative time spent at this "pre-steady-state" condition, leading to an

increase in $i(CH_4)$. Since the pulsed potential catalysis is a highly technique (and thus its effects on the surface morphology and reactants are), time-resolved in-situ techniques could aid to gain further insight into these processes. We thusly propose the use of in-situ AFM to elucidate the morphological changes, while time-resolved Raman spectroscopy can give powerful information about reactants and adsorbates during the pulsed CO_2ER.

The above discussed results are time-averaged gas product evolution resulting from GC analysis every 10 min. Seeing how product selectivity is dynamically sensitive to pulse conditions further insight could be gained if product formation could be assessed with greater time resolution, i.e., on the timescale of the potential pulses. Furthermore, faster analysis could overcome the time bottleneck and facilitate more rapid screening of pulse parameters E_c, E_a, t_c and t_a across a wider experimental space. This is the topic of the following Chapter.

3.4 Literature

(1)   Kuhl, K. P.; Hatsukade, T.; Cave, E. R.; Abram, D. N.; Kibsgaard, J.; Jaramillo, T. F. Electrocatalytic Conversion of Carbon Dioxide to Methane and Methanol on Transition Metal Surfaces. *J. Am. Chem. Soc.* **2014**, *136* (40), 14107–14113. https://doi.org/10.1021/ja505791r.

(2)   Feaster, J. T.; Shi, C.; Cave, E. R.; Hatsukade, T.; Abram, D. N.; Kuhl, K. P.; Hahn, C.; Nørskov, J. K.; Jaramillo, T. F. Understanding Selectivity for the Electrochemical Reduction of Carbon Dioxide to Formic Acid and Carbon Monoxide on Metal Electrodes. *ACS Catal.* **2017**, *7* (7), 4822–4827. https://doi.org/10.1021/acscatal.7b00687.

(3)   Bagger, A.; Ju, W.; Varela, A. S.; Strasser, P.; Rossmeisl, J. Electrochemical CO 2 Reduction: A Classification Problem. *ChemPhysChem* **2017**. https://doi.org/10.1002/cphc.201700736.

(4)   Chen, Y.; Li, C. W.; Kanan, M. W. Aqueous CO2 Reduction at Very Low Overpotential on Oxide-Derived Au Nanoparticles. *J. Am. Chem. Soc.* **2012**, *134* (49), 19969–19972. https://doi.org/10.1021/ja309317u.

(5)   Wuttig, A.; Surendranath, Y. Impurity Ion Complexation Enhances Carbon Dioxide Reduction Catalysis. *ACS Catal.* **2015**, *5* (7), 4479–4484. https://doi.org/10.1021/acscatal.5b00808.

(6)   Kuhl, K. P.; Hatsukade, T.; Cave, E. R.; Abram, D. N.; Kibsgaard, J.; Jaramillo, T. F. Electrocatalytic Conversion of Carbon Dioxide to Methane and Methanol on Transition Metal Surfaces. *J. Am. Chem. Soc.* **2014**, *136* (40), 14107–14113. https://doi.org/10.1021/ja505791r.

(7)   Kimura, K. W.; Fritz, K. E.; Kim, J.; Suntivich, J.; Abruña, H. D.; Hanrath, T. Controlled Selectivity of CO 2 Reduction on Copper by Pulsing the Electrochemical Potential. *ChemSusChem* **2018**, *11* (11), 1781–1786. https://doi.org/10.1002/cssc.201800318.

(8)   Kim, C.; Weng, L.-C.; Bell, A. T. The Impact of Pulsed Electrochemical Reduction of CO2 on the Formation of C2+ Products over Cu. *ACS Catal.* **2020**. https://doi.org/10.1021/acscatal.0c02915.

(9)   Clark, E. L.; Ringe, S.; Tang, M.; Walton, A.; Hahn, C.; Jaramillo, T. F.; Chan, K.; Bell, A. T. Influence of Atomic Surface Structure on the Activity of Ag for the Electrochemical Reduction of CO 2 to CO. *ACS Catal.* **2019**, *9* (5), 4006–4014. https://doi.org/10.1021/acscatal.9b00260.

(10)   Bohra, D.; Ledezma-Yanez, I.; Li, G.; de Jong, W.; Pidko, E. A.; Smith, W. A. Lateral Adsorbate Interactions Inhibit HCOO – While Promoting CO Selectivity for CO 2 Electrocatalysis on Silver. *Angew. Chemie Int. Ed.* **2019**, *58* (5), 1345–1349. https://doi.org/10.1002/anie.201811667.

(11)   Simon, G. H.; Kley, C. S.; Roldan Cuenya, B. Potential-Dependent Morphology of Copper Catalysts During CO2 Electroreduction Revealed by In Situ Atomic Force Microscopy. *Angew. Chemie Int. Ed.* **2021**, *60* (5), 2561–2568. https://doi.org/10.1002/ANIE.202010449.

(12)   Corson, E. R.; Kas, R.; Kostecki, R.; Urban, J. J.; Smith, W. A.; McCloskey, B. D.; Kortlever, R. In Situ ATR-SEIRAS of Carbon Dioxide Reduction at a Plasmonic Silver Cathode. *J. Am. Chem. Soc.* **2020**, *142* (27), 11750–11762. https://doi.org/https://doi.org/10.1021/jacs.0c01953.

(13)   Frumkin, A. N.; Petrii, O. A.; Damaskin, B. B. *Comprehensive Treatise of Electrochemistry*; Springer US: Boston, 1980.

(14)   Monteiro, M. C. O.; Dattila, F.; López, N.; Koper, M. T. M. The Role of Cation Acidity on the Competition between Hydrogen Evolution and CO 2 Reduction on Gold Electrodes. *J. Am. Chem. Soc.* **2021**. https://doi.org/10.1021/jacs.1c10171.

(15)   Wang, Y. H.; Zheng, S.; Yang, W. M.; Zhou, R. Y.; He, Q. F.; Radjenovic, P.; Dong, J. C.; Li, S.; Zheng, J.; Yang, Z. L.; Attard, G.; Pan, F.; Tian, Z. Q.; Li, J. F. In Situ Raman Spectroscopy Reveals the Structure and Dissociation of Interfacial Water. *Nat. 2021 6007887* **2021**, *600* (7887), 81–85. https://doi.org/10.1038/s41586-021-04068-z.

(16)   McCrum, I. T.; Koper, M. T. M. The Role of Adsorbed Hydroxide in Hydrogen Evolution Reaction Kinetics on Modified Platinum. *Nat. Energy 2020 511* **2020**, *5* (11), 891–899. https://doi.org/10.1038/s41560-020-00710-8.

(17)   Ito, M.; Yamazaki, M. A New Structure of Water Layer on Cu(111) Electrode Surface during Hydrogen Evolution. *Phys. Chem. Chem. Phys.* **2006**, *8* (31), 3623–3626. https://doi.org/10.1039/B606933A.

(18)   Liu, X.; Xiao, J.; Peng, H.; Hong, X.; Chan, K.; Nørskov, J. K. Understanding Trends in Electrochemical Carbon Dioxide Reduction Rates. *Nat. Commun.* **2017**, *8* (May), 15438. https://doi.org/10.1038/ncomms15438.

(19)   Bui, J. C.; Kim, C.; Weber, A. Z.; Bell, A. T. Dynamic Boundary Layer Simulation of Pulsed CO 2 Electrolysis on a Copper Catalyst. *ACS Energy Lett.* **2021**, 1181–1188. https://doi.org/10.1021/acsenergylett.1c00364.

4 Pulse parameter variation with rapid product detection

4.1 Further investigation of pulse time effects

Up to here, all data shown stemmed from very long experiments (typically run overnight), which made it very time consuming to study a broad range of parameter variations. DEMS allows the product detection with a second or even millisecond time resolution, which give us the chance to observe the product formation over the duration of a single pulse. We aimed to understand the effect of different pulse time durations for both the cathodic and the anodic pulse, while keeping the potentials fixed the E_c= −2.1 V and E_a= −0.5 V respectively.

The cell used is custom-made one compartment cell which contained a 3-electrode set-up (as described in section 2.5 and Figure 2). The catalyst is directly deposited on a hydrophobic membrane by magnetron sputtering, done in house. This has shown to maximize collection efficiency and minimize response times[1,2], due to decreasing the diffusion pathway for the products formed. The porous catalyst layer was about 600 nm thick, chosen as a result of an optimization series (not shown) using a range of thicknesses to determine which showed the highest signal of CO_2ER products due to optimal ratio of catalyst thickness vs sustained porosity. In the DEMS set-up the catalyst coated membrane served as the cathode, allowing products to be directly sucked into the mass spectrometer due to the vacuum that is present under the membrane. The cell is fed with a CO_2-saturated electrolyte, while a Pt-mesh served as a counter electrode. The exposed area of the catalyst layer in the cell was kept at 0.636 cm² defined by an O-ring with 9 mm inner diameter.

By monitoring the methane signal over time, we concluded that the sample activation in the DEMS cell under pulsed potential electrolysis (−2.1 V/−0.5 V, 5 s/5 s) is significantly shorter, up to 1.5 h, in comparison with the 4-5 h observed for the foil samples. This might be influenced by the higher porosity of the deposited metal layer on the PTFE membrane compared to the polished silver foils, as the nano-structured morphology might be easier to undergo surface reconstruction, or due to a different local pH in the porous catalyst. We therefore hereafter evaluate the mass signals of CO_2ER products only after 1.5 h to avoid convolution of pulse time effects with activation effects. In experiments where this was not feasible, we have to take the

lower/higher activation state into account. While the gas chromatographer can readily be calibrated, allowing the precise quantification of detected products, this is not trivial in DEMS. Due to the complex interplay of partial pressures within the MS vacuum, accurate product quantification, (especially when forming a complex mixture of products) can be challenging. We therefore refrained from converting the mass currents obtained from the DEMS and report them as exported from the system. Note that these currents are of a different origin and nature than the ones reported in the previous chapter on GC experiments. Table 3 lists the m/z ratio, corresponding fragments and the product they can be associated with, for the products of interest. The shown fragments are almost free of convolution and only contributed by a single product. The only exceptions are 28 m/z, which in addition to CO can also be attributed to ethylene (C_2H_4) and the fragmentation of CO_2 into CO and O. However, the GC experiments revealed that only neglectable amounts of ethylene are formed and we account for the fragmentation of CO_2 by subtracting 8 % of the CO_2 from the CO signal.

Table 3: m/z ratio, mass fragments and corresponding CO_2ER products investigated with DEMS. The colored species represent the products associated with the masses scanned, due to their higher formation rate.

m/z	2	15	28			44
Fragment	H_2	CH_3	CO	C_2H_4	CO	CO_2
Corresponding Product	H_2	CH_4	CO	C_2H_4	CO_2	CO_2

Since Hydrogen is the smallest and lightest gas detected here, it travels through the system the quickest, leading to a sharp rise in signal. Due to its low weight however the turbopumps have trouble taking out as efficiently as heavier gases, resulting a slow decay in signal. All other gases are sufficiently pumped out by the turbopump.

Scheme 4 illustrates the DEMS cell and the gas streams during the anodic and the cathodic pulse. During t_a we only draw CO_2 from the electrolyte into the mass spectrometer (MS), while during t_c the formed products are sucked into the MS.
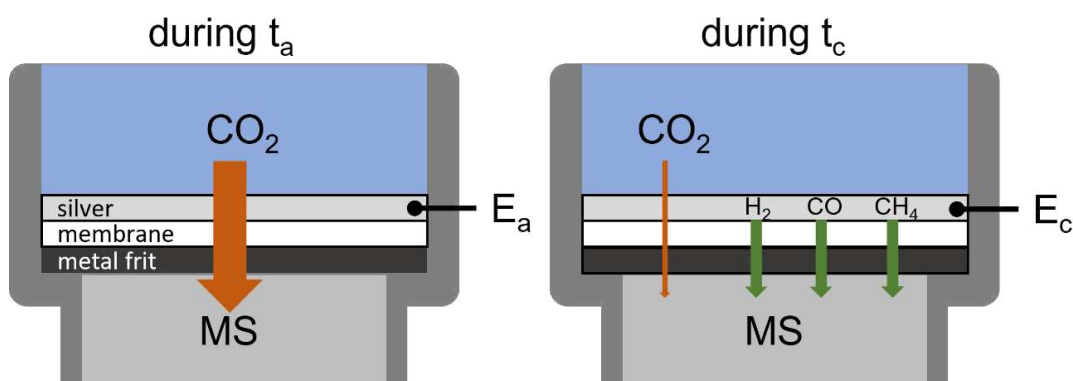
Scheme 4: DEMS cell scetch, visualizing gas flow during t_a and t_c.

The graphs in this chapter show continuous measurement of products (derived from raw m/z signal intensities) during electrochemical pulsing. The measured electrochemical currents (i(mA/cm²)) are shown in black, and the DEMS signals color coded. To facilitate comparison of the time-dependent behavior of the various species, the data are re-scaled to a common range and offset vertically, making the y-axis arbitrary (we do seek to perform quantitative analysis on these datasets).

We investigated the formation of the gaseous products that we observed in the H-cell experiments, namely H_2, CO and CH_4. As we were also interested in the consumption and diffusion of CO_2 back to the electrode surface, we also scanned for the corresponding mass signal. Figure 22 shows the mass signals as obtained from the mass spectrometer over the duration of one pulse cycle.
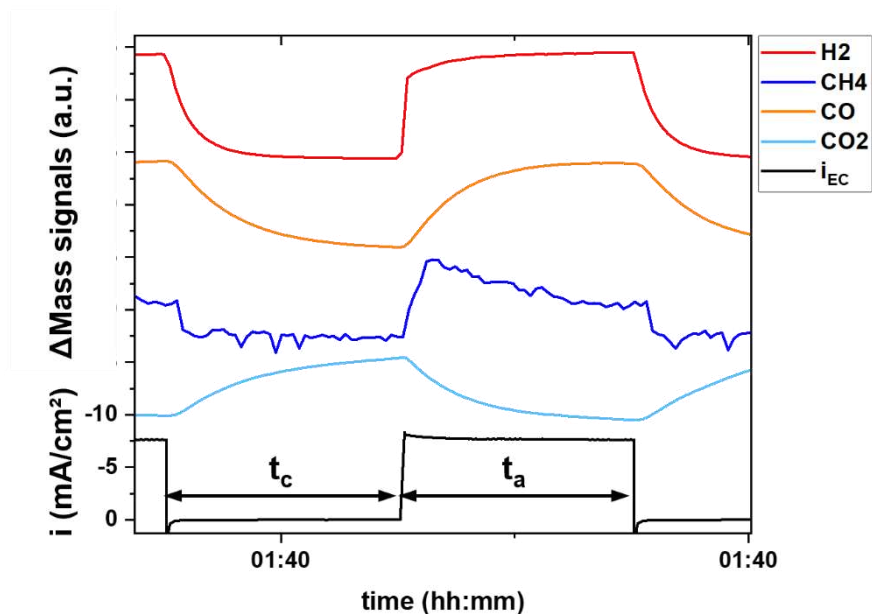
Figure 22: DEMS signals of major gaseous products formed under pulsed electrolysis at −2.1 V/−0.5 V, 5 s/5 s, and the simultaneously-measured current density through the electrode.

Figure 22 shows a snapshot of the DEMS experiment on an electrode already continuously operated under potential pulsing for >1.5 h. It can be seen that the MS signals corresponding to different chemical species rise and fall in conjunction with the applied pulsing period and the resulting electrochemical current density. First looking at the anodic pulse, we detect a steep decrease in CH_4 and H_2 signal, while CO shows a slower decay. The CO_2 signal grows over the time of the anodic pulse, since no reductive current flows during this, hence no CO_2 is reduced electrochemically, and it is replenished from the bulk solution during this period. The slower decay of the CO signal might be influenced by slow desorption of bound CO from the surface, indicating a stronger binding of *CO than expected from literature[3]. On reaching the cathodic pulse, we can observe an initial jump in the H_2 signal, which then slowly grows until is plateaus towards the end of the pulse. The CO signal behaves very similar to H_2 although showing a slower initial growth. The CO_2 signal decays due to it being converted into CO_2ER products, which appears faster over the first 1−1.5 s of the pulse and then slower over the remaining part. Most interestingly, CH_4 shows a distinct rise upon the potential switch, followed by a slow decay in signal over the rest of the cathodic pulse. This appears to support our previously mentioned hypothesis on the formation of methane – we see a non-uniform production of CH_4 over the

52

pulse, forming most significantly at the pulse start, which explains the increase in partial current density when employing shorter pulses.

The DEMS approach is therefore a powerful tool for quickly measuring products as a function of the pulse parameters and doing so with a time resolution sufficient to discern transient behaviors. We subsequently used this technique to evaluate a range of varied parameters. First, we progressively increased t_c while keeping t_a constant, aiming at gradually moving toward a behavior comparable to steady-state (potentiostatic) operation, interspersed with 5 s anodic pulses.

When extending the cathodic pulse length to 10 s, we observe similar signal shape as seen previously (under t_c= 5 s) for CO, CO_2 and CH_4, while the transient shape of the latter is more pronounced (Figure 23). Interestingly we see the methane signal slowly rising again after about 4.5 s of the cathodic pulse. The H_2 signal shape is different from the one at 5 s/5 s, as it shows a sharp initial rise, followed by a decay onto a plateau, resembling the transient shape of the methane signal. Such a behavior could be ascribed to lower CH_4 formation at t_c= 10 s, since we hypothesize CH_4 and H_2 to share a rate-limiting step, which typically results in a suppression of HER during the initial part of the cathodic pulse by the formation of CH_4.
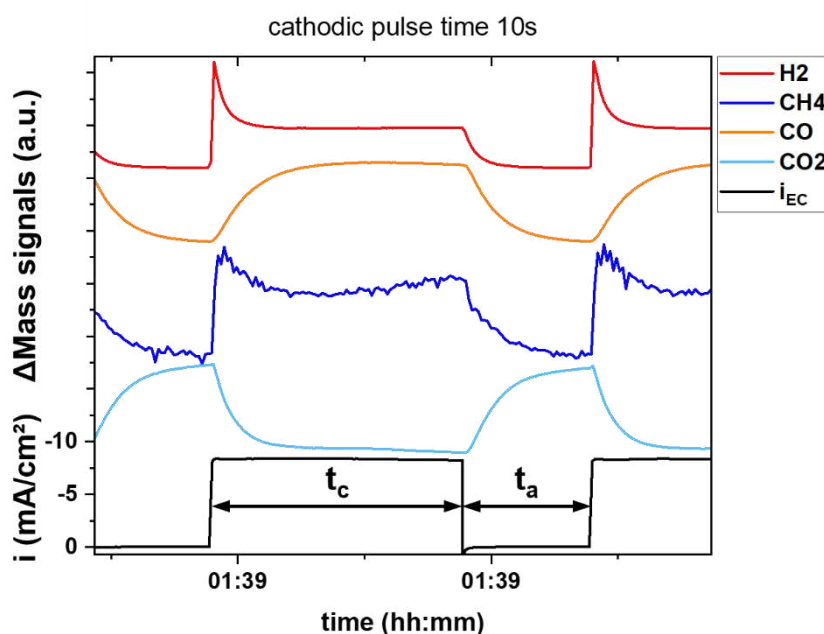
Figure 23: DEMS signals of major gaseous products formed under pulsed electrolysis at −2.1 V/−0.5 V, 10 s/5 s.

When extending the cathodic pulse duration (resulting in a higher t_c/t_a ratio), we create a higher local pH due to a longer reduction process. This could lead to a lower local CO_2 concentration due to bicarbonate/carbonate formation according to equation (9) and equation (10):
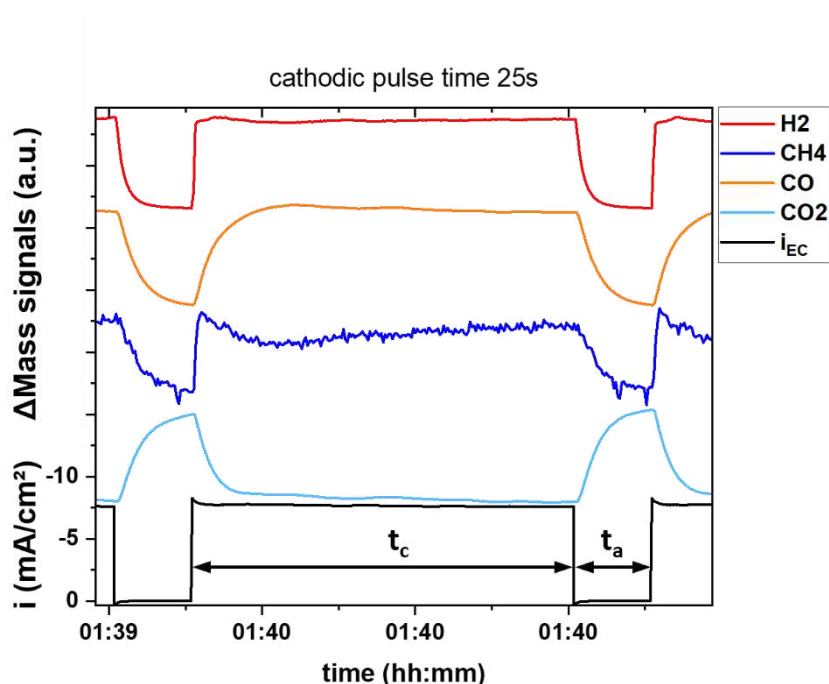
$$CO_2 + OH^- \leftrightarrow HCO_3^-$$ (9)

$$HCO_3^- + OH^- \leftrightarrow CO_3^{2-} + H_2O$$ (10)

Figure 24: DEMS signals of major gaseous products formed under pulsed electrolysis at −2.1 V/−0.5 V, 25 s/5 s.

Applying a cathodic potential for 25 s (see Figure 24: DEMS signals of major gaseous products formed under pulsed electrolysis at −2.1 V/−0.5 V, 25 s/5 s.), we observe a rapid increase in CH_4 signal (peaking after 0.6 s), followed by a similar transient decay as seen at shorter cathodic pulse duration. After about 5.5 s, the signal shows a slow rise over the rest of the cathodic pulse and a fast decline upon switching to the anodic pulse. A comparable signal shape is observed for the H_2 signal, whereas it shows a maximum at a later point of the pulse (after 1.4 s) and starts to slightly grow after about 6 s. The CO signal rises slowly, comparable to what we observed at t_c= 10 s and peaks after 6.7 s, followed by a moderate decrease over the remaining pulse. The similarity in peak shape between H_2 and CH_4, once again suggests that these species share some

54

commonality in some rate-determining factor, which is likely pH dependent. The transient signal thusly is affected by the pH dynamic in the pulsed electrolysis.[4] Most of the CO_2 is quickly consumed (~80 % after 3 s) as can be seen in the corresponding signal, which continues to decrease over the remaining cathodic pulse. Upon switching to the anodic pulse, the CO_2 signal recovers quickly.
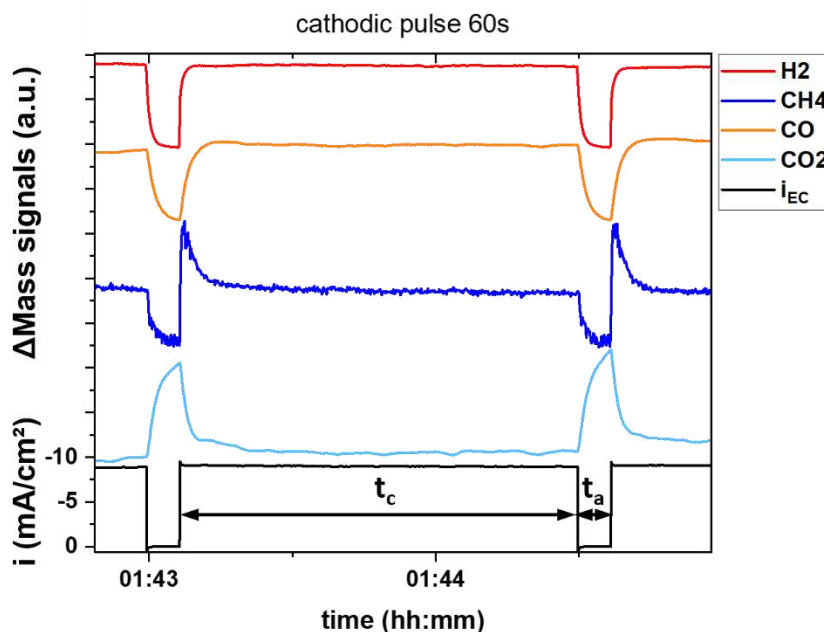
Figure 25: DEMS signals of major gaseous products formed under pulsed electrolysis at −2.1 V/−0.5 V, 60 s/5 s.

A cathodic pulse time of 60 s (while keeping t_a fixed at 5 s), shows comparable results to the previous experiment at t_c= 25 s. We observe a similar CH_4 signal shape, which rapidly grows after applying the cathodic potential and then decays to a steady level after about 4 s. Hydrogen shows a similar signal shape as in 5 s & 25 s cathodic pulse time, meaning a rise upon switching from anodic to cathodic potential, while showing no big spike as observed in Figure 23. The signal reaches its maximum after about 7.5 s and stays at this level for the remainder of the cathodic pulse. The CO signal shows a similar behavior as seen at t_c= 25 s – it grows to its maximum after 5.5 s, then shows a slight decrease over the following 5 s, where it stabilizes for the rest of the cathodic pulse. When the anodic pulse potential is applied all signals except for CO_2, drop rapidly. The CO_2 signal during the anodic pulse, shows an inverse shape of the CO signal, peaking at the potential switch, then shows a rapid decay during the cathodic pulse for 2.9 s, after which

the continuous decrease is flatter. We have observed little change in the methane signal peak maximum (correlating to the formation of product) when applying longer cathodic pulses. The signal decays typically after about 4 s to a steady state at which it remains or shows a minor growth for the remaining pulse time. Therefore, extending the pulse time of the cathodic pulse has no beneficial effect to methane formation rate, since it probably only leads to a higher local pH, which can lead to an actual lower local CO_2 concentration due to the CO_2/HCO_3^- equilibrium.

Since it is most likely that CO_2 and proton transport to the electrode surface is facilitated during a period of low current (during the anodic pulse), we systematically studied the effect of t_a modulation.
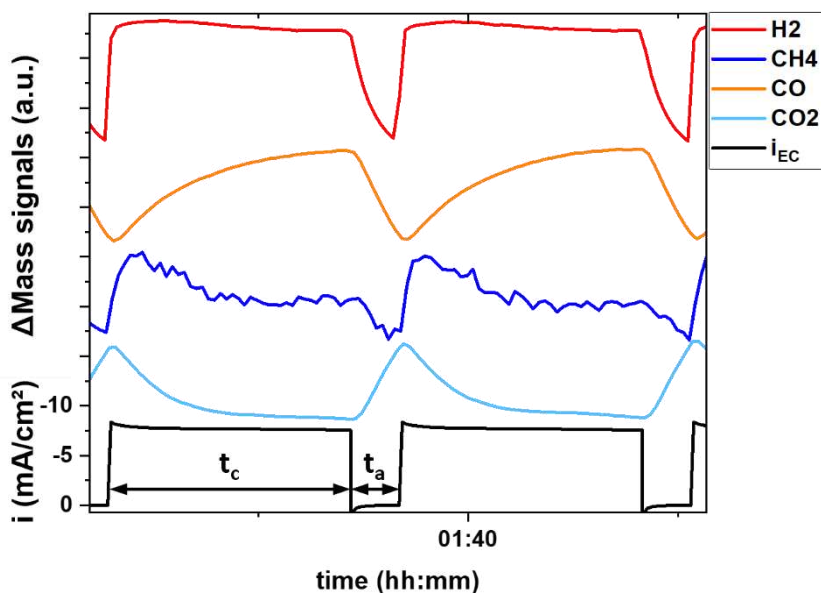
Figure 26: DEMS signals of major gaseous products formed under pulsed electrolysis at −2.1 V/−0.5 V, 5 s/1 s.

When applying a shorter anodic pulse like 1 s (as depicted in Figure 26), we observe a similar signal shape for H_2 as we have for t_c= 25 s (or even for t_c= 60 s). The signal rises sharply upon potential switch (from E_a to E_c), but peaks only after about 1 s, so slightly delayed to the CH_4 signal. It then shows a minor decay over the remaining cathodic pulse and quickly drops when turning to the anodic potential again. Whereas the CO signal shows a slow and long stretched growth over all the cathodic pulse, peaking at the last part of t_c, while decreasing similarly to the H_2 signal under anodic potential. The methane signal rises sharply upon employing the cathodic

potential, and shows a signal shape, like what we have observed at 5 s/5 s. The CO_2 signal shows a rather steep decay for the first few seconds and then exhibits a more moderate decrease for the rest of the cathodic pulse.
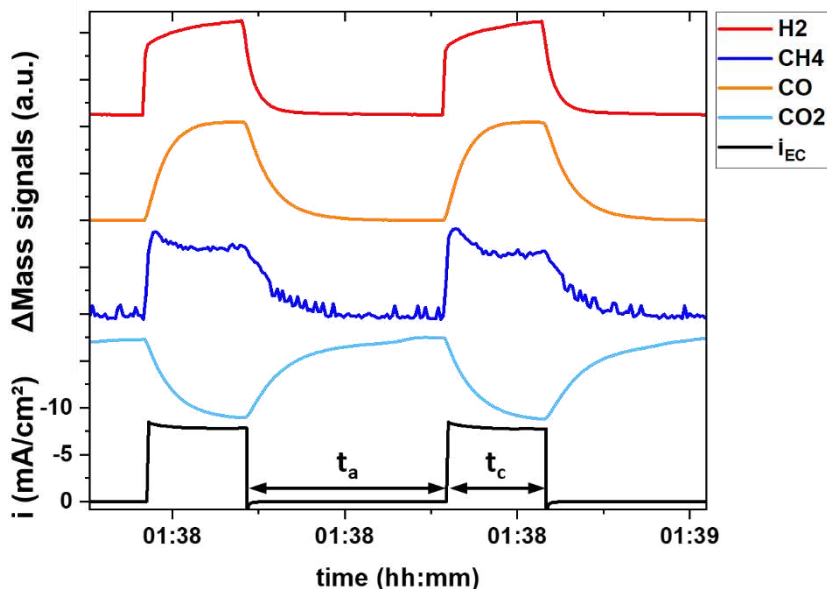
Figure 27: DEMS signals of major gaseous products formed under pulsed electrolysis at −2.1 V/−0.5 V, 5 s/10 s.

At an anodic pulse time of 10 s (Figure 27), we can observe an initial jump in the H_2 signal, followed by a moderate growth over the remaining cathodic pulse. Whereas the CO signal shows a similar peak shape as at a 5 s anodic pulse (cf. Figure 22). The CO_2 signal follows an inverse shape of the CO signal over both pulses, while the CH_4 signal shows as peak shape like during 10 s cathodic pulses (see Figure 23). Upon extending the anodic pulse time to 10 s, we can observe an increase in CO_2 signal, since it has a longer time to diffuse to the electrodes surface, before being reduced during the cathodic pulse.
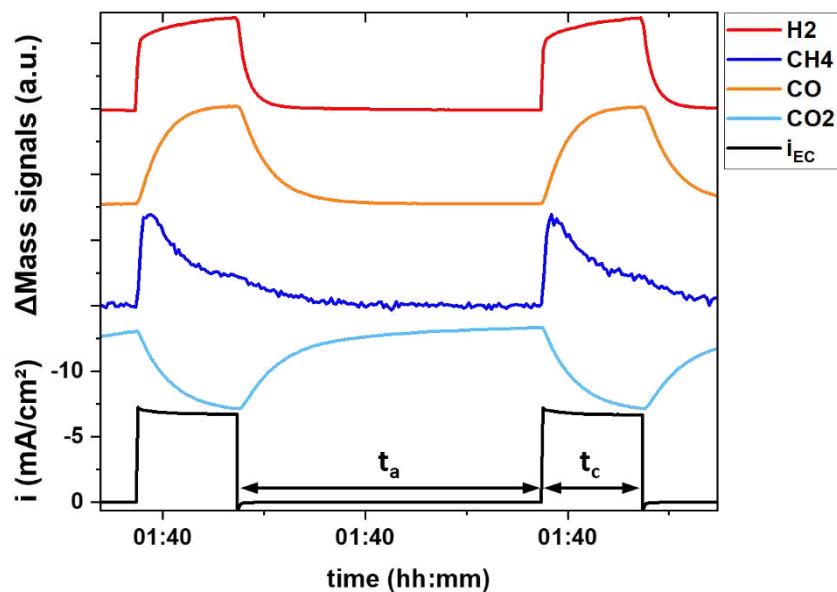
Figure 28: DEMS signals of major gaseous products formed under pulsed electrolysis at −2.1 V/−0.5 V, 5 s/15 s.

An anodic pulse time of 15 s yields mass signals as shown in Figure 28. We can see that Hydrogen, CO and CO_2 follow the same shape as we have seen at t_a= 10 s, while CH_4 shows a more pronounced signal peak after applying the cathodic potential, than what we have seen before. A similar observation can be made when extending the anodic pulse time to 25 s. We detect the same pulse shape for all gases measured, while the magnitude of the CO_2 signal and the methane signal is larger than at 15 s. The increase in methane signal can be explained by a higher local CO_2 concentration that is reached due to the extension of anodic pulse time. This can be also detected in the mass spectrometer, since the CO_2 signal magnitude (peak maximum – peak minimum) grows with increasing anodic pulse time. Furthermore, we observe also larger currents/densities, with longer anodic pulses, which can be explained by higher CO_2ER activity.
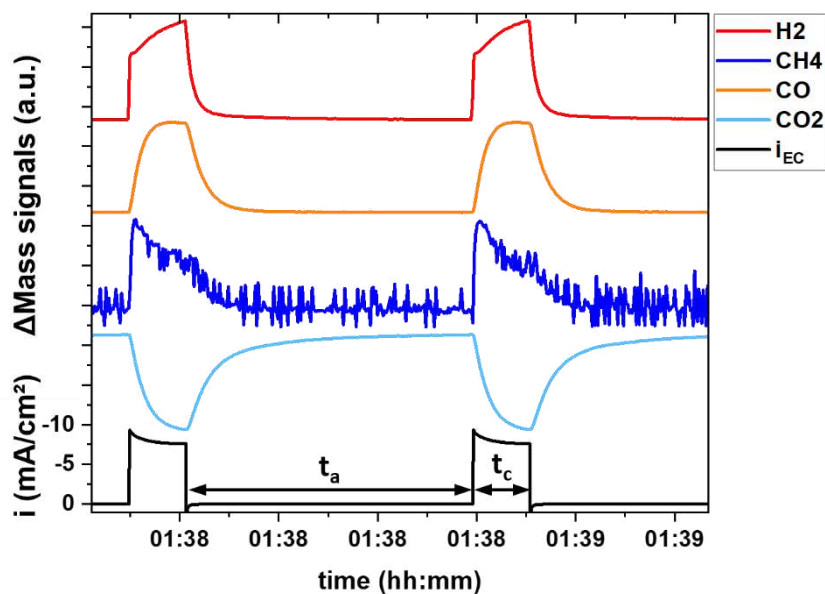
Figure 29: DEMS signals of major gaseous products formed under pulsed electrolysis at −2.1 V/−0.5 V, 5 s/25 s.

The DEMS signals shown so far were all re-scaled in order to facilitate comparison of their time-dependent behaviors. To get more quantitative insight about how product formation rates depend on pulse parameters, in order to extract comparative trends across the parameter space, we calculated for each product a MS signal difference (Δ(MS) = signal max @ Ec - baseline signal @ Ea)

Figure 30 A & B summarize the product formation rate trends extracted from the pulse time screening experiments. In these two figures the signal magnitudes are plotted with relation to the applied pulse time. For the cathodic pulse time screening (as displayed in Figure 30 A), we can observe a correlation between hydrogen and methane, where for conditions giving high CH_4 formation, we observe high H_2 evolution as well. However, we see no clear correlation between the cathodic pulse time and the methane signal. Since we quantify this behavior on the signal maximum, observed during the initial part of the pulse, little change in CH_4 with respect to t_c is a logical consequence. Due to the large datasets, the plotted values are obtained from signal maxima at the beginning of each cathodic and do not include the remaining part of the pulse. Going forward this will be targeted by development of a data analysis script capable of integrating signals over time during the pulse transients.

Figure 30 B shows the data extracted from the anodic pulse time screening experiments. We can see a clear correlation between longer anodic pulse times and CH_4 signal magnitudes, as well as lower CO_2 signal. Owing to the way of calculation of ΔMS the CO_2 ΔMS signal gives negative values. Hence the highest CO_2ER activity is observed at the most negative values for CO_2. Carbon monoxide grows with extended anodic pulse time, also owing to the higher local CO_2-concentration at longer t_a. Hydrogen does not show a clear correlation here, which makes further interpretation too speculative.
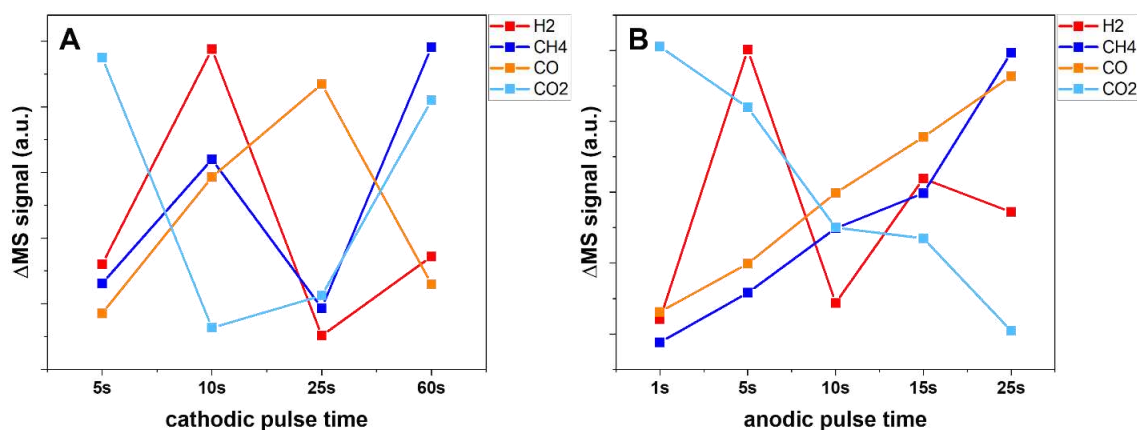
Figure 30: Averaged mass signal magnitudes over cathodic (A) and anodic (B) pulse time screening.

We have found little effect of t_c on the CH_4 signal, since we were looking at the signal maximum at the beginning of the cathodic pulse. Yet we found a significant effect of the anodic pulse time. Longer anodic pulses promote the methane formation, which might be explained by an increased replenishment of pH and local CO_2-concentration leading to higher activity in the initial part of the cathodic pulse. Yet this comes with the compromise that the duty cycle (and thus the overall time averaged CH_4 production) decreases when increasing t_a.

In addition to that we observed a decrease in HER whenever CH_4 is promoted and vice versa, suggesting that H_2 and CH_4 share a common rate limiting step (RLS), which is in agreement with observations made on copper.[5,6] Since this RLS likely to be pH dependent, we expect it to be influenced by pH transient under pulsing. Hence, the formation of CH_4 likely proceeds through a Langmuir-Hinshelwood mechanism, (as it was proposed for Cu catalysts), in which H* and CO* react with each other to form the *CHO intermediate, which can be further reduced to hydrocarbons.[5]

4.2 Screening a wide range of potentials using DEMS

We found significant methane formation at the potentials of −2.1 V/−0.5 V in the H-cell experiments. While optimizing the pulse potentials, we kept one pulse potential fixed, while varying the other. This showed us that the anodic potential can be varied between −0.4 V to −0.6 V at an E_c= −2.1 V (Figure 14 B), while still maintaining reasonable CH_4 selectivity. However, this does not rule out that other anodic potentials can result in even higher methane formation, if combined with the right cathodic potential and vice versa. We tested 154 potentials combinations by ranging E_c from −2.3 V to −1.0 V and E_a from −1.0 V to 0 V. Since running this screening with the classical H-cell/GC combination would have required continuous access to the gas chromatographer for weeks or even months, we made use of the fast response time of the DEMS set-up, which allowed us to detect products on a millisecond time scale. For the potential screening we applied each potential combination for 60 full pulse cycles (cathodic and anodic pulse) and for the data shown, we averaged the current and mass signals over the last 5 pulses. A new catalyst sputtered membrane was utilized for each anodic potential. Since inhomogeneities between the membranes from the deposition process could not be ruled out, slight differences between the experiments can also arise from different activities of each membrane. The trends that are observed on a single experiment however are conclusive. In addition, we observed little discrepancy in the initial linear sweep voltammetry (LSV) measured prior to each experiment, from which we can conclude that the difference in activity and permeability is minor. While the DEMS set-up we use does not allow for precise product quantification (as mentioned earlier), we can nonetheless observe trends and identify highly active potential combinations, which can subsequently be studied by follow-up tests with accurate product detection in the gas chromatographer.

We scanned the potential combinations by keeping one anodic pulse potential fixed, while varying the cathodic pulse potential. We followed this approach because we observed sample deactivation can occur at around −0.2 /−0.3 V (compare Figure 14 A & B) and wanted to avoid having this effect overlap with our experimental observations. We started each experiment at the highest cathodic overpotential (E_c= −2.3 V) and altered it stepwise in the anodic direction. The mass signals are plotted in arbitrary units (which are derived by the subtraction method described earlier), while the y-axis scale refers to the current density as obtained by the potentiostat.
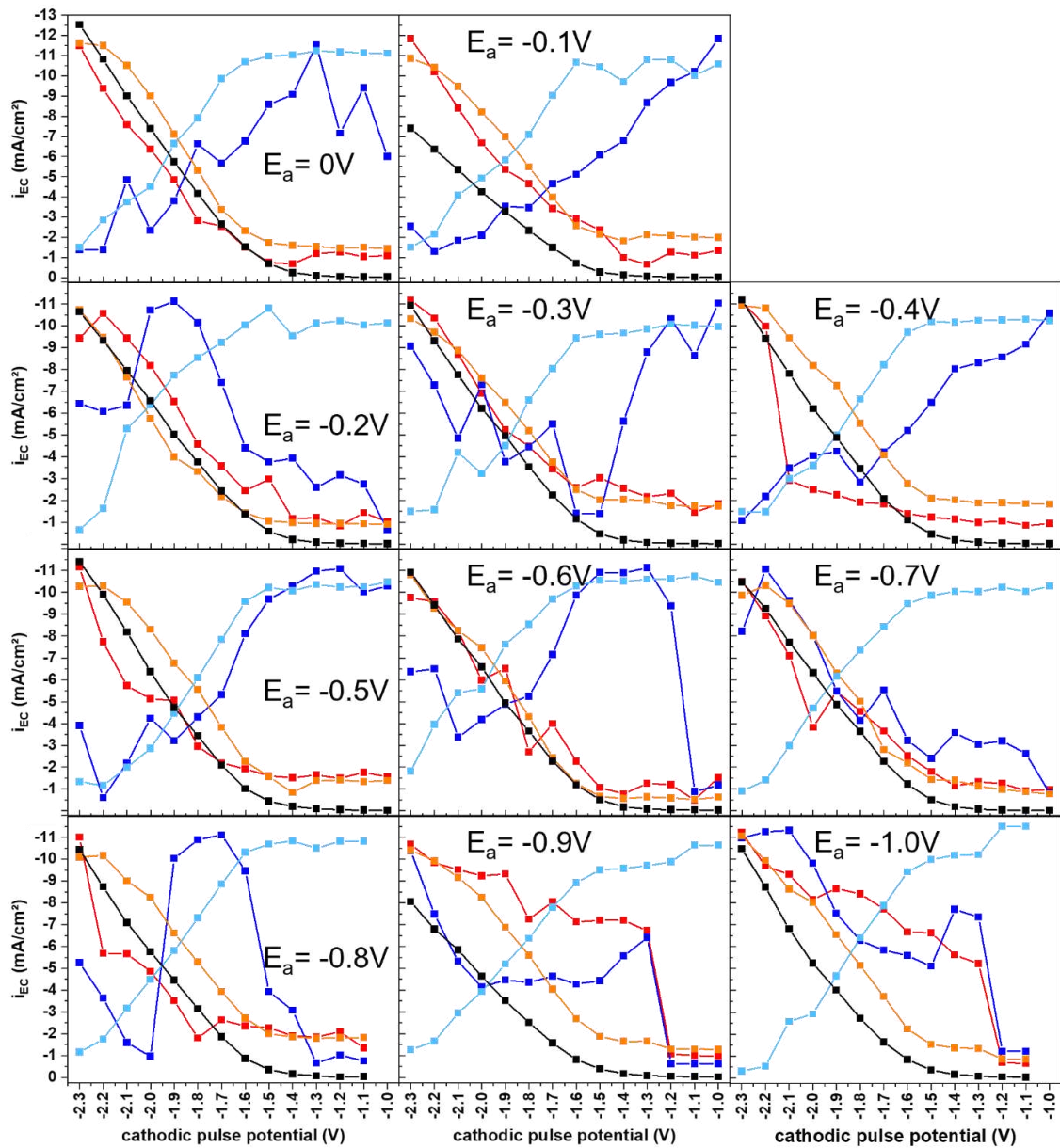
Figure 31: MS and current signal averages obtained at pulse potential screening with different fixed anodic pulse potentials. The y-axis shows a scalebar for the current density, while the mass signals are scaled in arbitrary units.

The results of the wide potential screening are plotted in Figure 31. For better comparability and all results are merged in a single figure. We can detect similar trends for H_2, and CO over all E_a tested (with slight variations), showing larger signals at higher (cathodic) overpotentials and decreasing towards lower overpotentials. The current density and CO_2 signal are inversely related as expected due to higher currents resulting CO_2 depletion. Most interestingly, CH_4 clearly exhibits large sensitivity to the different conditions applied.

Following the CH_4 in the anodic direction (of E_c) at an E_a of 0 V, we can observe the signal to grow significantly after −1.6 V and decrease at potentials of E_c> −1.3 V. This can either result from applying the right potential conditions or could be triggered by the longer electrolysis time that the sample has experience when reaching the less negative potentials, which then might lead to a higher state of "activation", as process discussed in the previous chapter. If the rise in CH_4 signal is due to a higher activation state (which should then be independent of the anodic pulse potential) we should observe this at the other anodic pulse potentials as well. H_2 show a minor increase between -1.4 V and -1.2 V.

At E_a= −0.1 V the CH_4 signal grows towards higher overpotentials and exhibits a maximum between −1.7 V and −2.0 V. This is in a similar potential range as the one identified in the previous chapter in the H-cell experiments, where we scanned E_c with E_a= −0.6 V. In contrast to the previous experiment where E_a= 0 V, we detect no elevated CH_4 evolution at lower overpotentials, but an actual decrease in line with the drop in current density.

For an E_a= −0.2 V, we detect a high CH_4 signal between -2.0 V and -1.7 V, followed by a decrease towards lower overpotentials. While at E_c= −1.4 V we can observe a small increase in CH_4, as well as a local minimum in CO_2 signal, indicating high CO_2ER activity. At a 100 mV lower pulse potential (E_a= −0.3 V), the CH_4 signal follows the previously observed trend as it rises with higher overpotential and resulting higher current density. It decreases from −2.3 V to −1.6 V and grows again in the anodic direction to a plateau between −1.2 V and −1.0 V, while we detect a small drop in signal at −1.1 V. This drop in signal (and especially its appearance over several different experiments) might suggest the formation of a different species, which shares a common RLS as CH_4 and H_2.

A more negative E_a of −0.4 V, yields a CH_4 signal that follows the trend of the CO_2 signal, by increasing towards lower overpotentials. In addition, we observe a small increase in CH_4 between −1.9 V and −2.3 V, as well as a slightly flatter increase between −1.4 V and −1.2 V. The CH_4 signal in region between −2.3 V and −1.9 V, resembles the trend observed for E_a= −0.2 V (but

shifted in E_c), where we have observed a rise in CH_4 formation between −2.0 V and −1.7 V. Hydrogen however shows a steep increase between −2.3 V and −2.2 V, which probably resembles a potential regime where CO_2 reaches mass transport limits. We then observe a suppressed HER once CO_2ER takes over, most likely due to a competition for surface sites and/or a lower local pH resulting from CO_2ER.

At an E_a= −0.5 V, we observe pronounced CH_4 formation between −1.6 V and −1.1 V with a maximum at −1.2 V, whereas the signal decreases towards more negative E_c, with a slight increase at −2.0 V and −2.3 V. In comparison to previous experiments the CH_4 formation is stretched over a broader range of cathodic pulse potentials (−1.7 V to −1.1 V). The small increase at −2 V is in well agreement with our observations made with the silver foil catalysts in the H-cell (see previous chapter). Between −2 V and −1.9 we also detect a deviation from the decrease in H_2 signal towards lower overpotentials, which again is in agreement with our findings in the H-cell experiments.

An anodic pulse potential of −0.6 V yields trends in signal growth that match our previous observations. The CH_4 signal shows a plateau between −2.3 V and −2.2 V, followed by a steep drop at −2.1 V. It then grows slowly to up to −1.8 V and then steeply from −1.7 V to −1.5 V, where it plateaus, followed by a decreases from −1.3 V to −1.1 V. We have observed higher CH_4 formation in a similar range at more posivite E_a (−0.5 V; −0.2 V), whereas the E_c potential range appears to be shifted to slightly higher overpotentials here. Another matching observation is the decrease at −1.1 V, which might suggest the formation of other species that compete for surface sites or intermediates.

When we apply an anodic pulse potential of −0.7 V, a striking difference to previously tested potentials is the reduction of CH_4 formation in the anodic direction (hence following the H_2 & CO trend). While it decreases steadily towards lower overpotentials, a little increase between −1.4 V and −1.1 V can be observed.

The results for −0.8 V: We observe a drastic rise in CH_4 signal at −1.9 V, and continuously high values for this product until E_c= −1.6 V, where the signal starts to decrease again up to −1.3 V. Hydrogen decreases from high overpotentials to lower ones, while showing a steep decrease after the first potential scanned, followed by a flatter decline between −2.2 V and −1.8 V up to a slight increase to −1.7 V where it almost plateaus up to −1.2 V. This is in agreement to what we have observed in our experiments with a silver foil catalyst, where HER increased at higher overpotentials, most probably caused by mass transport limited CO_2ER. Most interestingly CH_4

shows a signal shape as we have observed at −0.6 V but shifted towards more negative E_c. While we have observed E_a dependence on the methane formation in the previous chapter, we were limited to one cathodic potential for screening E_a and one E_a for screening E_c.

For an anodic pulse potential of −0.9 V, H_2 shows a similar signal shape with a less pronounced decrease, until it drops rapidly at $E_a \geq$ −1.2 V. The CH_4 signal decreases almost linearly from −2.3 V to −2 V, then plateaus from −2 V to −1.4 V, increases slightly to −1.3 V and then shows the same rapid decay as H_2 towards less negative E_c. The correlation between H_2 and CH_4 hints towards a shared RLS and is in agreement to our observations in the H-cell experiments.

As a final experiment in this section, we tested an E_a of −1 V. Hydrogen shows a decrease from very negative to more positive E_c while exhibiting an increase at −1.9 V and elevated levels until −1.2 V, where it drops abruptly, similar to what we have observed at E_a= −0.9 V. The CH_4 signal increases in the anodic direction from −2.3 V to −2.1 V, followed by a decrease up to −1.5 V. It then shows a rise between −1.4 V and −1.3 V and drops rapidly as the H_2 at −1.2 V. The graph shows no data for E_a= −1 V, since here E_a equals E_c, hence no pulsing is applied. The drastic drops at very low overpotentials (as observed for several E_a) is due to the extremely low currents at these potential combinations, producing extremely small signals, that can barely be separated from noise.

We hypothesize the formation of CH_4 to be dependent on an optimal coverage of *CO and *H. While higher overpotentials increase the chance of *CO reduction before it is desorbed[7] (Ag shows a low binding energy towards CO)[3], the anodic pulse potential could have a strong effect on the adsorbed species and H* (as it is postulated that anodic pulses could lead to specific desorption, most likely at less cathodic E_a). Hence a shift in cathodic pulse potential needed to drive the efficient formation of CH_4 is observed with respect to the applied E_a.

For direct comparison of the potential combinations on each species (and the current density), the data from the above experiments is summarized in the following 2D and 3D graphs.
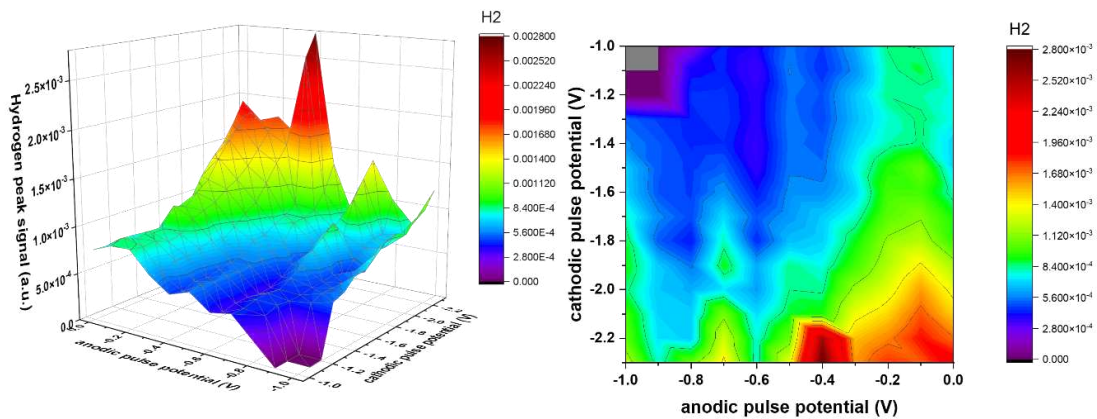
Figure 32: 3D and 2D plot of pulse potential screening data for H_2.

Figure 32 directly correlates the effect of pulse potential on the HER. We can see highly active potential combinations (dark red) and regions of less HER (dark blue/purple). While we can see a correlation between high overpotentials and a resulting higher current density (Figure 36) we also note a higher activity over a wide range of cathodic pulse potentials for an E_a of −0.1 V. Since we aim to suppress HER, operating at potential combinations resulting in low H_2 formation (as depicted in blue), suggests best conditions.
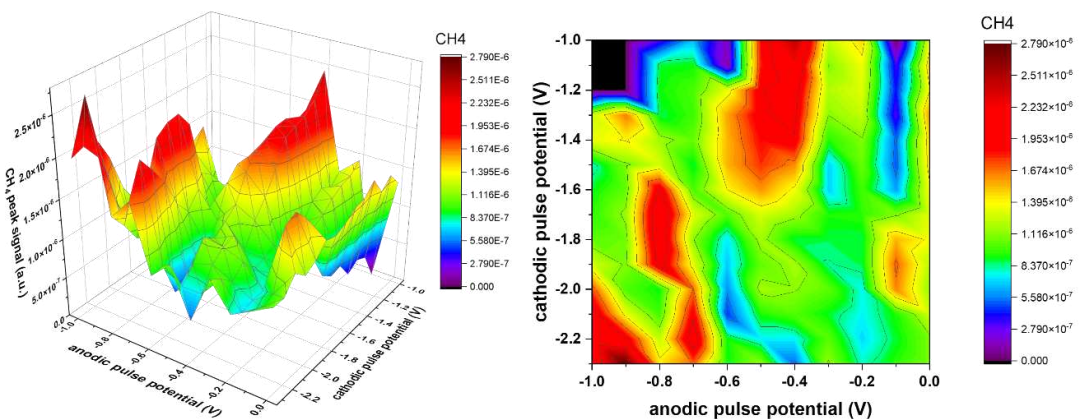
Figure 33: 3D and 2D plot showing the effect of pulse potential variation on CH_4.

The 2D and 3D plots in Figure 33 reveal highly active potential combinations for CH_4 ranging over several regions that haven't been tested by GC yet. This shows the strength of the DEMS

screening approach and testing these potential combinations offer a great potential for further rate improvement. We can identify a diagonal shift in methane activity from the most negative E_c and E_a combinations (−2.3 V/−0.9 V) to "milder" potentials (e.g., −1.2 V/−0.4 V). We propose the strong dependency of CH_4 activity on the anodic pulse potential to be related to adsorbed species, influencing the reaction pathway.
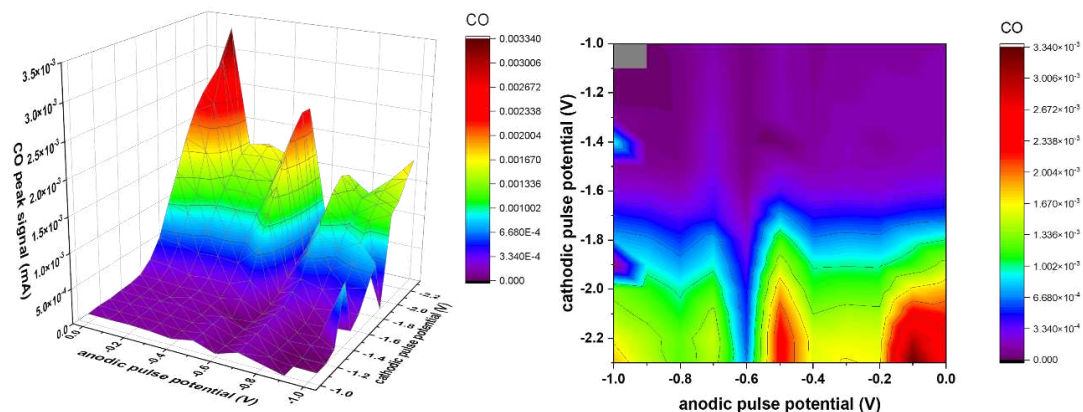
Figure 34: 3D and 2D plot showing the effect of pulse potential variation on CO.

Figure 34 depicts the correlation between observed CO signal and the applied potential combination. We observe higher signals towards higher E_c, similar to what has been observed for H_2 in Figure 32. In contrast to CH_4, we detect no areas of high CO formation at lower overpotentials.
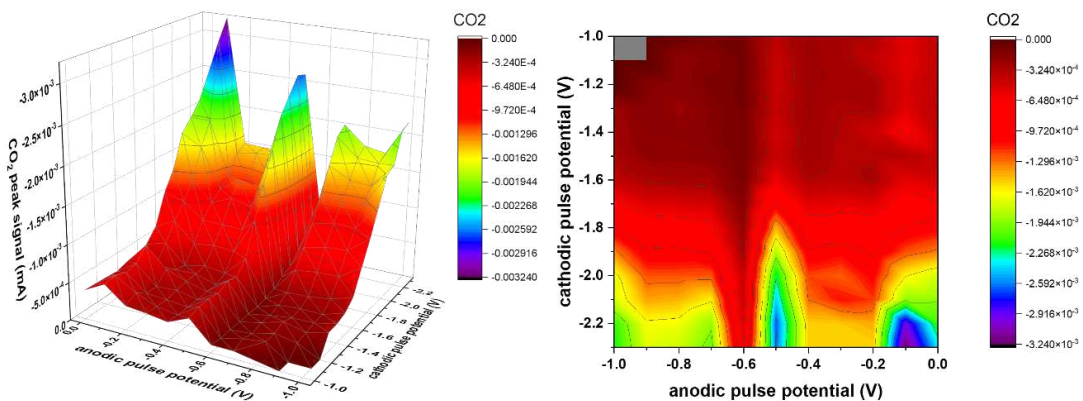
Figure 35: 3D and 2D plot showing the effect of pulse potential variation on CO_2 signal.

The summary graphs in Figure 35 show the CO_2 signal correlated with the applied pulse potentials. We can see regions of higher CO_2ER depicted in purple and dark blue, while regions with lower CO_2ER are depicted in red. In agreement with the results for other products, CO_2 consumption is highest at high overpotentials resulting from higher reductive currents (cf. Figure 36). Yet we can locate regions of lower CO_2ER. While a low signal for E_a= −0.6 V (for all gases) also hints to a lower permeability through the membrane.
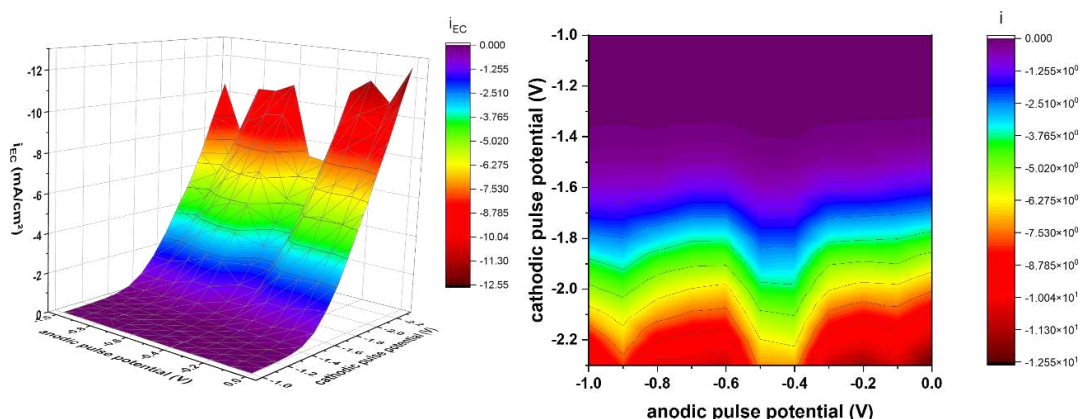
Figure 36: 3D and 2D plot showing the effect of pulse potential variation on i_{EC}.

The above graphs show the partial current densities plotted with respect to the applied pulse potentials. Since the sample area was defined by an O-ring it is the same for all samples (a new sample was used for each E_a), differences in i_{EC} are likely to originate from the applied potential combination. We can see the higher current density at combinations of highly cathodic E_c and very anodic E_a. This trend is in line with our observations from Figure 34 (CO) and Figure 35 (CO_2), indicating that a large part of the current stems from CO_2 to CO reduction.

Shorter pulses are highly beneficial for the promotion of CH_4 over the other gas products. We ascribe this to the non-uniform formation of CH_4 with respect to the pulse duration (t_c). Most of the CH_4 is formed during an initial state of the cathodic pulse, where a high local CO_2 concentration is present, while we still have an elevated local pH. We also didn't observe any direct correlation between an extended cathodic pulse length and an increase in CH_4, while we observed higher methane peak signals at longer t_a. This is in agreement with the observation that high local CO_2 concentrations promote the CH_4 formation. However, since no product formation is detected under the anodic pulse, extending t_a might not yield actual higher CH_4 rates. We therefore refrain from applying asymmetric potential pulses. Shorter pulses (like the

ones tested in the GC, in the millisecond timescale) will be subject of future investigations with the DEMS set-up.

The wide potential screening revealed regions of possible higher CH_4 formation that have not been tested yet with accurate product quantification. The observed high CH_4 peak signals especially at lower overpotentials are of great interest since they offer a more energy efficient way of CH_4 production than what we have tested so far. A possible explanation for these high signals at significantly lower potentials, could be the difference in surface morphology between the silver foils tested in chapter 3 and the here employed sputtered porous silver layers. The resulting confined pores in the porous Ag-films have substantially different mass transport conditions than the flat foils, thus giving for example formed CO more time to re-adsorb to the surface and be further reduced and can additionally create a larger local pH, which can aid the HER suppression. In addition to that, a change in mass transport is inherent to the different cell architectures used in both set-ups. While in the H-cell experiments a constant stream of CO_2 was fed into the cell, creating some convection to the otherwise stagnant electrolyte, we needed to employ a flow cell architecture in the DEMS experiments discussed in this chapter. This is due to the high CO_2 consumption by the mass spectrometer, which constantly takes out CO_2 from the solution into the high vacuum. By establishing electrolyte flow, the catalyst is constantly fed with fresh CO_2-saturated $KHCO_3$ solution, allowing for more realistic CO_2ER conditions. Further studies will include testing the promising potential combinations identified in the GC. In addition, picking the optima from the pulse time experiments and running them for potential optimization or vice versa, with the goal of optimizing this four-parameter space, would be an intriguing field to research. This however seems not feasible to do experimentally yet would be well suited for an AI/machine learning algorithm[8,9] to study based on data-sets like the one presented here.

4.3 Literature

(1) Clark, E. L.; Bell, A. T. Direct Observation of the Local Reaction Environment during the Electrochemical Reduction of CO2. *J. Am. Chem. Soc.* **2018**, *140* (22), 7012–7020. https://doi.org/10.1021/jacs.8b04058.

(2) Baltruschat, H. Differential Electrochemical Mass Spectrometry. *J. Am. Soc. Mass Spectrom.* **2004**, *15* (12), 1693–1706. https://doi.org/10.1016/j.jasms.2004.09.011.

(3) Bagger, A.; Ju, W.; Varela, A. S.; Strasser, P.; Rossmeisl, J. Electrochemical CO 2 Reduction: A Classification Problem. *ChemPhysChem* **2017**, *18* (22), 3266–3273. https://doi.org/10.1002/cphc.201700736.

(4) Bui, J. C.; Kim, C.; Weber, A. Z.; Bell, A. T. Dynamic Boundary Layer Simulation of Pulsed CO 2 Electrolysis on a Copper Catalyst. *ACS Energy Lett.* **2021**, 1181–1188. https://doi.org/10.1021/acsenergylett.1c00364.

(5) Schreier, M.; Yoon, Y.; Jackson, M. N.; Surendranath, Y. Competition between H and CO for Active Sites Governs Copper-Mediated Electrosynthesis of Hydrocarbon Fuels. *Angew. Chemie Int. Ed.* **2018**, *57* (32), 10221–10225. https://doi.org/10.1002/anie.201806051.

(6) Cheng, T.; Xiao, H.; Goddard, W. A. Full Atomistic Reaction Mechanism with Kinetics for CO Reduction on Cu(100) from Ab Initio Molecular Dynamics Free-Energy Calculations at 298 K. *Proc. Natl. Acad. Sci. U. S. A.* **2017**, *114* (8), 1795–1800. https://doi.org/10.1073/pnas.1612106114.

(7) Kuhl, K. P.; Hatsukade, T.; Cave, E. R.; Abram, D. N.; Kibsgaard, J.; Jaramillo, T. F. Electrocatalytic Conversion of Carbon Dioxide to Methane and Methanol on Transition Metal Surfaces. *J. Am. Chem. Soc.* **2014**, *136* (40), 14107–14113. https://doi.org/10.1021/ja505791r.

(8) Guo, Y.; He, X.; Su, Y.; Dai, Y.; Xie, M.; Yang, S.; Chen, J.; Wang, K.; Zhou, D.; Wang, C. Machine-Learning-Guided Discovery and Optimization of Additives in Preparing Cu Catalysts for CO2Reduction. *J. Am. Chem. Soc.* **2021**, *143* (15), 5755–5762. https://doi.org/https://doi.org/10.1021/jacs.1c00339.

(9)   Blanco, D. E.; Lee, B.; Modestino, M. A. Optimizing Organic Electrosynthesis through Controlled Voltage Dosing and Artificial Intelligence. *Proc. Natl. Acad. Sci.* **2019**, *116* (36), 17683–17689. https://doi.org/10.1073/PNAS.1909985116.

5 Probing adsorbates during p-CO$_2$ER with in-situ Raman spectroscopy

5.1 Data acquisition and analysis

Raman spectroscopy is a form of vibrational spectroscopy, meaning it can give information about vibrational modes of molecules or solids. It is dependent on inelastic scattering of photons. Here a monochromatic light source provides photons, which are inelastically scattered and upon interaction with the substrate, result in a shift in energy. Silver is very suitable for this technique since it has a plasmon resonance frequency in the relevant range, able to induce enhancement of near-surface signals. In our particular case, we can use this energy shift to extract information about the molecules adsorbed to the surface or in close proximity to it (~3 nm)[1–3]. We applied this powerful technique in-situ during our pulsed electrolysis on Ag foil catalysts to gain information about I) The activation process leading to the rise in CH$_4$ production during the experiment and II) The effect of the potential switch (or alternation) between E$_c$ and E$_a$ on the surface composition.

Figure 37 A & B show a comparison of four Raman spectra, acquired over a pulse experiment (conducted at −2.1 V/−0.5 V; 5 s/5 s). In order to gain detailed information about the system and its changes, we collected one spectrum every 400 ms over a total experimental time of 40 min (compare Scheme 3 in the Materials and Methods section). For a better signal-to-noise ratio, the collected spectra (6000) were separated into three segments (each segment thus corresponding to 2000 spectra, equal to about 13 min of the experiment), which are then averaged with regards to the applied pulse potential i.e., E$_a$ or E$_c$ during their collection. With the reported time resolution of 400 ms per spectrum, we collected 12.5 spectra per potential pulse (t$_c$= t$_a$= 5 s). The data shown (so each trace corresponding to a pulse potential, cf. Figure 37 A & B) is an average of 10 spectra per potential pulse, with one spectrum omitted at the beginning and at the end of the potential pulse, as well as the spectrum collected at the potential switch. For the sake of clarity, the spectra representing the middle 2000 spectra are omitted. For technical reasons the spectra collection was split into two segments, with a range from 150 to 2000 cm^{-1} collected during the first 40 min of the pulse experiment and 1800-3200 cm^{-1}, collected during the following 40 min of the pulse experiment.
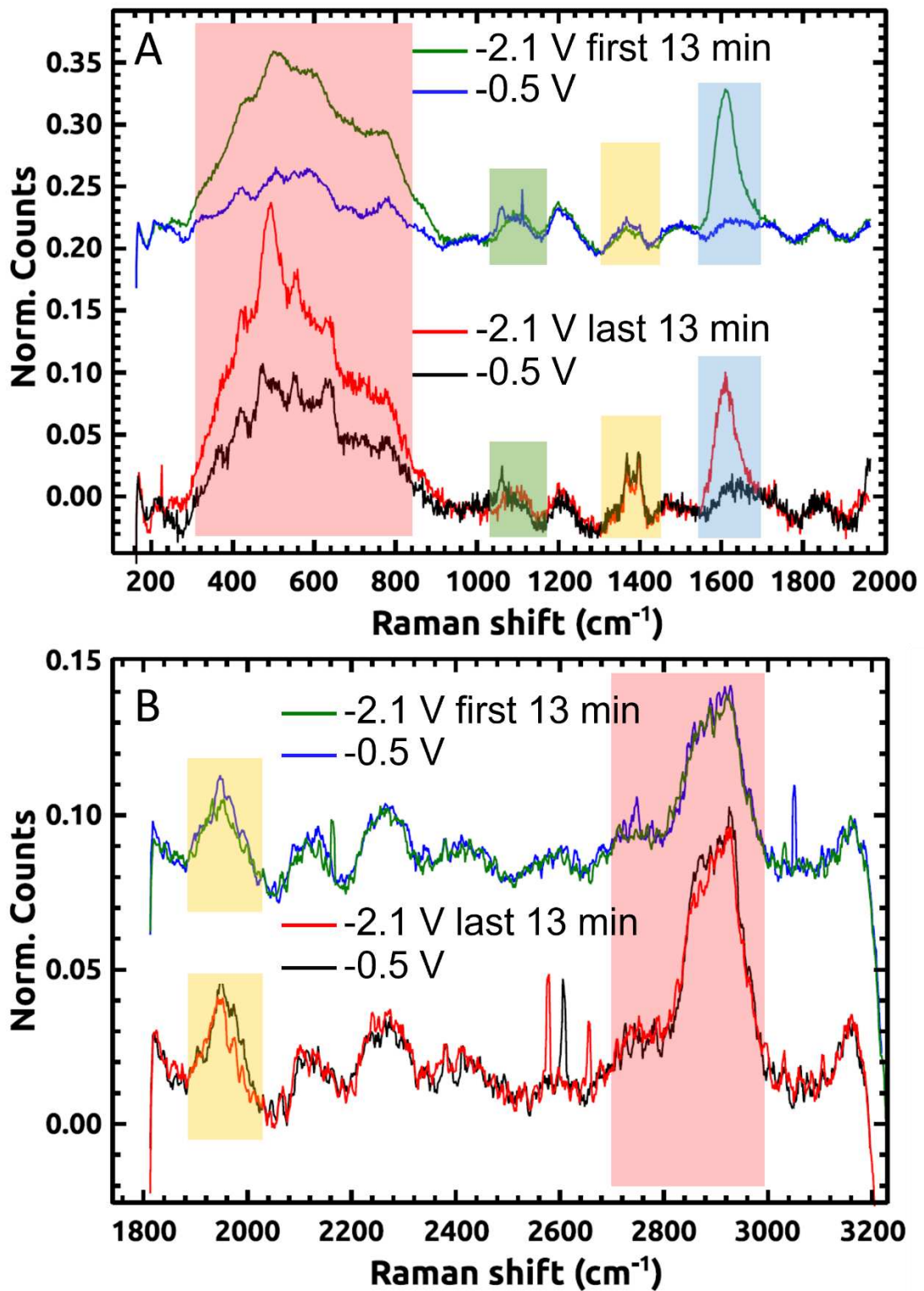
Figure 37: Raman spectra for a 40 min pulse experiment (conducted at −2.1 V/−0.5 V; 5 s/5 s). 6000 spectra were collected over the pulse experiment and subsequently split into 3 segments of ~13 min each, for which the data was averaged. Here shown are the averaged spectra over the first 13 min, blue line: −0.6 V & green line: −2.1 V; as well as the last 13 min, with black line: −0.6 V and red line: −2.1 V. Regions of interest are marked with colored rectangles. A) shows the Raman region from 150-2000 cm^{-1}, while B) shows the data from 1800-3200 cm^{-1}.

Figure 37 A shows the spectra obtained in the range between 150-2000 cm^{-1}. Regions of interest are labeled with colored rectangles. Herein, we can observe significant changes, both over the duration of the experiment (so difference between first 13 min and last 13 min) as well as over one pulse cycle, that is the difference between the average spectra during E_c and E_a respectively. Most prominent are the differences in signal magnitude between E_c and E_a steps (green/blue). The region with the lowest Raman shift (red rectangle, ~300-840 cm^{-1}) encompasses a range of species, which can include Ag-O species[4], Ag-O interaction with carbonated species[5], Ag-CO_x interactions[6], or C-O interactions.[7]

In the spectral region between 1800-3200 cm^{-1} (Figure 37 B), two distinct regions are marked. The peak at ~1950 cm^{-1} in the yellow region could be assigned to surface bound CO. While it appears at lower wavenumbers than usual, it can stem from CO being bound in a bridge configuration as reported previously.[12,13] This peak shows a slight rise over the duration of the experiment (first 13 min vs last 13 min), as well an increase when E_a is applied. The increase over the experiment duration points to an increase in CO surface coverage, while a larger signal at E_a suggests that CO is bound preferably during the anodic pulse and further reduced during the cathodic pulse. The spiking signals around 2600 cm^{-1} for the red and black trace, as well as the blue trace at ~3060 cm^{-1} are artefacts and do not correspond to molecular vibrations. The region in red is most likely contributed by C−H interactions. The signal for CH_4 (2917 cm^{-1})[14], falls in the same region, supporting our observations that methane is formed under the cathodic pulse (as shown chapter 2). This observation, as well as the absence of graphitic carbon signals (1360 cm^{-1} and 1580 cm^{-1})[15,16], refutes the hypothesis of Shiratsuchi et al. that CH_4 on silver is formed during the anodic pulse by a reaction of a [C] intermediate (see introduction on silver CO_2ER).

The in-situ Raman results presented above represent a preliminary analysis enabled by a time-resolved technique very recently developed by collaborators.[17] Further experiments and comprehensive analysis of the data are being conducted in a follow-up study for subsequent publication.

5.2 Literature

(1) Masango, S. S.; Hackler, R. A.; Large, N.; Henry, A.-I.; McAnally, M. O.; Schatz, G. C.; Stair, P. C.; Van Duyne, R. P. High-Resolution Distance Dependence Study of Surface-Enhanced Raman Scattering Enabled by Atomic Layer Deposition. *Nano Lett.* **2016**, *16* (7), 4251–4259. https://doi.org/10.1021/acs.nanolett.6b01276.

(2) Liu, S.; D'Amario, L.; Jiang, S.; Dau, H. Selected Applications of Operando Raman Spectroscopy in Electrocatalysis Research. *Curr. Opin. Electrochem.* **2022**, *35*, 101042. https://doi.org/10.1016/j.coelec.2022.101042.

(3) Wei, W.; Li, S.; Millstone, J. E.; Banholzer, M. J.; Chen, X.; Xu, X.; Schatz, G. C.; Mirkin, C. A. Surprisingly Long-Range Surface-Enhanced Raman Scattering (SERS) on Au–Ni Multisegmented Nanowires. *Angew. Chemie Int. Ed.* **2009**, *48* (23), 4210–4212. https://doi.org/10.1002/ANIE.200806116.

(4) Iwasaki, N.; Sasaki, Y.; Nishina, Y. Ag Electrode Reaction in NaOH Solution Studied by In-Situ Raman Spectroscopy. *Surf. Sci.* **1988**, *198* (3), 524–540. https://doi.org/10.1016/0039-6028(88)90382-2.

(5) Bohra, D.; Ledezma-Yanez, I.; Li, G.; de Jong, W.; Pidko, E. A.; Smith, W. A. Lateral Adsorbate Interactions Inhibit HCOO – While Promoting CO Selectivity for CO 2 Electrocatalysis on Silver. *Angew. Chemie Int. Ed.* **2019**, *58* (5), 1345–1349. https://doi.org/10.1002/anie.201811667.

(6) Harris, T.; Chartrand, D.; Heidary, N.; Pardo-Perez, L. C.; Ly, K.; Kornienko, N. Surface Chemistry Modulates CO2 Reduction Reaction Intermediates on Silver Nanoparticle Electrocatalysts. *ChemRxiv* **2020**. https://doi.org/10.26434/chemrxiv.12014910.v1.

(7) Bohra, D.; Ledezma-Yanez, I.; Li, G.; de Jong, W.; Pidko, E. A.; Smith, W. A. Lateral Adsorbate Interactions Inhibit HCOO – While Promoting CO Selectivity for CO 2 Electrocatalysis on Silver. *Angew. Chemie* **2019**, *131* (5), 1359–1363. https://doi.org/https://doi.org/10.1002/anie.201811667.

(8) Rudolph, W. W.; Irmer, G.; Königsberger, E. Speciation Studies in Aqueous HCO 3 – –CO 3 2– Solutions. A Combined Raman Spectroscopic and Thermodynamic Study. *Dalt. Trans.* **2008**, No. 7, 900–908. https://doi.org/10.1039/B713254A.

(9)   Chernyshova, I. V.; Somasundaran, P.; Ponnurangam, S. On the Origin of the Elusive First Intermediate of CO 2 Electroreduction. *Proc. Natl. Acad. Sci.* **2018**, *115* (40), E9261–E9270. https://doi.org/10.1073/pnas.1802256115.

(10)   Bui, J. C.; Kim, C.; Weber, A. Z.; Bell, A. T. Dynamic Boundary Layer Simulation of Pulsed CO 2 Electrolysis on a Copper Catalyst. *ACS Energy Lett.* **2021**, 1181–1188. https://doi.org/10.1021/acsenergylett.1c00364.

(11)   Oda, I.; Ogasawara, H.; Ito, M. Carbon Monoxide Adsorption on Copper and Silver Electrodes during Carbon Dioxide Electroreduction Studied by Infrared Reflection Absorption Spectroscopy and Surface-Enhanced Raman Spectroscopy. *Langmuir* **1996**, *12* (4), 1094–1097. https://doi.org/10.1021/la950167j.

(12)   Schmitt, K. G.; Gewirth, A. A. In Situ Surface-Enhanced Raman Spectroscopy of the Electrochemical Reduction of Carbon Dioxide on Silver with 3,5-Diamino-1,2,4-Triazole. *J. Phys. Chem. C* **2014**, *118* (31), 17567–17576. https://doi.org/10.1021/jp503598y.

(13)   Mahoney, M. R.; Howard, M. W.; Cooney, R. P. Raman Spectra of Carbon Monoxide Adsorbed on Silver Electrodes. *J. Electroanal. Chem. Interfacial Electrochem.* **1984**, *161* (1), 163–167. https://doi.org/10.1016/S0022-0728(84)80257-0.

(14)   Magnotti, G.; KC, U.; Varghese, P. L.; Barlow, R. S. Raman Spectra of Methane, Ethylene, Ethane, Dimethyl Ether, Formaldehyde and Propane for Combustion Applications. *J. Quant. Spectrosc. Radiat. Transf.* **2015**, *163*, 80–101. https://doi.org/10.1016/j.jqsrt.2015.04.018.

(15)   Mahoney, M. R.; Howard, M. W.; Cooney, R. P. Carbon Dioxide Conversion to Hydrocarbons at Silver Electrode. *Chem. Phys. Lett.* **1980**, *71* (1), 59–63. https://doi.org/https://doi.org/10.1016/0009-2614(80)85289-4.

(16)   Cooney, R. P.; Mahoney, M. R.; Howard, M. W. Intense Raman Spectra of Surface Carbon and Hydrocarbons on Silver Electrodes. *Chem. Phys. Lett.* **1980**, *76* (3), 2–6. https://doi.org/https://doi.org/10.1016/0009-2614(80)80645-2.

(17)   D'Amario, L.; Stella, M. B.; Edvinsson, T.; Persico, M.; Messinger, J.; Dau, H. Towards Time Resolved Characterization of Electrochemical Reactions : Electrochemically-Induced Raman Spectroscopy. *ChemRxiv* **2022**.

6 Conclusion and Outlook

6.1 Conclusion

Driving the electrochemical CO_2 reduction (CO_2ER) with renewable energy is a promising way of creating carbon neutral commodity chemicals and fuels, thus helping to mitigate from fossil sources of carbon and energy. Pulsed potential CO_2ER (p-CO_2ER) has shown potential as a simple but versatile way of directing the product formation without complex synthesis of catalysts. We have investigated the p-CO_2ER as a way of controlling the selectivity on an Ag-foil catalyst, with significant changes compared to potentiostatic control. We found that the silver undergoes an activation period during the first ~4 h after which it shows the unique behavior of producing large amounts of CH_4. Pulsing also suppressed the competing hydrogen evolution reaction. We observe a change in surface roughness and morphology due to the pulsing. The surface restructuring might lead to a higher concentration of undercoordinated sites, that could exhibit a higher binding strength towards the key intermediate CO.[1,2] We were able to show that pulsing the potential leads to an increased local CO_2 concentration, able to suppress HER and promote CO_2ER. The pulsed potential approach also yielded enhanced stability for over 20 h, without showing any signs of degradation.

We probed the product evolution in real-time and have confirmed that methane is indeed formed during the cathodic part of the pulse cycle, refuting a working hypothesis of Shiratsuchi et al.[3] The employment of fast product detection via DEMS allowed us to probe a wide range of pulse parameters (E_c, E_a, t_c and t_a), revealing higher CH_4 formation during ms pulses and identifying promising potential combinations for further optimized CH_4 formation, which will be focus of forthcoming experiments.

A preliminary analysis of in-situ Raman spectroscopy complemented our observations, showing significant differences in adsorbed species between both potentials (E_c and E_a) as well as over the duration of the experiment. While differences between the applied potentials give information about the effect of pulsing, changes over the duration of the experiment hints towards processes relating to surface activation.

These findings refute the mechanism proposed by Shiratsuchi et al.[3], which proposed hydrocarbon formation to take place during the anodic pulse, via the reaction of a graphitic carbon intermediate with H*. We propose a mechanism closer to what has been suggested for

Cu, where CO is reduced to a *CHO intermediate, followed by reduction to C-H intermediates and subsequently CH_4.[2,4]

Pulsing might also enable re-adsorption of CO onto the surface (on different surface sites, than where it was formed initially). So it might be that CO conversion sites are formed during pulsing, while CO forming sites are already present from the start, which could be investigated by CO reduction experiments.

6.2 Outlook

The roughening observed during pulsing poses the questions whether undercoordinated sites with higher CO binding strength are forming. This could be investigated by (in-situ) AFM, with the aim to provide a detailed view of surface structure evolution during the activation process. This gained insight in combination with density-functional theory (DFT) calculation on undercoordinated sites on silver (which hasn't been done for CO_2ER to our knowledge) can help to understand whether such sites may have a role in CO reduction.

Since we have identified potential combinations of high CH_4 selectivity in the DEMS experiment, we will investigate those with accurate product quantification aiming to obtain even higher CH_4 rates. The obtained in-situ Raman data will be analyzed in more detail, in order to identify adsorbed species and gain insight into the deactivation mechanism that is observed at less negative E_a (−0.3 V to −0.1 V). Investigating cation effects on the p-CO_2ER on silver is of large interest, due to their ability to further promote CO_2ER and suppress HER. Further we will study pulsed potential CO reduction on silver, targeting liquid products, as DFT studies have suggested that silver shows potential for efficient ethanol formation.[5] Future experiments will also include the use of a gas-fed electrolyzer in p-CO_2ER experiments, allowing operation at significantly higher (industrially relevant) current densities.

6.3 Literature

(1)   Dutta, A.; Morstein, C. E.; Rahaman, M.; Cedeño López, A.; Broekmann, P. Beyond Copper in CO 2 Electrolysis: Effective Hydrocarbon Production on Silver-Nanofoam Catalysts. *ACS Catal.* **2018**, *8* (9), 8357–8368. https://doi.org/10.1021/acscatal.8b01738.

(2)   Liu, X.; Xiao, J.; Peng, H.; Hong, X.; Chan, K.; Nørskov, J. K. Understanding Trends in Electrochemical Carbon Dioxide Reduction Rates. *Nat. Commun.* **2017**, *8* (May), 15438. https://doi.org/10.1038/ncomms15438.

(3)   Shiratsuchi, R.; Nogami, G. Pulsed Electroreduction of CO2 on Silver Electrodes. *J. Electrochem. Soc.* **1996**, *143* (2), 582–586. https://doi.org/10.1149/1.1836484.

(4)   Cheng, T.; Xiao, H.; Goddard, W. A. Full Atomistic Reaction Mechanism with Kinetics for CO Reduction on Cu(100) from Ab Initio Molecular Dynamics Free-Energy Calculations at 298 K. *Proc. Natl. Acad. Sci. U. S. A.* **2017**, *114* (8), 1795–1800. https://doi.org/10.1073/pnas.1612106114.

(5)   Hanselman, S.; Koper, M. T. M.; Calle-Vallejo, F. Computational Comparison of Late Transition Metal (100) Surfaces for the Electrocatalytic Reduction of CO to C 2 Species. *ACS Energy Lett.* **2018**, *3* (5), 1062–1067. https://doi.org/10.1021/acsenergylett.8b00326.

7 Publications

(1) Pardo Pérez, L. C.; **Arndt, A**.; Stojkovikj, S.; Ahmet, I. Y.; Arens, J. T.; Dattila, F.; Wendt, R.; Guilherme Buzanich, A.; Radtke, M.; Davies, V.; Höflich, K.; Köhnen, E.; Tockhorn, P.; Golnak, R.; Xiao, J.; Schuck, G.; Wollgarten, M.; López, N.; Mayer, M. T. Determining Structure-Activity Relationships in Oxide Derived Cu-Sn Catalysts During CO2 Electroreduction Using X-Ray Spectroscopy. *Adv. Energy Mater.* **2022**, *12* (5). https://doi.org/10.1002/AENM.202103328.

(2) Pulse Potential CO2 reduction for Tuning Product Selectivity on Silver – *in preparation*